

EUROPEAN ORGANISATION FOR NUCLEAR RESEARCH (CERN)



Submitted to: JINST



CERN-EP-2024-342
20th December 2024

Expected Tracking Performance of the ATLAS Inner Tracker at the High-Luminosity LHC

The ATLAS Collaboration

The high-luminosity phase of LHC operations (HL-LHC), will feature a large increase in simultaneous proton–proton interactions per bunch crossing up to 200, compared with a typical leveling target of 64 in Run 3. Such an increase will create a very challenging environment in which to perform charged particle trajectory reconstruction, a task crucial for the success of the ATLAS physics program, and will exceed the capabilities of the current ATLAS Inner Detector (ID). A new all-silicon Inner Tracker (ITk) will replace the current ID in time for the start of the HL-LHC. To ensure successful use of the ITk capabilities in Run 4 and beyond, the ATLAS tracking software has been successfully adapted to achieve state-of-the-art track reconstruction in challenging high-luminosity conditions with the ITk detector. This paper presents the expected tracking performance of the ATLAS ITk based on the latest available developments since the ITk technical design reports.

© 2024 CERN for the benefit of the ATLAS Collaboration.

Reproduction of this article or parts of it is allowed as specified in the CC-BY-4.0 license.

arXiv:2412.15090v1 [hep-ex] 19 Dec 2024

Contents

1	Introduction	2
2	The ATLAS Inner Tracker	3
2.1	Overview	3
2.2	ITk layout	3
3	Simulation	7
3.1	Geometry description and material	7
3.2	Simulation samples	11
3.3	Simulation of digitized readout signals	12
4	Reconstruction	12
4.1	Track reconstruction and selection	12
4.2	Vertex reconstruction and selection	15
5	Expected tracking and vertexing performance	16
5.1	Seeding performance	16
5.2	Efficiency	17
5.3	Number of tracks, mis-reconstructed and fake track rates	22
5.4	Track parameter resolution	25
5.5	Primary vertex reconstruction and identification	26
6	Conclusion	29

1 Introduction

The Large Hadron Collider (LHC) [1] has enabled detailed exploration of the energy frontier since 2009 with a successful program of proton–proton and heavy-ion collisions. It is slated to be upgraded in time for its fourth period of operation (Run 4) to deliver a nominal luminosity of $5.0 \times 10^{34} \text{cm}^{-2} \text{s}^{-1}$ to the general-purpose detectors ATLAS [2] and CMS [3], in a configuration known as high-luminosity LHC (HL-LHC) [4]. Such an increase in instantaneous luminosity creates a very challenging environment for particle detectors since it is achieved at the cost of a drastic increase in the average number of proton–proton interactions in the same bunch crossing ($\langle \mu \rangle$, also known as “pile-up”), expected to rise up to as much as 140 in the ATLAS detector during Run 4, as compared with a typical leveling target of 64 during Run 3. For subsequent runs, further luminosity increases up to $7.5 \times 10^{34} \text{cm}^{-2} \text{s}^{-1}$ are under discussion, which would bring the pile-up up to 200, extreme conditions under which the reconstruction will have to maintain robust performances. Moreover, the performance of the ATLAS Inner Detector subsystem [5, 6] is already affected by radiation damage [7, 8], which degrades its operational capabilities. Furthermore, the subsystem will face challenges in addressing the increased fluence and occupancy resulting from HL-LHC collisions, with bandwidth limitations and the need to minimize the material budget likely exacerbating these issues. Therefore, the ATLAS Collaboration will install a new all-silicon tracking detector, the Inner Tracker (ITk) [9, 10], as a part of its Phase-II detector upgrade program [11, 12] in preparation for HL-LHC data-taking. Following the publication of the technical design reports, further refinements were made to the detector design, which are detailed in this document.

The reconstructed trajectories (tracks) of charged particles produced in collisions are a key input to many other reconstruction algorithms [13–18], and they are also used directly by a number of physics analyses (for example Refs. [19–21]). To achieve high tracking efficiency, the ATLAS tracking chain [22, 23] is designed around a combinatorial variant of the well-known Kalman filter algorithm [24], augmented by an ambiguity solving stage designed to keep the low-quality and duplicate track creation rates at a minimum. This paper presents the expected performance of a version of this track reconstruction chain tuned specifically for the challenging environment of HL-LHC collisions and using the ITk detector.

The ATLAS Collaboration has produced notes detailing the expected performance of flavor-tagging [25, 26] as well as the integrated performance of the whole Run 4 detector [27, 28]. Reports about the concomitant upgrade to the CMS detector can be found in Refs. [29, 30]. Extensive information about the physics prospects at the HL-LHC for both the ATLAS and CMS collaborations can be found in Refs. [31, 32].

The rest of this paper is structured as follows: the ITk detector layout is detailed in Section 2; the simulation framework and samples, and the track reconstruction strategy are described in Section 3 and 4, respectively; the expected ITk tracking and vertexing performance is reported in Section 5; and concluding remarks can be found in Section 6.

2 The ATLAS Inner Tracker

2.1 Overview

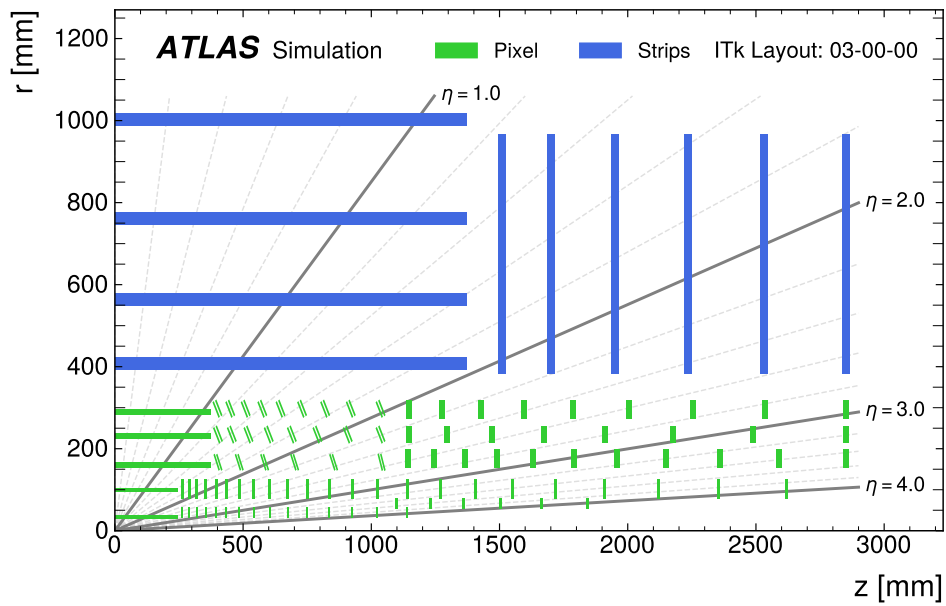
The ITk is designed to be a silicon-based detector that comprises a pixel [10] and a strip subsystem [9]. The pixel subsystem covers a pseudorapidity¹ range of $|\eta| < 4.0$ and consists of five flat barrel layers and five layers of inclined or vertical rings for forward region coverage. The strip subsystem spans $|\eta| < 2.7$ and includes four strip layers in the barrel region and six disks in the endcaps, all using double-sided modules. The active area of the detector will be shielded from the neutron flux coming from the calorimeters by a neutron moderator surrounding the strip detector.

The ITk will operate within a solenoidal magnetic field of 2 T, which is aligned with the beam axis. This magnetic field plays a crucial role by bending the trajectories of charged particles, allowing to estimate their transverse momentum, p_T . The overall ITk configuration aims to achieve a minimum of nine measurements per track across the entire expected beam spot size, assuming a Gaussian distribution with a longitudinal width of 50 mm, and aims to reconstruct tracks left by charged particles with $p_T > 1$ GeV passing through the detector in the $|\eta| < 4.0$ range.

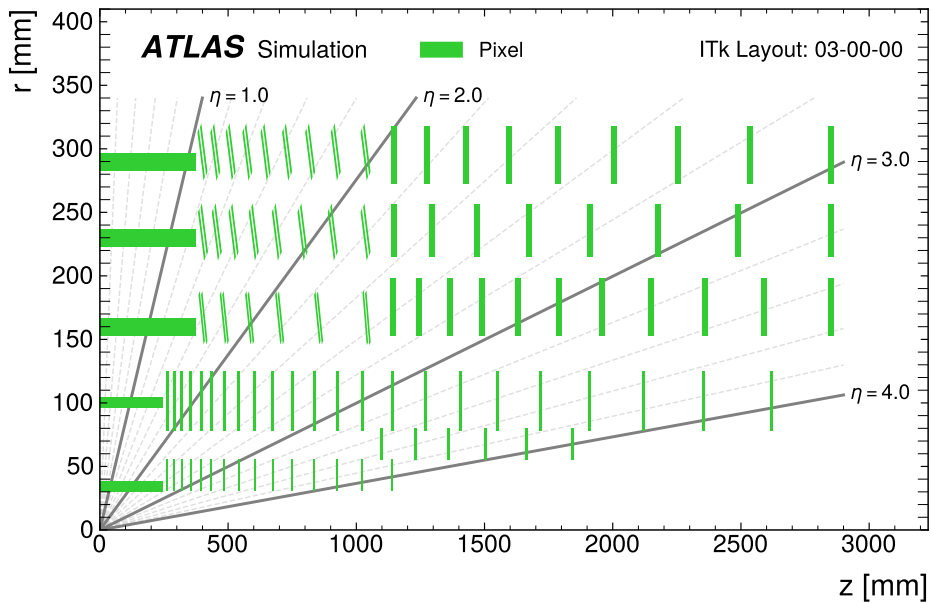
2.2 ITk layout

After the release of the technical design reports [9, 10], the detector design underwent additional refinement, as outlined in the following description. The resulting ITk layout is labeled as 03-00-00 and is presented in Figure 1.

¹ ATLAS uses a right-handed coordinate system with its origin at the nominal interaction point (IP) in the center of the detector and the z -axis along the beam pipe. The x -axis points from the IP to the center of the LHC ring, and the y -axis points upwards. Polar coordinates (r, ϕ) are used in the transverse plane, ϕ being the azimuthal angle around the z -axis. The pseudorapidity is defined in terms of the polar angle θ as $\eta = -\ln \tan(\theta/2)$ and is equal to the rapidity $y = \frac{1}{2} \ln \left(\frac{E+p_z}{E-p_z} \right)$ in the relativistic limit. Angular distance is measured in units of $\Delta R \equiv \sqrt{(\Delta y)^2 + (\Delta \phi)^2}$.



(a)



(b)

Figure 1: (a) A schematic depiction of the ITk Layout 03-00-00 as presented in this document. (b) A zoomed-in view of the pixel detector. In each case, only one quadrant and only active detector elements are shown. The horizontal axis is along the beam line with zero being the nominal interaction point. The vertical axis is the radius measured from the interaction point. Thicker lines in the flat barrel sections are due to their tilt in the ϕ -direction, while thicker lines in the endcap disks are due to their staggering along the z -direction, where z -positions vary between distinct values as a function of ϕ location.

Updates were made to the tilt angles in the azimuthal direction of the barrel strip modules in the first two layers, and the radius of the first layer was modified. These changes were implemented to ensure sufficient space during installation, while still maintaining ample overlap between the modules of adjacent staves for alignment purposes and hermeticity², as detailed in Table 1. Following the decision to incorporate the high-granularity timing detector (HGTD) [33] into the Phase-II upgrade of ATLAS, necessary adjustments were also made to the overall spatial dimensions of the ITk to accommodate the HGTD. Table 2 provides a summary of the resulting disk locations. The innermost pixel layer uses smaller modules based on 3D pixel sensor technology. These modules consist of a single active element with front-end (FE) read-out chips bump-bonded to the sensors and grouped in triplets. In contrast, all other layers use planar “quad” modules, where four FE chips are bump-bonded to the silicon sensor.

Table 1: Radius, extent in the z direction, tilt angle and strip length for the strip barrel in the ITk Layout 03-00-00. The number of staves reported are for the full barrel.

Barrel layer	Number of staves	Radius [mm]	$ z $ [mm]	Tilt angle [degrees]	Strip length [cm]
0	56	399	0 – 1372	13	2.5
1	80	562	0 – 1372	12	2.5
2	112	762	0 – 1372	12	5
3	144	1000	0 – 1372	11	5

Table 2: Position of disks of the strip endcap in the ITk Layout 03-00-00.

Disk	Radius [mm]	Position [mm]
0	385	1512
1	385	1702
2	385	1952
3	385	2237
4	385	2532
5	385	2850

A redesign of the pixel endcap ring system took into consideration the altered envelope along the z -axis and the need to provide space for service routing in the radial direction. To meet the latter requirement, adjustments were made to the radial extent of the support tube in the inner pixel barrel. The redesign of the inner two layers of the pixel system involved incorporating staves for the traditional barrel region, featuring “flat” modules parallel to the beam line, and replacing the former inclined section with coupled rings sharing the same support structure for the two layers. This change has the advantage of allowing the services to be routed to modules in the innermost pixel layer outward in the radial direction, thereby minimizing the material in the innermost part of the detector. The transition to coupled rings required a re-optimization of the ring locations in the previously inclined section to ensure hermeticity and an adequate number of predicted hits within the constraints of the new support structure.

A substantial redesign was also implemented in the three outermost layers of the barrel pixel system to help the incorporation of quad modules, each consisting of 2×2 readout chips, within the inclined section. These modules in the inclined sections are mounted on rings supported by a shell structure. The transition from the initially planned dual chip (2×1) to quad chip modules results in a 50% reduction in the total

² Hermeticity is the ability of the detector to provide complete coverage of the particle trajectories in all directions, without any gaps or regions where particles could potentially escape detection.

number of rings. This adjustment allows the entire ITk to be equipped with both single- and quad-chip modules, eliminating the necessity for dual-chip modules. Additionally, it contributes to a reduction in the length of the inclined outer barrel. The inclination angles of the modules in the $r - z$ plane were re-optimized in accordance with the new layout. Furthermore, the length of the flat section in the three outermost pixel barrel layers was shortened to accommodate nine quad modules.

One of the most recent and significant modifications pertains to the innermost pixel layer. Following an extensive technical review, the ATLAS Collaboration decided in early 2020 to adjust the ITk layout, bringing this layer closer to the beam line to enhance the tracking performance. Consequently, the radius of the barrel section for this pixel layer was reduced from 39 to 34 mm, and the innermost point of the endcap rings was shifted inward from 36 to 33.2 mm. The reduction in the radius of the barrel section allowed a decrease in the number of staves from 16 to 12, and a re-optimization of the number and position of endcap rings in the innermost pixel layers, maintaining hit coverage equivalent to the previous layout. Additionally, the pixel sensor dimensions for the innermost pixel layer in the barrel were adjusted to $25 \mu\text{m}$ in the transverse plane and $100 \mu\text{m}$ in the longitudinal plane, while the rest of the pixel detector uses the original $50 \times 50 \mu\text{m}^2$ pixels. While the innermost layer will suffer higher radiation damage with this smaller radius, the two innermost pixel layers are designed to be replaceable before the end of the HL-LHC data-taking.

The updated layout of the pixel barrel and endcaps is summarized in Tables 3 and 4. A display of the full ITk layout presented in this document is shown in Figures 2 and 3.

Table 3: Parameters for the pixel flat barrel and inclined rings in the ITk Layout 03-00-00. The number of sensors per row refers to a complete staff in the central, flat part of the barrel where sensors are placed parallel to the beam line. The number of inclined rings refers to both sides of the detector. “Triplets” consist of three connected read-out chips, each associated with a $2 \times 2 \text{ cm}^2$ sensor, while “quad” modules are made of four connected read-out chips associated with a single $4 \times 4 \text{ cm}^2$ sensor.

Barrel layer	Radius [mm]	Rows of sensors	Flat barrel $ z $ [mm]	Flat sensors per row	Incl. rings $ z $ [mm]	Incl. rings	Module type	Sensor dim. [μm^2]
0	34	12	0 – 245	24	–	–	triplets	25×100
1	99	20	0 – 245	12	–	–	quads	50×50
2	160	32	0 – 372	18	380 – 1035	2×6	quads	50×50
3	228	44	0 – 372	18	380 – 1035	2×8	quads	50×50
4	291	56	0 – 372	18	380 – 1035	2×9	quads	50×50

Table 4: Parameters for the pixel endcaps in the ITk Layout 03-00-00. The radii refer to the innermost point of the sensors on a ring. The number of rings refers to both sides of the detector. “Triplets” consist of three connected read-out chips, each associated with a $2 \times 2 \text{ cm}^2$ sensor, while “quad” modules are made of four connected read-out chips associated with a single $4 \times 4 \text{ cm}^2$ sensor.

Ring layer	Radius [mm]	$ z $ [mm]	Rings	Sensors per ring	Module type	Sensor dim. [μm^2]
0	33.20	263 – 1142	2×15	18	triplets	50×50
0.5	58.70	1103 – 1846	2×6	30	triplets	50×50
1	80.00	263 – 2621	2×23	20	quads	50×50
2	154.50	1145.5 – 2850	2×11	32	quads	50×50
3	214.55	1145.5 – 2850	2×8	44	quads	50×50
4	274.60	1145.5 – 2850	2×9	52	quads	50×50

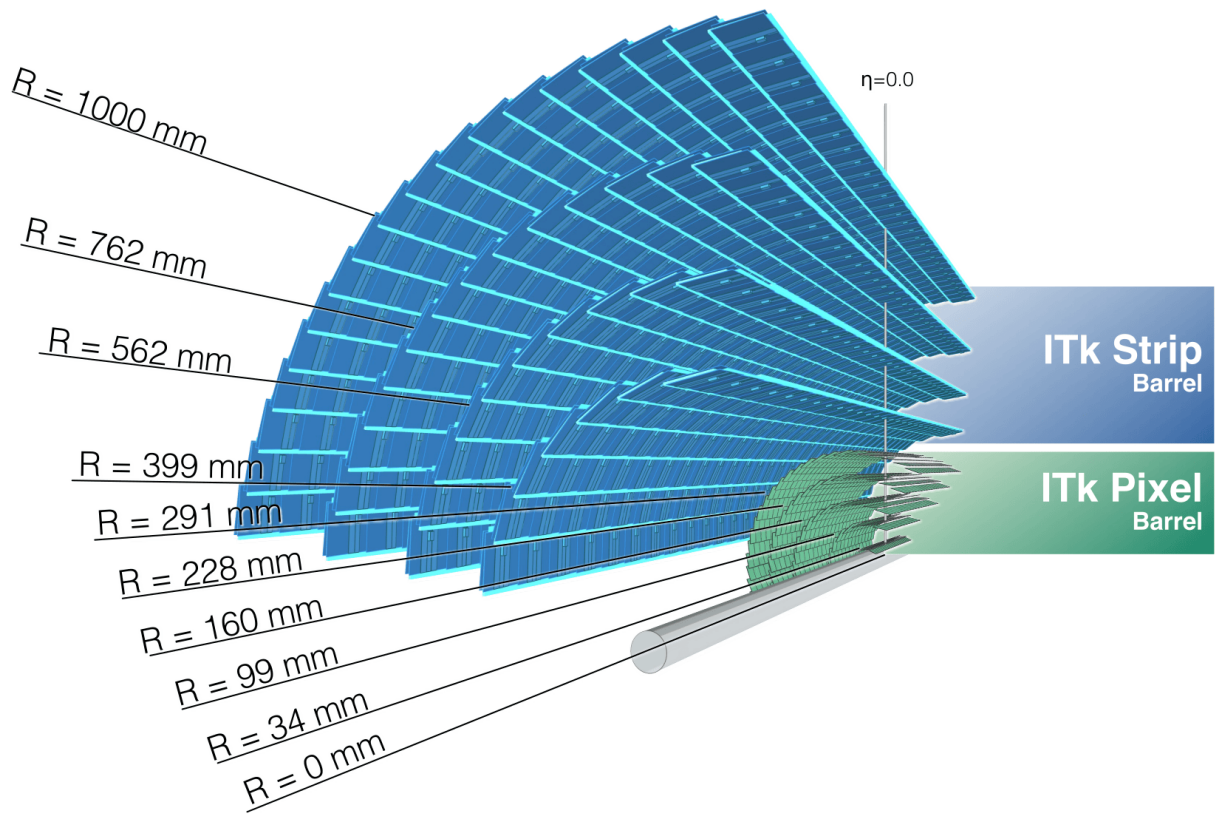


Figure 2: Transverse view of the Inner Tracker Layout 03-00-00 presented in this document.

Figure 4 depicts the overall count of expected pixel and strip measurements along a track depending on its pseudorapidity. The data are derived from simulated single-muon events with a transverse momentum of 1 GeV. Across the entire detector acceptance, a minimum of nine measurements is maintained, with rare exceptions occurring only in cases where tracks pass through the gaps between pixel or strip barrel modules, in particular for particles produced at $z = 0$ cm and $\eta \sim 0$. This feature is enhanced in Figure 4 given the generation of particles at $z = 0$ cm.

3 Simulation

3.1 Geometry description and material

A major effort has been put over the last years in a new implementation of the simulation of the ITk Pixel and Strip detectors using the ATLAS software suite [34]. This new implementation makes use of the GeoModel tool suite [35] and relies on atomic XML configuration files assembled to create the full detector. It benefits from a significantly improved clarity and long-term maintainability, the latter guaranteed by

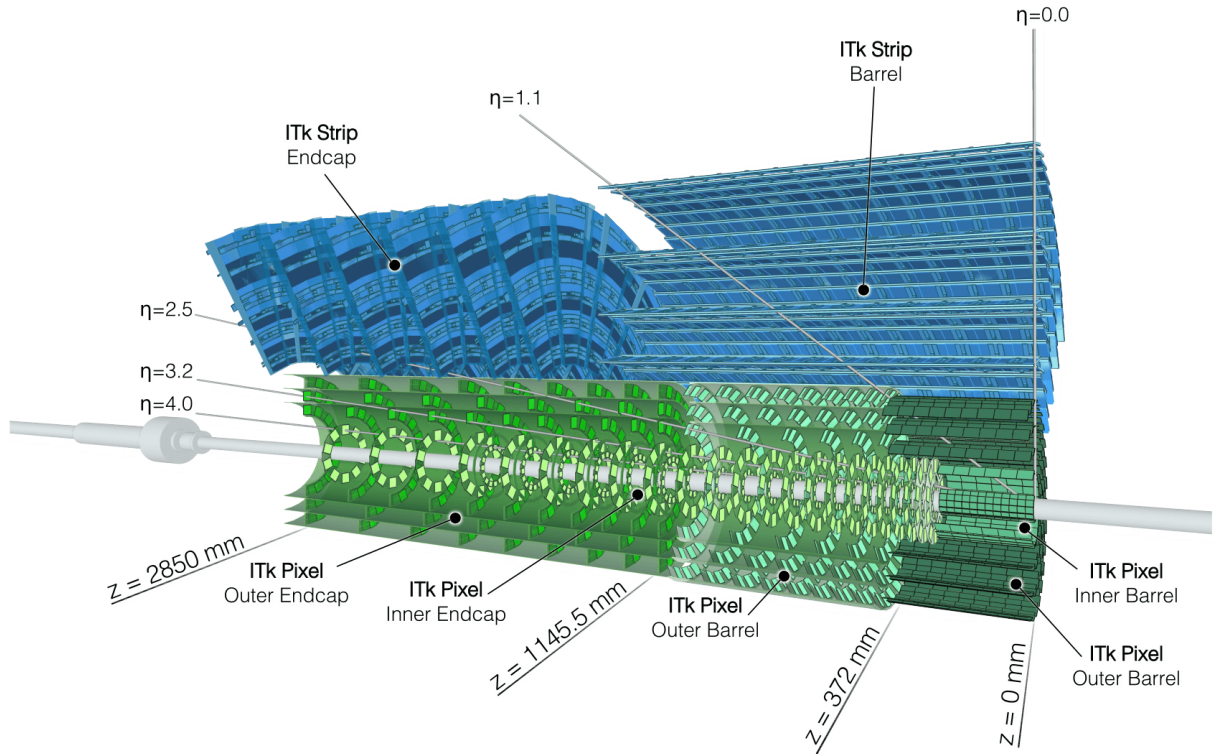


Figure 3: Longitudinal view of the Inner Tracker Layout 03-00-00 presented in this document.

the commitment of the ATLAS Collaboration to use the GeoModel library as the basis for its detector simulation for Run 4 and beyond [36].

Figures 5 and 6 present the integrated radiation length (X_0) and nuclear interaction length (Λ_0)³ traversed by a straight track as a function of the absolute pseudorapidity at the exit of the ITk volume. The position of the origin of those tracks follows the expected HL-LHC beam spot distribution. The mean radiation and interaction lengths traversed by particles before reaching the minimum number of hits required for track reconstruction (see Section 4.1) is shown in Figure 7. The material budget in the central region $|\eta| < 1.5$ demonstrates an increase of up to 50% relative to the Run 3 Inner Detector, while significant reductions in the material are present in the more forward region. The material location in the $r - z$ frame simulated for the studies presented here is illustrated in Figure 8.

³ The radiation length is defined as the average distance after which an electron's energy is decreased to $1/e$ of its initial value by material interactions, while the nuclear interaction length is defined as the mean distance between nuclear interactions sustained by a hadron.

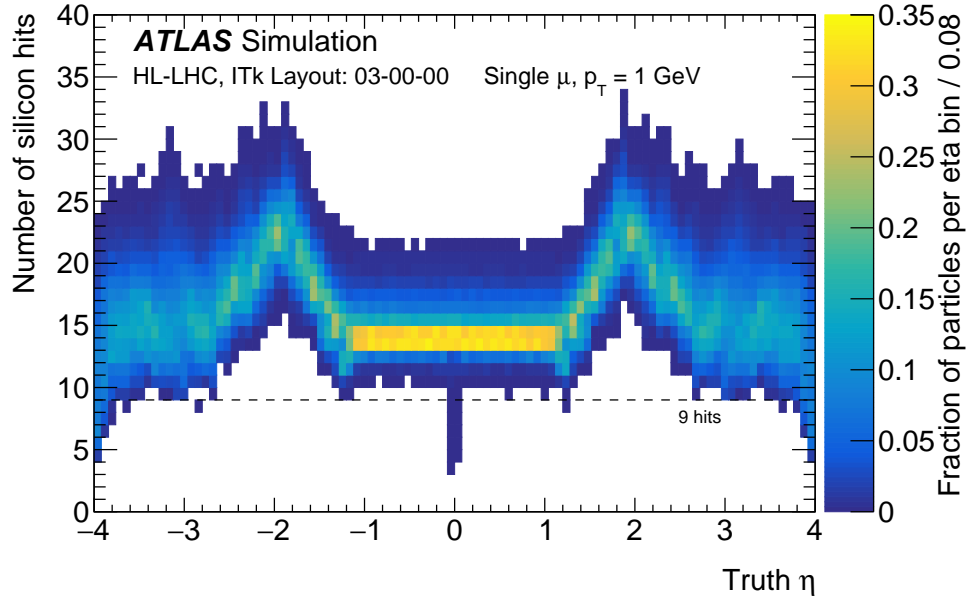


Figure 4: Number of combined potential strip and pixel measurements along a particle trajectory as a function of the truth particle pseudorapidity for the ITk Layout 03-00-00. A sample of single-muon events with $p_T = 1$ GeV is used. The muons are produced with a uniform distribution between 0 to 2 mm in transverse distance to the beam line and at fixed values of $z = -15$ cm, 0 cm, and 15 cm, in equal amounts.

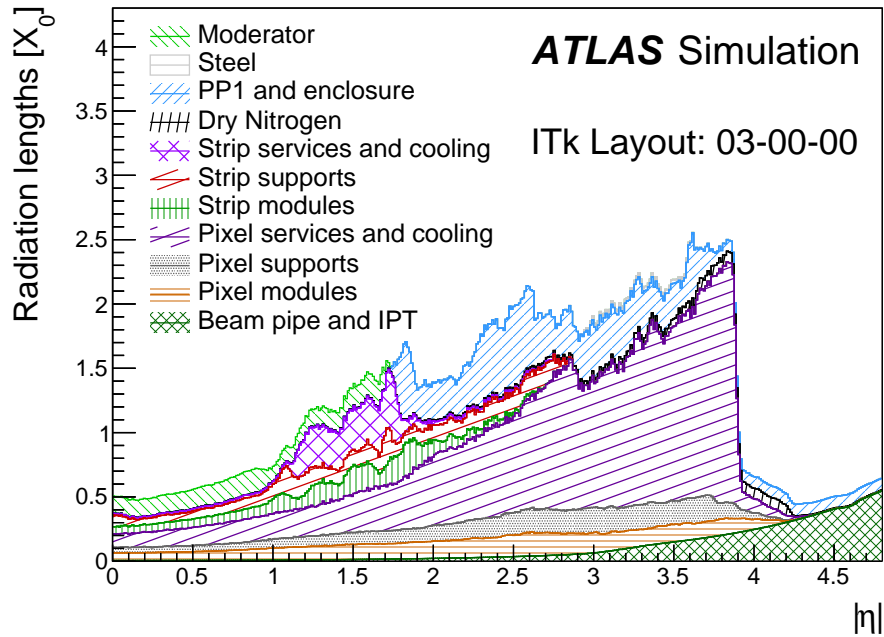


Figure 5: Integrated radiation length (X_0) traversed by a straight track as a function of the absolute pseudorapidity $|\eta|$ at the exit of the ITk volume for the ITk Layout 03-00-00, broken down by sub-system and material category. The Inner Positioning Tube (IPT) is a support carbon-fibre cylinder just outside the beam pipe. The Patch Panel 1 (PP1) is an interface located in the endcaps that facilitates power distribution, signal transmission, and optical conversion between the detector modules and external systems. The moderator is located beyond the active detector area.

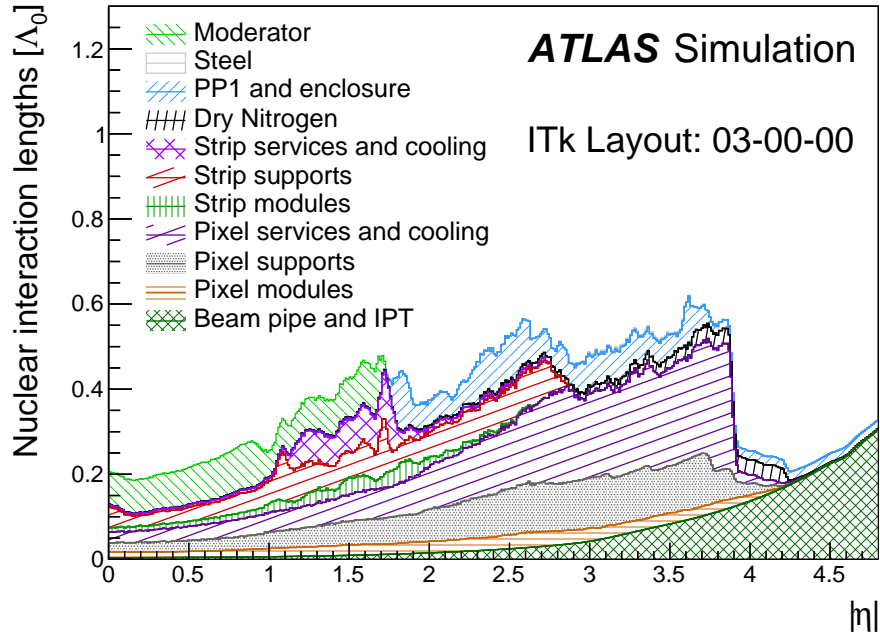


Figure 6: Integrated nuclear interaction length (Λ_0) traversed by a straight track as a function of the absolute pseudorapidity $|\eta|$ at the exit of the ITk volume for the ITk Layout 03-00-00, broken down by sub-system and material category. The Inner Positioning Tube (IPT) is a support carbon-fibre cylinder just outside the beam pipe. The Patch Panel 1 (PP1) is an interface located in the endcaps that facilitates power distribution, signal transmission, and optical conversion between the detector modules and external systems. The moderator is located beyond the active detector area.

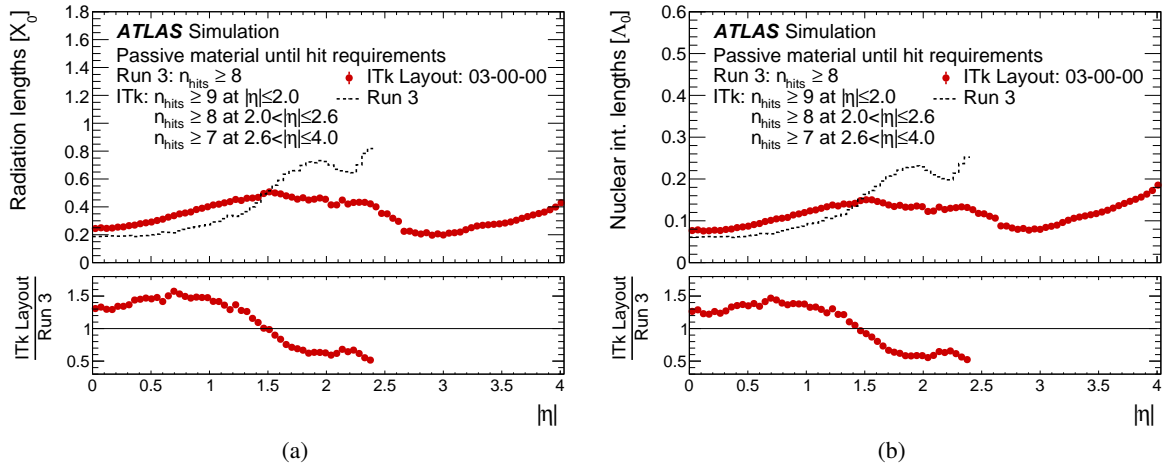


Figure 7: Material thickness in (a) radiation lengths (X_0) and (b) nuclear interaction lengths (Λ_0) seen by particles until reaching the minimum number of hits required for track reconstruction. The ITk detector is compared with the Run 3 detector.

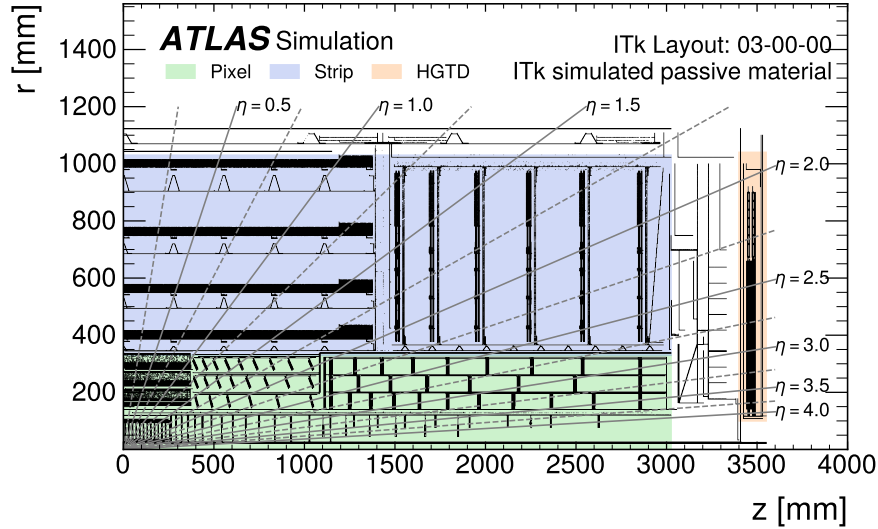


Figure 8: Location of the material for one quadrant of the ITk Layout 03-00-00.

3.2 Simulation samples

To evaluate the performance of the generic track reconstruction, single-particle (muon, electron and charged pion) samples are simulated with a uniform η distribution for $|\eta| < 4.0$ and a fixed transverse momentum of 2, 10, or 100 GeV. To replicate the expected HL-LHC beam spot dimensions and positions, the particle origin positions are generated based on a Gaussian distribution with a width of 50 mm centered at $z = 0$ in the longitudinal direction, while a width of $12 \mu\text{m}$ centered at $r = 0$ is used for the transverse direction.

In addition, a $t\bar{t}$ sample at $\sqrt{s} = 14$ TeV is simulated to assess the performance of the track and vertex reconstruction, with different average pile-up ranges from 50 to 70, 130 to 150, and 190 to 210, labeled respectively as $\langle\mu\rangle = 60, 140$ and 200 . For every simulated event, the number of pile-up interactions is randomly sampled from a Poisson distribution with a mean corresponding to the average pile-up. For comparison with the Run 3 detector performance, a $t\bar{t}$ sample at $\sqrt{s} = 13.6$ TeV produced with the Run 3 detector geometry and a uniform pile-up profile between 0 and 80 is used. The production of $t\bar{t}$ events is modeled using the POWHEG Box v2 [37–40] generator at next-to-leading-order in QCD with the NNPDF3.0NLO [41] parton distribution functions (PDF) and the h_{damp} parameter⁴ fixed to $1.5 m_{\text{top}}$ [42], with $m_{\text{top}} = 172.5$ GeV used for the top-quark mass. The events are interfaced to PYTHIA 8.230 [43] to model the parton shower, hadronization, and underlying event, with the A14 set of tuned parameters [44] and using the NNPDF2.3LO set of PDFs [45]. The decays of bottom and charm hadrons are performed by EVTGEN 1.6.0 [46]. Only $t\bar{t}$ events with a single leptonic W boson decay are considered. Minimum bias simulation samples are used in addition for specific studies, in which the average pile-up ranges are extended to cover the ranges 0 to 105, 95 to 175 and 165 to 210.

Finally, a sample of hypothetical Z' particles with a mass of $m_{Z'} = 4$ TeV decaying with roughly equal probabilities into b -, c -, and light-quark jets is used to study the tracking performance in the core of high- p_{T} jets. The sample is constructed so that the resulting jet p_{T} spectrum is roughly uniform up to

⁴ The h_{damp} parameter is a resummation damping factor and one of the parameters that controls the matching of POWHEG matrix elements to the parton shower and thus effectively regulates the high- p_{T} radiation against which the $t\bar{t}$ system recoils.

5 TeV. The Z' events are produced with the PYTHIA 8.307 [47] Monte Carlo generator, using the A14 set of tuned parameters and the NNPDF2.3_{LO} PDF set. The decay of heavy-flavor hadrons is handled by the EVTGEN 2.1.1 [46] package. No additional proton–proton interactions are included in this sample.

The simulated events are processed through the full ATLAS detector simulation [48] based on the GEANT4 toolkit [49].

3.3 Simulation of digitized readout signals

The energy depositions created by GEANT4 undergo a digitization process to mimic the behavior of detector electronics and produce the readout signals [7]. This involves utilizing the energy deposited during each GEANT4 step within the active silicon volume to calculate both the free charge and the drift time to the readout surface. These calculations take into account various parameters such as sensor thickness, carrier mobility, depletion and bias voltages, and effects due to the magnetic field such as the directional drift of electrons, known as the Lorentz shift. Additionally, the simulation accounts for contributions from noise and capacitive coupling to neighboring channels. The algorithm then assesses the amount of charge collected in each channel, and if it surpasses a predetermined threshold, the corresponding channel is labeled as having fired.

The Bichsel straggling function [50] is used to simulate realistic charge depositions for thin pixel sensors. Modules in the innermost layer of the barrel, equipped with pixels with a pitch of $25 \times 100 \mu\text{m}^2$, use a discriminator threshold of 900 e , while all other modules use a threshold of 600 e . Those thresholds are motivated by the expected behavior of the ITkPixV2 front-end chip to be used for the ITk Pixel detector [51]. When a pixel registers a charge exceeding the discriminator threshold, a 4-bit measurement of time-over-threshold (ToT) is emulated through a calibration function. This emulation results in an average ToT of seven bunch crossings for a charge of 10000 e . All hits with a charge surpassing the threshold are attributed to the specific bunch crossing associated with the particle that contributed the most to the charge. Noise is added to the charge from ionizing particles with a standard deviation of 75 e (100 e for the innermost barrel layer); however, random/thermal noise is not yet included in the modeling. The resolution of the charge measurement is in any case expected to be primarily influenced by the limited number of bits in the ToT measurement rather than the noise. In the innermost layer, 3D pixel sensors are approximated as planar sensors, with Lorentz effects disabled to mimic the 3D sensor designs.

4 Reconstruction

4.1 Track reconstruction and selection

The track reconstruction process⁵ begins by creating clusters from the individual channels within the strip and pixel subdetectors. In the case of the pixel detector, ToT information from each channel is accessible and is transformed into a representative charge measurement. The ToT-based calibration exploits the charge distribution within the cluster, enhancing the precision of the cluster position determination and its

⁵ This section describes the main tracking reconstruction pass, aiming to reconstruct prompt particles originating from the interaction point. In addition, there exist some specialized passes, for instance aiming to reconstruct tracks produced away from the interaction point (i.e., large-radius tracking), or a calorimeter-seeded back-tracking pass aiming to recover tracks from photon conversions. Describing such passes is outside the scope of this work.

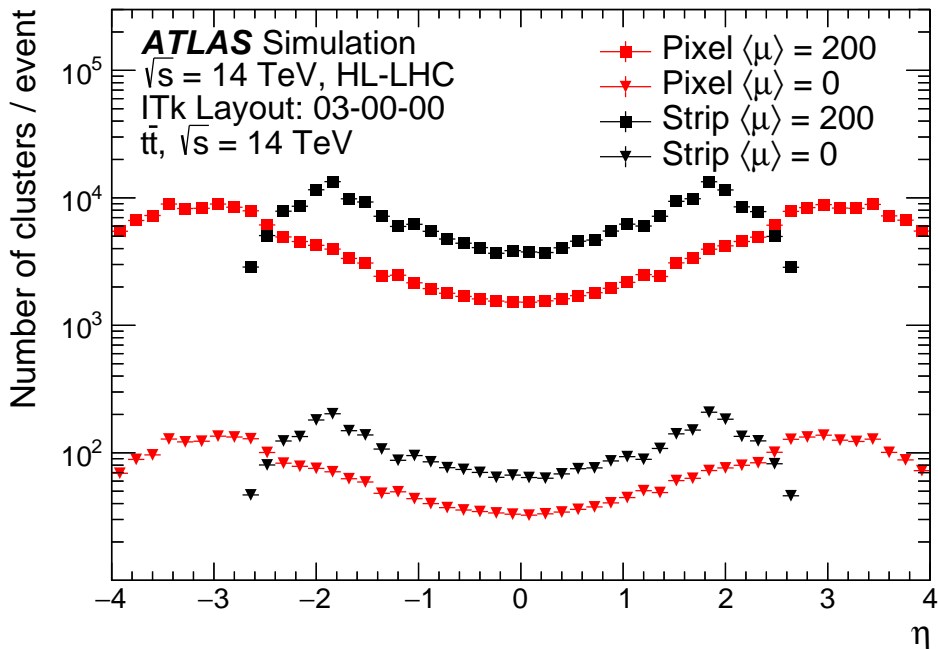


Figure 9: Distribution of the mean number of pixel and strip clusters vs η , at $\langle\mu\rangle = 0$ and $\langle\mu\rangle = 200$.

estimated uncertainty [52]. Additionally, the position estimate incorporates an assessment of the local incident angle of the track to further refine the cluster measurements. The distribution of pixel and strip clusters can be seen in Figure 9, showing a total occupancy of approximately 5×10^5 clusters per event at $\langle\mu\rangle = 200$.

Pixel and strip clusters are transformed into three-dimensional representations, referred to as space-points. Strip space-points are constructed combining clusters on opposite module sides, incorporating the relative stereo angle between the strips on the two sides and assuming that the track trajectory points to the interaction region.

Track finding starts with the track seeding stage [53], during which seeds are built from triplets of pixel or strip space-points compatible with a helical track model. These seeds define a search path, and a combinatorial Kalman filter (CKF) [24, 54] identifies track candidates compatible with the initial seed parameters, extending the seeds with additional space-points. In the CKF, the material interactions and noise contributions are approximated based on the number of detector layers crossed, rather than relying on detailed material and magnetic field description, which are used only in the final track fit. Seeds are skipped if they are constructed from clusters already associated with a track candidate. Two iterations of track finding are carried out sequentially, starting with strip seeds followed by pixel seeds, to enhance the overall track reconstruction efficiency. Strip seeding is performed first, as cluster density is lower in the outermost regions of the detector. This approach allows pixel clusters associated with a strip seed to be removed, reducing the number of possible pixel cluster combinations in the subsequent pixel seeding, which is computationally advantageous. Initially, a pion hypothesis is adopted to model the energy loss resulting from particle interactions with the detector material. If a track seed cannot be extended to form a complete track but aligns with an electromagnetic cluster detected in the calorimeter, the track finding algorithm is applied under an electron hypothesis. This electron hypothesis accommodates energy losses

of up to 30% due to bremsstrahlung during each interaction with a detector material layer.

In the final stage of track reconstruction, an ambiguity-solving algorithm is executed to determine the definitive assignment of clusters to competing tracks. During this stage, a precision fit is performed using a global χ^2 -minimization technique [55], incorporating precise data regarding the material model and magnetic field. Holes, defined as missing measurements on a track where active sensors should have registered hits, are assessed based on the track trajectory and information about the detector geometry and status. The tracks are ranked according to their hit count and the quality of their fit. Ambiguities between multiple track candidates are resolved by comparing their respective scores, and the track with the highest score is retained [23, 56].

In a high track density environment, such as the core of high- p_T jets, the separation between different charged particles is close to the detector granularity. In such cases, charge depositions from different particles can overlap and be reconstructed as single merged clusters. Tracks that share clusters are penalized in the ambiguity solver stage and they may consequently fail to satisfy the quality criteria and be rejected. The identification and special treatment of merged clusters is thus crucial for ensuring a high track reconstruction performance in dense environments, as it has a strong impact on the track reconstruction efficiency and the precision of the reconstructed track parameters. To optimize the tracking performance in this regime in Run 1, 2 and 3, ATLAS uses machine-learning-based algorithms dedicated to distinguishing clusters compatible with deposits from a single or multiple charged particles [57, 58]. This identification is performed only when a cluster is used by multiple tracks. The implementation and optimization of such algorithms for the ITk geometry is ongoing as of this writing, and an emulation of those algorithms based on particle-level information that reproduces the performance of the Run 3 machine-learning based algorithms is conservatively used in the meantime.

The accepted tracks must satisfy the η -dependent criteria outlined in Table 5. The criteria are made η -dependent to accommodate for the non-trivial detector layout, both in terms of number of sensitive elements and of distribution of the material as a function of η . They give in particular the possibility to maintain a uniform track reconstruction efficiency through the detector.

Table 5: Set of requirements applied during the track reconstruction in different pseudorapidity intervals. A hole is an intersection of the predicted trajectory of the particle with an active sensor element from which no measurement is assigned to the track (inactive sensors are not taken into account). The hole counting does not consider layers before the first and after the last hit. The longitudinal and transverse impact parameters, z_0 and d_0 , are defined relative to the mean position of the beam spot.

Requirements	Pseudorapidity interval		
	$ \eta \leq 2.0$	$2.0 < \eta \leq 2.6$	$2.6 < \eta \leq 4.0$
Pixel + strip hits	≥ 9	≥ 8	≥ 7
Pixel hits	≥ 1	≥ 1	≥ 1
Holes	≤ 2	≤ 2	≤ 2
p_T [MeV]	> 900	> 400	> 400
$ d_0 $ [mm]	< 2.0	< 2.0	< 10.0
$ z_0 $ [cm]	< 20.0	< 20.0	< 20.0

4.2 Vertex reconstruction and selection

To distinguish the different proton–proton collisions in a single bunch crossing, the reconstructed tracks are used to identify the position of the interactions along the beam axis. These are referred to as primary vertices (PVs). Typically, only a single pp interaction per recorded bunch crossing generates physics of interest for analysis. The corresponding PV is known as the *hard-scatter* vertex and is selected among all the reconstructed PVs. The position of the hard-scatter vertex is used for example as a reference for pile-up rejection, or in flavor-tagging algorithms.

Primary vertex reconstruction, both with the Run 3 Inner Detector and ITk, relies on the adaptive multi-vertex finder (AMVF) algorithm [59], which simultaneously reconstructs multiple vertices, allowing tracks to be associated with several vertices at the same time. The primary vertex finding process incorporates only a subset of the entire set of reconstructed tracks. In addition to the track selection criteria applied during reconstruction, the selections outlined in Table 6 are imposed to ensure reliable impact parameter estimates.

Table 6: Set of requirements applied to tracks during the AMVF vertex reconstruction, for the ID Run 3 and ITk Run 4 configurations. The uncertainties associated with d_0 and $z_0 \sin \theta$, $\sigma(d_0)$ and $\sigma(z_0 \sin \theta)$, are estimated from the global χ^2 fit used in the track reconstruction, taking into account individual hit position uncertainties.

Requirements	ID Run 3	ITk Run 4
Pixel hits	≥ 1	≥ 3
Pixel holes	≤ 1	≤ 1
SCT / Strip hits	≥ 4	≥ 0
Silicon hits	≥ 6	≥ 7
p_T [MeV]	> 500	> 900
$ d_0 $ [mm]	< 4.0	< 1.0
$\sigma(d_0)$ [mm]	< 5	< 0.35
$\sigma(z_0 \sin \theta)$ [mm]	< 10	< 2.5

The AMVF uses a vertex seed finder to identify potential vertex candidates along the beamline in the z -direction:

- Each track is represented by a Gaussian probability distribution $P(r, z)$ centered at its point of closest approach (d_0, z_0) . The track densities are summed to identify global maxima in track density, representing the initial seeds used to reconstruct vertices.
- Through an iterative process, a new vertex candidate, along with all tracks with z_0 agreeing with the vertex candidate within a 0.5 mm window, is added to the pool of vertex candidates managed by the adaptive Kalman filter multi-vertex fit.
- All vertices undergo a refitting process using the adaptive Kalman filter multi-vertex fit, where each track may contribute to multiple vertices. Tracks with a low adaptive weight in the fit, computed based on a χ^2 compatibility criterion with the vertex position described in Ref. [59], are eliminated from the fit of a specific vertex.
- The new vertex candidate is preserved if the vertex is identified with more than two tracks, the cumulative adaptive weights are not excessively low, and the new vertex is more than three standard deviations away from any other candidate.

- This procedure is reiterated until there are no more vertex candidates or the maximum number of iterations is reached.

Among all of the reconstructed vertices in each event, the one with the largest Σp_T^2 of its associated tracks, referred to as the hard-scatter vertex, is selected as the one of interest. This choice is motivated by the fact that pile-up events are dominated by soft QCD interactions.

5 Expected tracking and vertexing performance

5.1 Seeding performance

The performance of the seeding algorithm is assessed using different figures of merit that rely on associating seeds with stable charged particles produced by Monte Carlo simulation. A seed is considered matched with a particle if more than half of its measurements originate from this particle, and the fraction of particles matched to at least one seed is defined as the *physics* seeding efficiency.

The *technical* seeding efficiency represents the efficiency to find seeds for reconstructable particles, and is defined as the fraction of seed matches among particles providing at least three measurements in the detector. By construction, this efficiency does not depend on the detector material or on the layout hermeticity, allowing the isolation of the algorithmic seeding efficiency.

Figure 10 displays the physics seeding efficiency as a function of the particle η and p_T (labeled as “Truth η ” and “Truth p_T ”) in $t\bar{t}$ events with an average pile-up of 200, for particles from the hard-scatter event with p_T larger than 1 GeV. The technical and physics seeding efficiencies combining pixel and strip seeding are both displayed in Figure 11. The η -dependence of the seeding efficiency directly reflects the number of available measurements in the detectors, which can be inferred from the detector layout visible in Figure 1. An inclusive physics seeding efficiency larger than 85% is achieved over the whole phase space and reaches 95% or more for particles with p_T larger than 10 GeV. The lower efficiency at low p_T is related to material interactions, more likely to affect low- p_T particles. This affects strip seeds more significantly, as they are reconstructed after the particles have crossed a larger amount of material. The very high technical efficiency confirms that most of the physics inefficiency is indeed associated with material interactions.

While the pixel physics seeding efficiency is very close to the combined physics seeding efficiency, the strip seeds provide some useful redundancy in case of potential pixel detector defects. Figure 12 presents the number of seeds per particle as a function of η and p_T . On average, more than six seeds are found for all particles, as a particle typically leaves many hits in the detector, allowing for the construction of multiple triplets (seeds) from these hits. This abundance of seeds ensures the robustness of the seeding process against potential detector defects or misalignment.

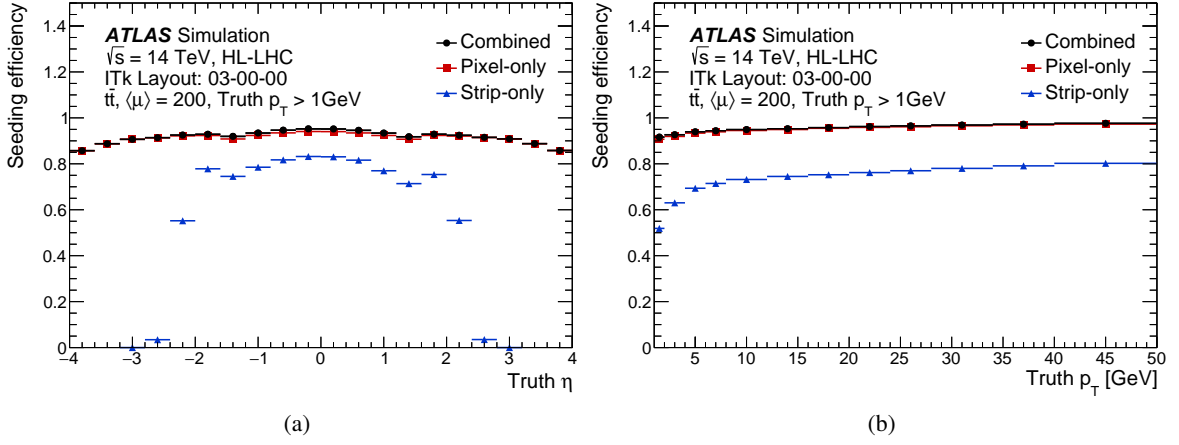


Figure 10: Expected physics seeding efficiency as a function of (a) η and (b) p_T for $t\bar{t}$ events at $\langle\mu\rangle = 200$ for hard-scatter particles with $p_T > 1$ GeV. The seeding efficiency is shown separately for pixel-only, strip-only and both combined.

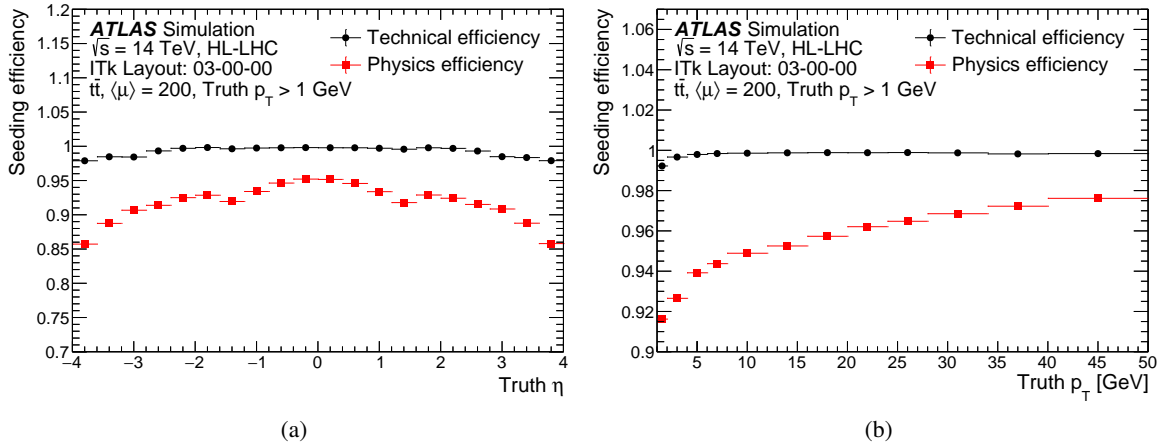


Figure 11: Expected technical and physics seeding efficiencies as a function of (a) η and (b) p_T for $t\bar{t}$ events at $\langle\mu\rangle = 200$ for hard-scatter particles with $p_T > 1$ GeV. The efficiency is shown for the combined pixel and strip seeding.

5.2 Efficiency

Similarly to seeds, two different definitions of the tracking efficiency are used to distinguish between pattern recognition effects and detector effects. The physics tracking efficiency is defined as the fraction of charged particles associated with a reconstructed track. To do the particle-to-track matching, information about individual particle contributions to a given simulated silicon hit is used. The matching criterion is based on the weighted fraction of measurements used to reconstruct a track common with the charged particle of interest, defined as

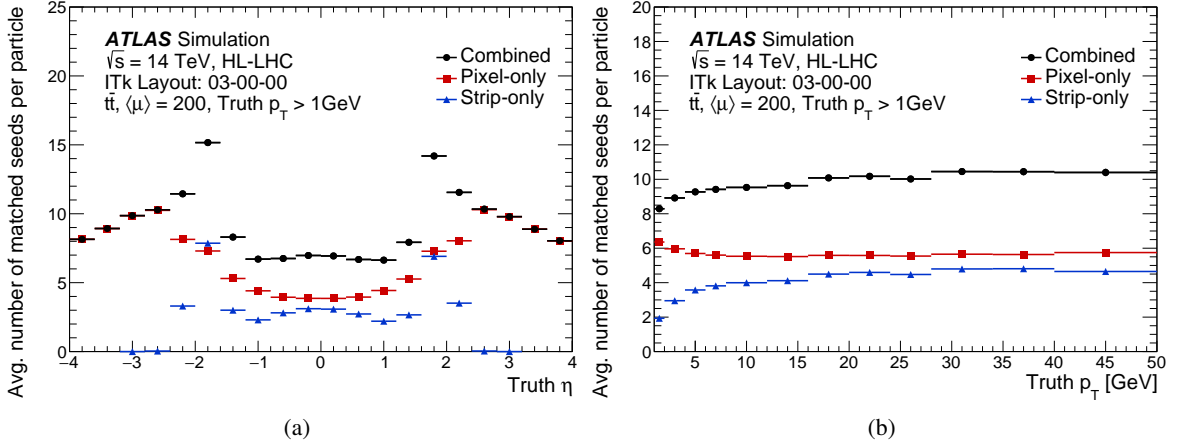


Figure 12: Expected number of seeds per particle as a function of (a) η and (b) p_T for $t\bar{t}$ events at $\langle\mu\rangle = 200$ for hard-scatter particles with $p_T > 1$ GeV, shown separately for pixel-only, strip-only and both combined.

$$R_{\text{match}} = \frac{2 \times N_{\text{common}}^{\text{pix}} + N_{\text{common}}^{\text{strip}}}{2 \times N_{\text{reco}}^{\text{pix}} + N_{\text{reco}}^{\text{strip}}}, \quad (1)$$

with $N_{\text{reco}}^{\text{pix/strip}}$ ($N_{\text{common}}^{\text{pix/strip}}$) representing the number of clusters from the different subdetectors used in the reconstruction of a given track (associated both to the particle and the reconstructed track). Since strip sensors are installed in back-to-back stereo pairs, a particle crossing a strip module will usually acquire two silicon hits, as opposed to a single hit per pixel module; the different weights therefore give equal importance to the two measurement types. A charged particle is considered to be reconstructed if it is matched to a track with $R_{\text{match}} > 0.5$.

The *technical* tracking efficiency represents the fraction of track matches among the charged particles providing enough measurements in the detector to satisfy the reconstruction cuts. It is used to assess the algorithmic efficiency of the tracking reconstruction and decouple it from the detector material or the layout hermeticity.

The physics tracking efficiency for muons with $p_T = 2, 10$ and 100 GeV without pile-up is presented in Figure 13. The expected efficiency is compatible with the one obtained with the ATLAS Run 3 detector. The efficiency is above 99.5% for 2 GeV muons and compatible with 100% for larger p_T up to $|\eta| = 3.6$. A small drop of efficiency down to 99% is present in the very forward region of the ITk detector, due to the smaller number of available measurements in that region. The physics tracking efficiency for 10 GeV muons, electrons and pions is shown in Figure 14. Although the tracking efficiency for electrons and pions is lower due to their higher interaction rate with the detector material, it is expected to remain above 85% for all types of prompt and stable charged particles. In the forward region ($|\eta| > 3.0$), Figure 7 illustrates a steeper increase in nuclear interaction lengths compared with radiation lengths. Consistent with these material distributions, the tracking efficiency for pions in this region is more significantly reduced than that for electrons.

Figure 15 emphasizes the expected tracking performance at $\langle\mu\rangle = 200$, showcasing the physics efficiency in $t\bar{t}$ events for particles with $p_T > 1$ GeV within the detector acceptance, stemming from the hard-scatter

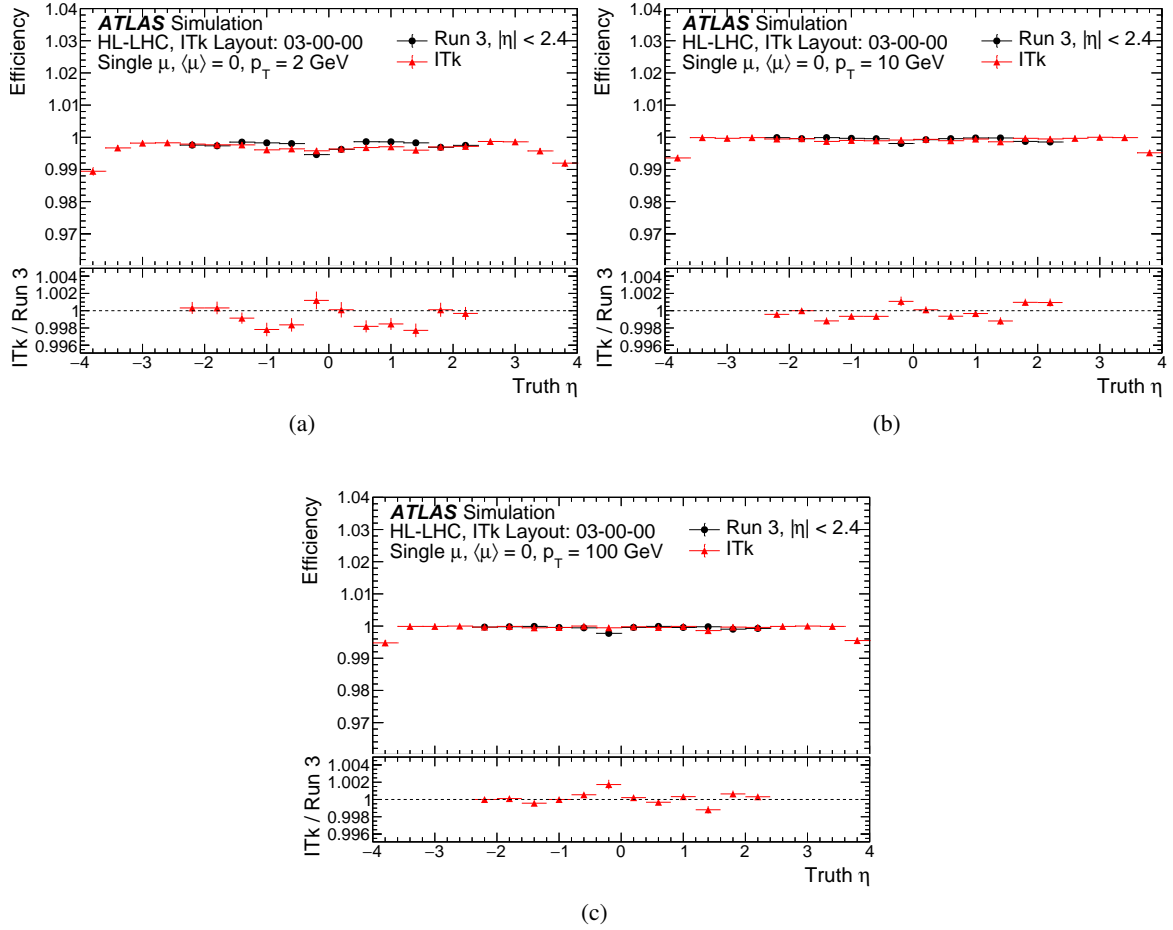


Figure 13: Expected physics tracking efficiency for single muons with (a) $p_T = 2$, (b) 10 and (c) 100 GeV without pile-up. The results are compared for muons between the ITk and the Run 3 detector.

interaction. A comparison is made between this efficiency and that obtained with the Run 3 detector, in conditions with a uniform $\langle\mu\rangle$ distribution between 0 and 80. The physics efficiency in the central region of the ITk detector is expected to be maintained within 5% of that of the Run 3 detector, despite the larger material budget of ITk discussed in Section 3.1. The efficiency achieved in the newly accessible forward region with $2.5 < |\eta| < 4.0$ is similar to the one achieved in the central region of ITk.

Figure 16 shows the technical tracking efficiency and the physics tracking efficiency for tracks from the hard-scatter interaction in $t\bar{t}$ events at $\langle\mu\rangle = 200$. The difference between the two quantities originates mainly from interactions of charged particles with detector material before reaching the required number of measurements.

The stability of the physics tracking efficiency at different pile-up conditions and in different $|\eta|$ ranges is shown in Figures 17 and 18. The efficiency at $\langle\mu\rangle = 200$ is within 0.5% of the efficiency achieved at $\langle\mu\rangle = 0$. A similar pile-up robustness is observed in the different $|\eta|$ ranges considered.

In the following, the performance of track reconstruction within jets is shown for a $Z'(m = 4 \text{ TeV})$ Monte Carlo sample, where the rate of cluster merging is much higher than in $t\bar{t}$ events due to the larger fraction

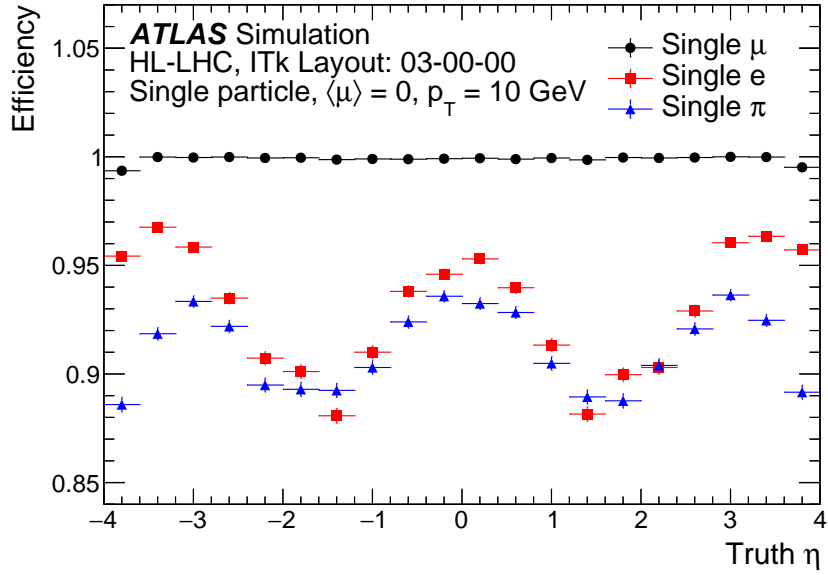


Figure 14: Expected physics tracking efficiency for single muons, electrons and pions with $p_T = 10$ GeV without pile-up.

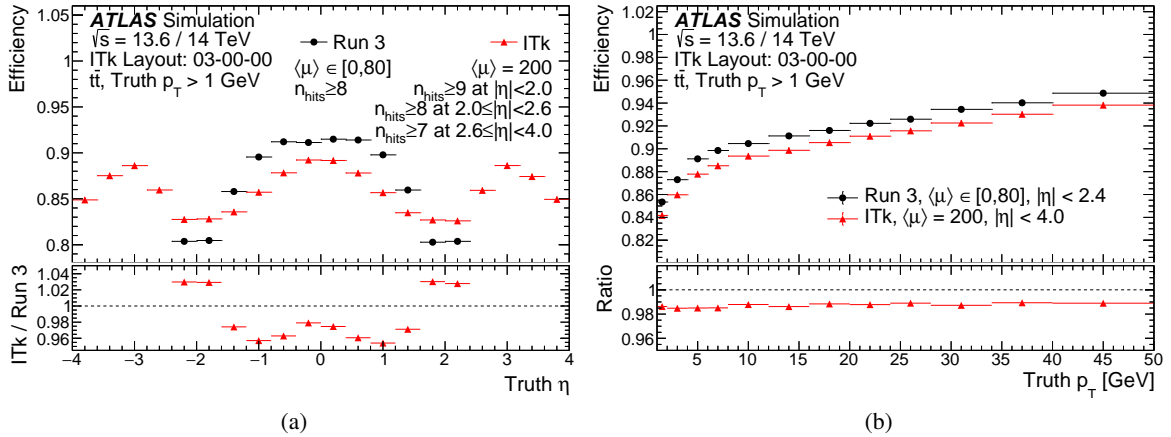


Figure 15: Expected physics tracking efficiency as a function of (a) η and (b) p_T in $t\bar{t}$ events at $\langle\mu\rangle = 200$ for hard-scatter particles with $p_T > 1$ GeV with the ITk detector compared with the Run 3 detector, in conditions with a uniform $\langle\mu\rangle$ distribution between 0 and 80.

of high- p_T jets. For the studies presented here, jets are reconstructed by clustering energy deposits in the calorimeter with the anti- k_r algorithm [60] with a radius parameter $R = 0.4$, implemented in FASTJET [61]. Tracks are matched to jets based on their angular separation $\Delta R(\text{track}, \text{jet})$ from the jet axis, required to be lower than 0.4. To isolate the effects correlated with dense hadronic environments from those due to interactions with the detector material, the efficiency is presented for jets with $|\eta| < 1.2$, in the central region where the material budget is the lowest, and for particles with $p_T > 10$ GeV, less impacted by material effects.

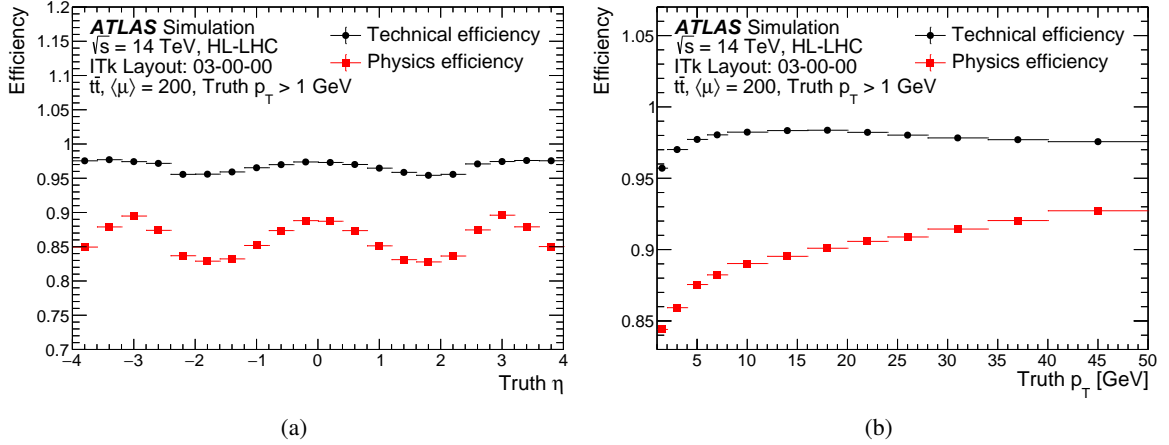


Figure 16: Comparison between the expected technical and physics tracking efficiencies as a function of (a) η and (b) p_T in $t\bar{t}$ events at $\langle\mu\rangle = 200$ for hard-scatter particles with $p_T > 1$ GeV with the ITk detector.

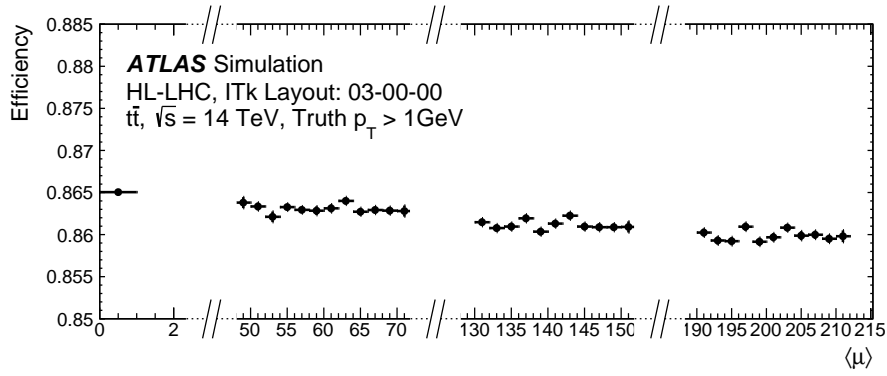


Figure 17: Expected physics tracking efficiency as a function of pile-up in $t\bar{t}$ events for hard-scatter particles with $p_T > 1$ GeV with the ITk detector.

Figure 19(a) highlights the physics tracking efficiency expected for charged particles within high- p_T jets when no dedicated merged cluster identification is used. Tracks located in the core of the jets have on average a larger p_T , which explains why the efficiency is higher in the core of jets for a jet p_T up to 700 GeV. On the other hand, the particle density increases with the jet p_T , inducing a decrease in the physics tracking efficiency. This effect is more pronounced in the core of the jets where the particle density is highest. The potential benefit from a dedicated algorithm used for identifying merged clusters is shown in figure 19(b), which compares the performance obtained when no merged pixel cluster identification or when a perfect truth-based identification is used. To optimize the tracking performance in high track-density environments, ATLAS uses a machine-learning-based merged pixel cluster identification algorithm [57, 58] that has not yet been adapted for use in Run 4. The commissioning of dedicated algorithms for the ITk pixel detector will be one of the main focuses of upcoming developments.

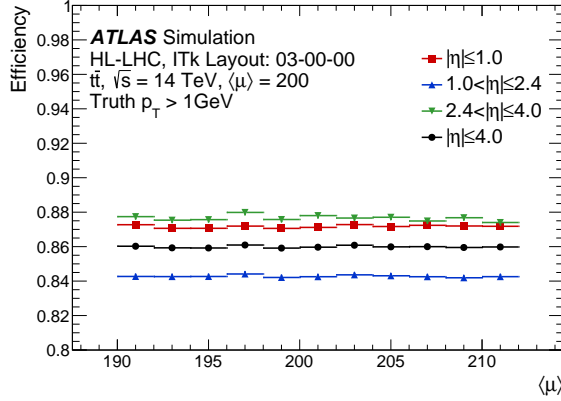


Figure 18: Expected physics tracking efficiency as a function of pile-up in $t\bar{t}$ events at $\langle\mu\rangle = 200$ for hard-scatter particles with $p_T > 1$ GeV with the ITk detector in different $|\eta|$ ranges.

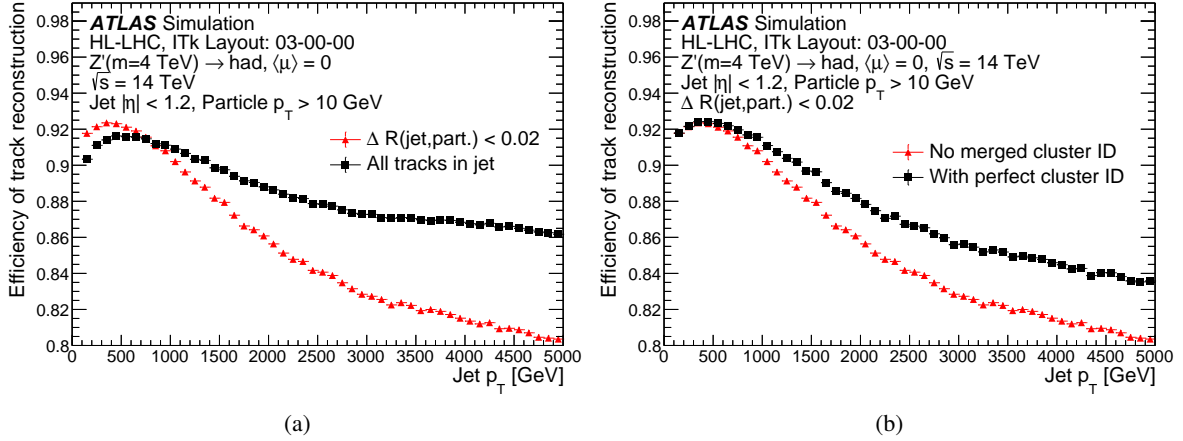


Figure 19: Physics tracking efficiency for tracks in jets as a function of the jet p_T in Z' events in which the Z' decays hadronically, comparing (a) the inclusive efficiency for all tracks matched to the jet ($\Delta R < 0.4$) or within the jet core ($\Delta R < 0.02$) and (b) reconstruction scenarios with perfect, or no, classification of merged clusters in the jet core.

5.3 Number of tracks, mis-reconstructed and fake track rates

Figure 20 illustrates the count of reconstructed tracks with $p_T > 1$ GeV at $\langle\mu\rangle = 200$ in $t\bar{t}$ events. In the ideal case where all tracks are well-reconstructed and the tracking efficiency is not reduced with pile-up, a linear increase in the number of tracks as a function of the number of interactions⁶ is expected. In reality, a small quadratic component is observed in the number of reconstructed tracks as a function of the number of interactions, caused for instance by a certain fraction of particles that would not be reconstructed due to the minimum number of hits requirement (c.f. Table 5) but which are assigned to tracks also containing mis-attributed hits from pile-up particles, allowing them to satisfy the reconstruction criteria. There also exist a small fraction of tracks arising from combinations of hits not closely corresponding to any charged particle, known as fake tracks. Tracks from either source are collectively referred to as mis-reconstructed

⁶ The number of interactions follows a Poisson distribution with mean $\langle\mu\rangle$.

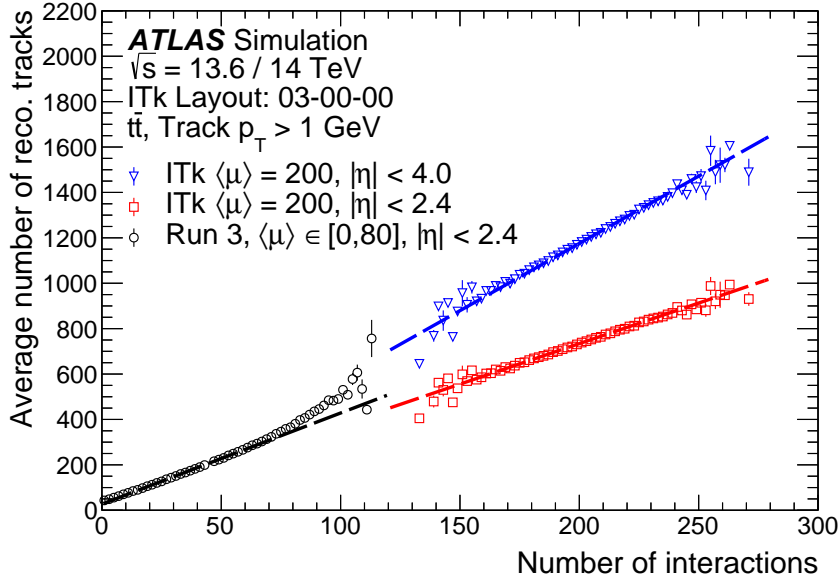


Figure 20: Number of reconstructed tracks per event with $p_T > 1 \text{ GeV}$ as a function of the number of interactions for $t\bar{t}$ events at $\langle\mu\rangle = 200$ with the ITk detector compared with the Run 3 detector, in conditions with a uniform $\langle\mu\rangle$ distribution between 0 and 80. The dashed lines illustrate the results of linear fits performed over the limited range corresponding to $\langle\mu\rangle$ between 120 and 280 for the ITk and between 20 and 60 (extrapolated to 0–120) for the Run 3 detector to illustrate the pile-up dependence of this quantity.

tracks, and their number is expected to scale super-linearly with the number of interactions. The number of well-reconstructed tracks as a function of the number of interactions can be estimated by fitting a linear function to the number of tracks distribution in the low pile-up regime, where the number of fake and mis-reconstructed tracks is expected to be negligible. The slope of this linear fit is then reduced linearly as a function of μ , to take into account the relative efficiency reduction of up to 0.7% at $\langle\mu\rangle = 200$. On the other hand, the total number of reconstructed tracks as a function of the number of interactions follows a quadratic function; therefore the fraction of mis-reconstructed tracks can be estimated from the difference between a quadratic fit to the number of tracks distribution and this linear fit, extrapolated to the full pile-up range. This fraction, shown in Figure 21 for a minimum bias sample, reaches at most 2% at $\langle\mu\rangle = 200$. As a comparison, in Run 3 the mis-reconstructed track rate at the typical Run 3 leveling target of $\langle\mu\rangle = 64$ is approximately 6.5%. This reduction in the rate of mis-reconstructed tracks is primarily due to the optimized layout of the ITk detector, which provides in particular a greater number of silicon hits. These additional hits enhance the track reconstruction precision by enabling tighter selection criteria. The expected fake track creation rate can be estimated from Monte Carlo simulation, using the same matching probability distribution used to calculate the tracking efficiency. Figure 22 shows the expected fraction of tracks with a matching probability lower than 50% and features an expected fake track creation rate of approximately 3×10^{-4} at $\mu = 200$, showcasing the excellent fake track suppression capabilities of the ITk. Moreover, a comparison with Figure 21 shows that fake tracks are not expected to be a dominant source of mis-reconstructed tracks.

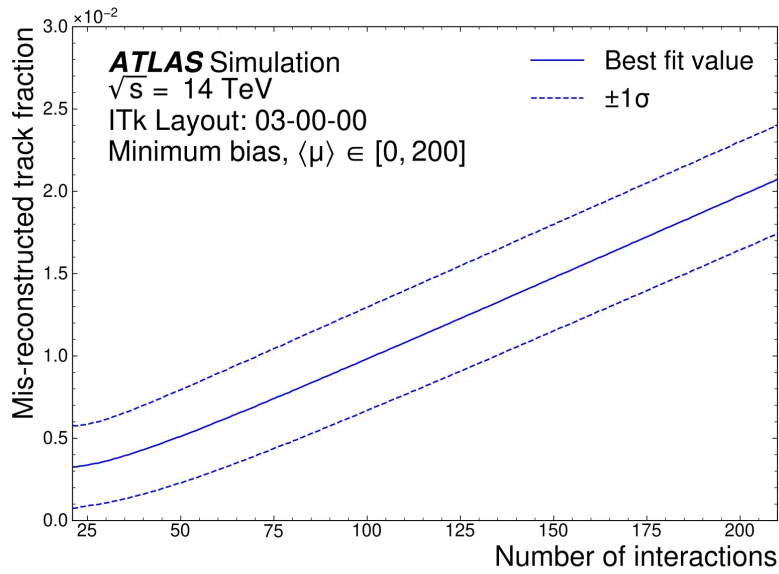


Figure 21: Fraction of mis-reconstructed tracks, defined as the difference between a quadratic fit in the full μ range and a linear fit extrapolated from the $\mu < 20$ region. The number of tracks corresponding to real particles and containing enough hits to satisfy the reconstruction criteria is expected to scale linearly with pile-up. The mis-reconstructed track population is composed of fake tracks not corresponding to any particle and tracks corresponding to actual particles but that include mis-attributed hits from pile-up particles, and is expected to increase faster than linearly with pile-up.

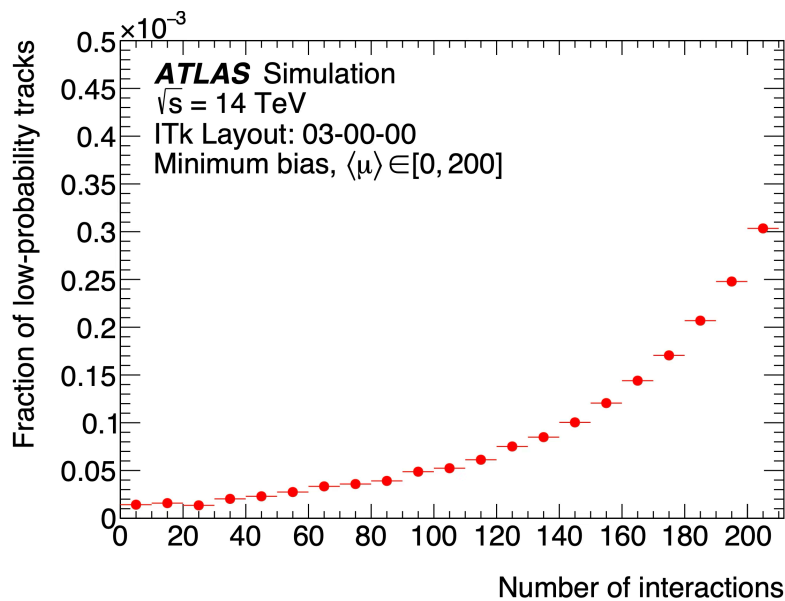


Figure 22: Fraction of all tracks with matching probability less than 50% as computed in Monte Carlo simulation, which estimates the fraction of tracks not closely corresponding to a charged particle, also known as the fake track creation rate.

5.4 Track parameter resolution

The resolution on track parameters is estimated from reconstructed tracks associated with charged particles. The distribution of the difference between the reconstructed track parameter and the corresponding quantity for the simulated particle is iteratively truncated from its outliers, which lie more than three standard deviations away from the mean of the distributions, until the distribution is left invariant. Up to 5% (1%) of the tracks associated with muons with $p_T = 2$ GeV (100 GeV) are found to be outliers in the process. The standard deviation of the core distribution is defined as the intrinsic measurement resolution of the track parameters.

Figures 23 to 25 display the expected resolution on the transverse (d_0) and longitudinal (z_0) impact parameters and the transverse momentum for simulated muons with $p_T = 2$ and 100 GeV, compared between the ITk and the Run 3 ATLAS detector. The slight worsening of the z_0 resolution observed near $\eta = 0$ in Figure 24 is associated with the fact that position measurements from the pixel detector are calibrated taking into account the charge distribution within the cluster and the angle of incidence of the track. As particles with $\eta \sim 0$ typically create one-pixel-wide clusters with normal incident angles, there is therefore no information to be exploited to improve the position resolution in such cases. Due to the comparable radius of the innermost pixel layers and thanks to the smaller pixel pitch (25×100 or $50 \times 50 \mu\text{m}^2$ for ITk, $50 \times 250 \mu\text{m}^2$ for the Run 3 detector [62, 63]), the d_0 resolution is improved by up to 20% and the z_0 resolution by up to a factor of two with ITk for 2 GeV muons, mainly in the central part of the detector where the material budget is minimal. This advantage is even more pronounced for 100 GeV muons, which are less affected by multiple scatterings from material. In this case, the d_0 and z_0 resolutions are significantly improved, by a factor of up to two and four respectively. The transverse momentum resolution with ITk is expected to surpass the Run 3 resolution due to the superior resolution in the bending plane provided by the silicon microstrip sensors in ITk compared with the straw tubes in the Run 3 detector. While the transverse momentum resolution in the forward region appears relatively poor for 100 GeV muons, the rate of such muons in that region of the detector is expected to be extremely low, since they correspond to forward muons with an energy of around 3 TeV.

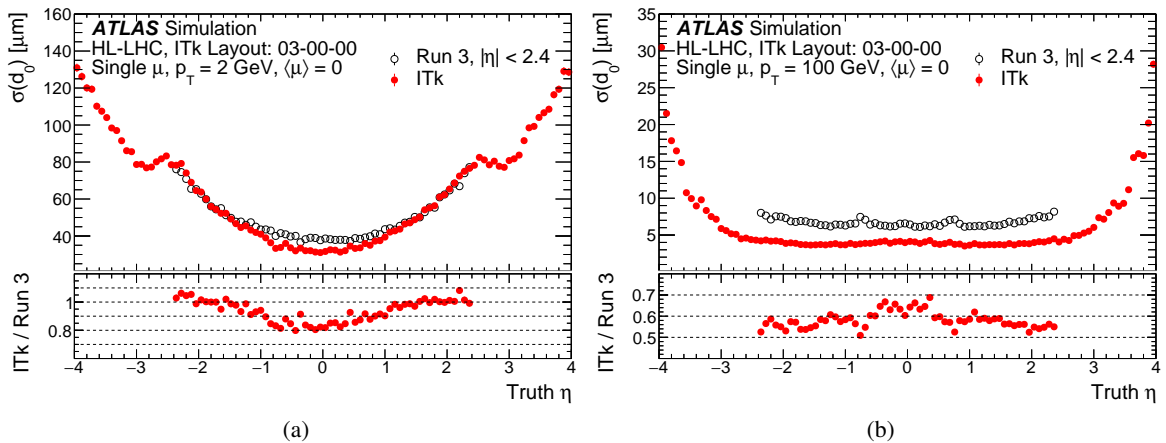


Figure 23: Transverse impact parameter (d_0) resolution as a function of η for (a) 2 GeV and (b) 100 GeV muons without pile-up, compared between the ITk and the Run 3 detector.

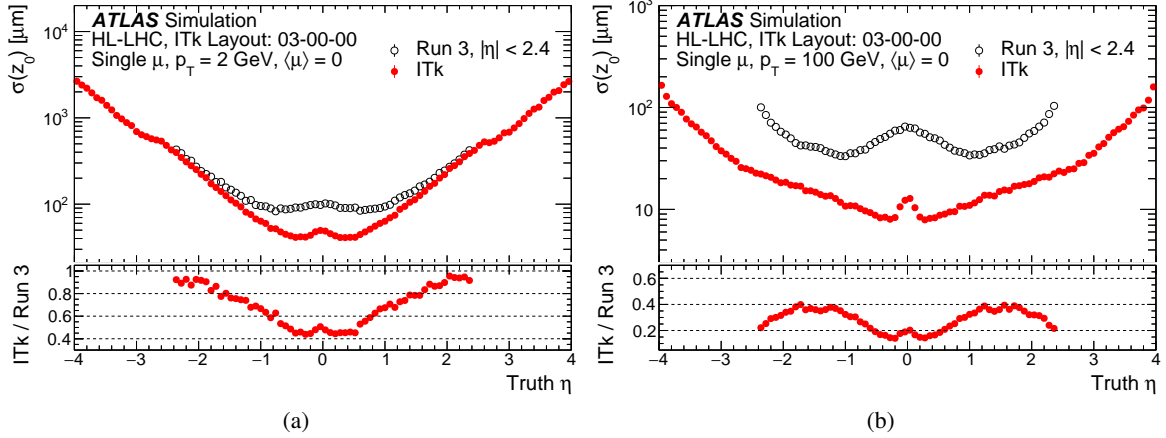


Figure 24: Longitudinal impact parameter (z_0) resolution as a function of η for (a) 2 GeV and (b) 100 GeV muons without pile-up, compared between the ITk and the Run 3 detector.

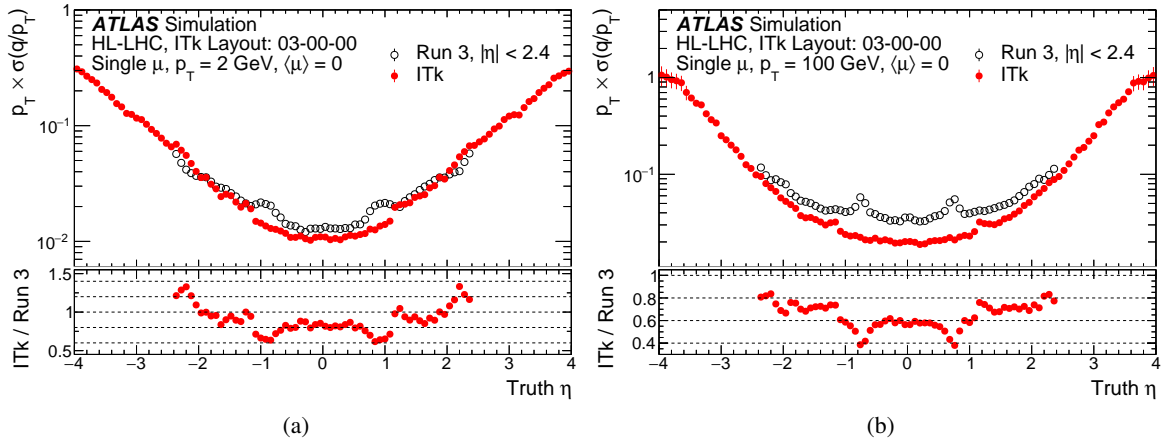


Figure 25: Relative transverse momentum resolution as a function of η for (a) 2 GeV and (b) 100 GeV muons without pile-up, compared between the ITk and the Run 3 detector.

5.5 Primary vertex reconstruction and identification

The local pile-up density is defined as the number of proton–proton interactions within a 4 mm window around the true hard-scatter vertex, normalized by this distance. In Figure 26(a), the local pile-up density under HL-LHC conditions with $\langle \mu \rangle$ of 200 is shown, in comparison to the one used in the Run 3 sample. Figure 26(b) exhibits the efficiency of the hard-scatter vertex reconstruction, described in Section 4.2, denoting the fraction of events in which a vertex is reconstructed within 0.1 mm of the true hard-scatter position along the longitudinal direction. The figure underscores the resilient performance achieved even under the highest expected pile-up density in HL-LHC conditions.

Another relevant metric is the selection efficiency of the signal hard-scatter vertex, defined as the reconstructed primary vertex that has the largest number of tracks matched to true particles originating from the simulated hard-scatter interaction. The combined reconstruction and selection efficiency, i.e.,

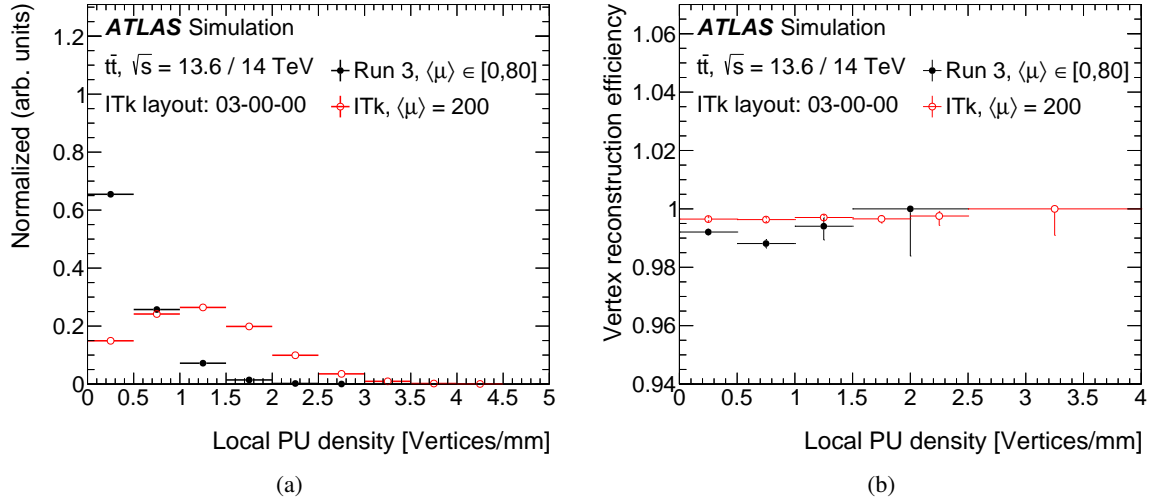


Figure 26: (a) Distribution of the number of local pile-up density around the hard-scatter vertex, evaluated in $t\bar{t}$ events with $\langle\mu\rangle = 200$ in the ITk sample and with a uniform pile-up profile between 0 and 80 in the Run 3 sample. (b) Primary vertex reconstruction efficiency evaluated in $t\bar{t}$ events with $\langle\mu\rangle = 200$ as a function of the local pile-up density around the hard-scatter vertex. For comparison, the performance obtained with the Run 3 ATLAS detector with a uniform pile-up profile between 0 and 80 is also shown.

the fraction of events in which the hard-scatter vertex is reconstructed and selected as the highest Σp_T^2 primary vertex, is expected to be influenced by various factors. The highest- Σp_T^2 vertex is chosen as the vertex of interest, but this choice may be compromised if the hard-scatter vertex is split into multiple reconstructed vertices due to nearby pile-up vertices. This effect is expected to be primarily correlated with the local pile-up density, and the efficiency is demonstrated to be highly robust against this variable in Figure 27(a).

True pile-up vertices may also be merged into a single reconstructed vertex, increasing its associated Σp_T^2 . Finally, there is a small probability for a pile-up interaction to genuinely yield a larger Σp_T^2 than the simulated hard-scatter process, even with a perfect vertex reconstruction algorithm. These effects are expected to be largely correlated with the number of interactions. Figure 27(b) displays the combined reconstruction and selection efficiency as a function of this variable. The efficiency is expected to be reduced down to 92% on average at a pile-up of 200.

The longitudinal position resolution obtained with the ITk detector is presented in Figure 28 and exhibits a strong robustness against pile-up, being maintained at about $10 \mu\text{m}$ up to high pile-up density, improving by more than a factor of two the performance of the Run 3 detector. Strongly correlated with the improved track parameter resolution, this feature is thus expected to greatly benefit pile-up rejection in jets, hadronic τ reconstruction, lepton isolation, and flavor-tagging algorithms.

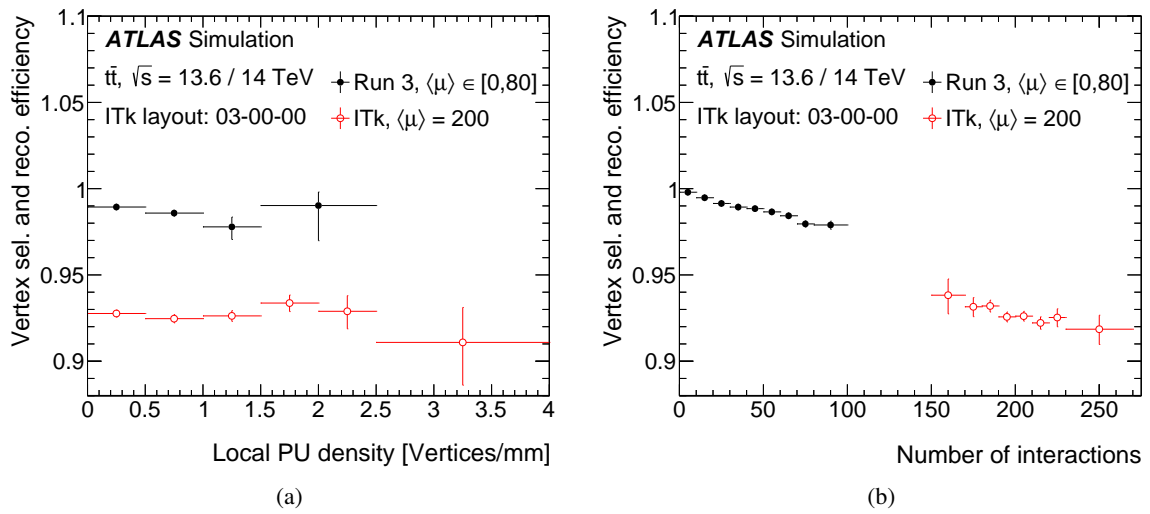


Figure 27: Primary vertex combined reconstruction and selection efficiency evaluated in $t\bar{t}$ events with $\langle\mu\rangle = 200$. The efficiency is presented as a function of (a) the local pile-up density around the hard-scatter vertex and (b) the number of interactions. For comparison, the performance obtained with the Run 3 ATLAS detector with a uniform pile-up profile between 0 and 80 is also shown.

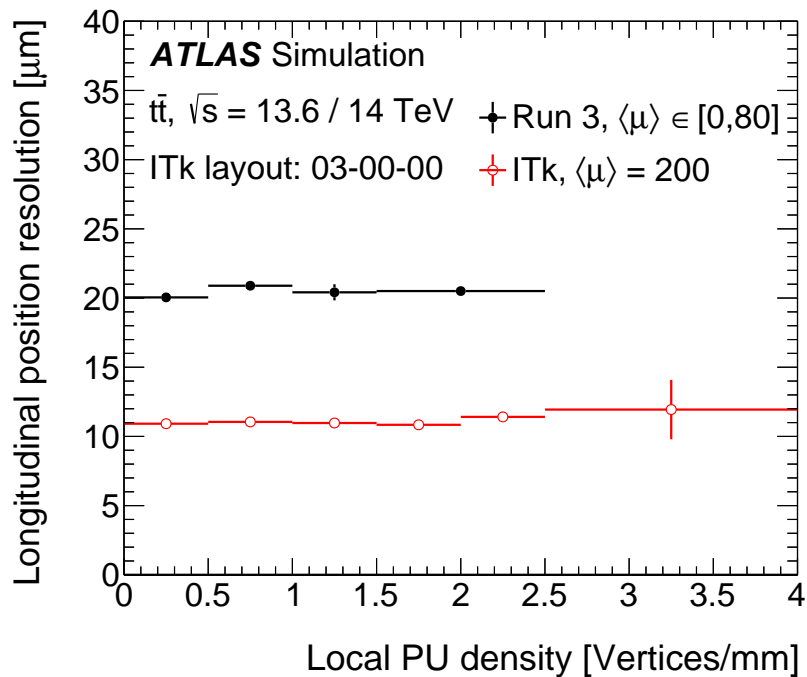


Figure 28: Longitudinal position resolution of the reconstructed primary vertex, evaluated in $t\bar{t}$ events with $\langle\mu\rangle = 200$. For comparison, the performance obtained with the Run 3 ATLAS detector with a uniform pile-up profile between 0 and 80 is also shown.

6 Conclusion

This paper presents the state-of-the-art tracking performance expected with the ITk detector during the high-luminosity LHC operation phase. The combination between the ITk design and the ATLAS tracking software is expected to perform to a high standard in very challenging high pile-up conditions. The track seeding performance exploits in particular the large multiplicity of high-precision silicon measurements to guarantee a high efficiency and redundancy, offering a strong robustness against detector misalignment or sensor defects. The full tracking efficiency is found to reach levels similar to Run 3, while the multiple high-precision silicon measurements on each track enables a quasi-linear scaling of the track multiplicity with pile-up, indicating much lower numbers of fake tracks expected than in Run 3 despite the increased pile-up expected at high luminosity. The resolution on track parameters, critical for the flavor-tagging and pile-up rejection performances, are significantly improved relative to the Run 3 detector thanks to the smaller pixel pitch used in the ITk. The tracking performance in the forward region with $2.4 < |\eta| < 4.0$, which will be newly covered by the ITk, is also shown to reach very high standards, compatible with the requirements expected from high-level object reconstruction and identification algorithms. The vertex position resolution is also improved relative to the Run 3 performance, while the vertex reconstruction and selection efficiency shows a very strong robustness against pile-up. Finally, the tracking performance is found to be degraded in the core of high- p_T jets due to the presence of merged charge clusters, and mitigation techniques inspired by the ones used with the Run 3 detector will have to be put in place for the ITk track reconstruction to guarantee high tracking performance in this challenging environment, which is crucial for many beyond-the-Standard-Model searches. The results presented in this paper represent a solid baseline for future developments expected to happen in the coming years, and will be used in particular as a reference for the expected evolution of the ATLAS tracking software before the start of the Run 4 data-taking.

Acknowledgements

We thank CERN for the very successful operation of the LHC and its injectors, as well as the support staff at CERN and at our institutions worldwide without whom ATLAS could not be operated efficiently.

The crucial computing support from all WLCG partners is acknowledged gratefully, in particular from CERN, the ATLAS Tier-1 facilities at TRIUMF/SFU (Canada), NDGF (Denmark, Norway, Sweden), CC-IN2P3 (France), KIT/GridKA (Germany), INFN-CNAF (Italy), NL-T1 (Netherlands), PIC (Spain), RAL (UK) and BNL (USA), the Tier-2 facilities worldwide and large non-WLCG resource providers. Major contributors of computing resources are listed in Ref. [64].

We gratefully acknowledge the support of ANPCyT, Argentina; YerPhI, Armenia; ARC, Australia; BMWFW and FWF, Austria; ANAS, Azerbaijan; CNPq and FAPESP, Brazil; NSERC, NRC and CFI, Canada; CERN; ANID, Chile; CAS, MOST and NSFC, China; Minciencias, Colombia; MEYS CR, Czech Republic; DNRF and DNSRC, Denmark; IN2P3-CNRS and CEA-DRF/IRFU, France; SRNSFG, Georgia; BMBF, HGF and MPG, Germany; GSRI, Greece; RGC and Hong Kong SAR, China; ICHEP and Academy of Sciences and Humanities, Israel; INFN, Italy; MEXT and JSPS, Japan; CNRST, Morocco; NWO, Netherlands; RCN, Norway; MNiSW, Poland; FCT, Portugal; MNE/IFA, Romania; MSTDI, Serbia; MSSR, Slovakia; ARIS and MVZI, Slovenia; DSI/NRF, South Africa; MICIU/AEI, Spain; SRC and Wallenberg Foundation, Sweden; SERI, SNSF and Cantons of Bern and Geneva, Switzerland; NSTC, Taipei; TENMAK, Türkiye; STFC/UKRI, United Kingdom; DOE and NSF, United States of America.

Individual groups and members have received support from BCKDF, CANARIE, CRC and DRAC, Canada; CERN-CZ, FORTE and PRIMUS, Czech Republic; COST, ERC, ERDF, Horizon 2020, ICSC-NextGenerationEU and Marie Skłodowska-Curie Actions, European Union; Investissements d’Avenir Labex, Investissements d’Avenir Idex and ANR, France; DFG and AvH Foundation, Germany; Herakleitos, Thales and Aristeia programmes co-financed by EU-ESF and the Greek NSRF, Greece; BSF-NSF and MINERVA, Israel; NCN and NAWA, Poland; La Caixa Banking Foundation, CERCA Programme Generalitat de Catalunya and PROMETEO and GenT Programmes Generalitat Valenciana, Spain; Göran Gustafssons Stiftelse, Sweden; The Royal Society and Leverhulme Trust, United Kingdom.

In addition, individual members wish to acknowledge support from Armenia: Yerevan Physics Institute (FAPERJ); CERN: European Organization for Nuclear Research (CERN DOCT); Chile: Agencia Nacional de Investigación y Desarrollo (FONDECYT 1230812, FONDECYT 1230987, FONDECYT 1240864); China: Chinese Ministry of Science and Technology (MOST-2023YFA1605700, MOST-2023YFA1609300), National Natural Science Foundation of China (NSFC - 12175119, NSFC 12275265, NSFC-12075060); Czech Republic: Czech Science Foundation (GACR - 24-11373S), Ministry of Education Youth and Sports (FORTE CZ.02.01.01/00/22_008/0004632), PRIMUS Research Programme (PRIMUS/21/SCI/017); EU: H2020 European Research Council (ERC - 101002463); European Union: European Research Council (ERC - 948254, ERC 101089007, ERC, BARD, 101116429), European Union, Future Artificial Intelligence Research (FAIR-NextGenerationEU PE00000013), Italian Center for High Performance Computing, Big Data and Quantum Computing (ICSC, NextGenerationEU); France: Agence Nationale de la Recherche (ANR-20-CE31-0013, ANR-21-CE31-0013, ANR-21-CE31-0022, ANR-22-EDIR-0002); Germany: Baden-Württemberg Stiftung (BW Stiftung-Postdoc Eliteprogramme), Deutsche Forschungsgemeinschaft (DFG - 469666862, DFG - CR 312/5-2); Italy: Istituto Nazionale di Fisica Nucleare (ICSC, NextGenerationEU), Ministero dell’Università e della Ricerca (PRIN - 20223N7F8K - PNRR M4.C2.1.1); Japan: Japan Society for the Promotion of Science (JSPS KAKENHI JP22H01227, JSPS KAKENHI JP22H04944, JSPS KAKENHI JP22KK0227, JSPS KAKENHI JP23KK0245); Norway: Research Council of Norway (RCN-314472); Poland: Ministry of Science and Higher Education (IDUB AGH, POB8, D4 no 9722), Polish National Agency for Academic Exchange (PPN/PPO/2020/1/00002/U/00001), Polish National Science Centre (NCN 2021/42/E/ST2/00350, NCN OPUS 2023/51/B/ST2/02507, NCN OPUS nr 2022/47/B/ST2/03059, NCN UMO-2019/34/E/ST2/00393, UMO-2020/37/B/ST2/01043, UMO-2021/40/C/ST2/00187, UMO-2022/47/O/ST2/00148, UMO-2023/49/B/ST2/04085, UMO-2023/51/B/ST2/00920); Spain: Generalitat Valenciana (Artemisa, FEDER, IDIFEDER/2018/048), Ministry of Science and Innovation (MCIN & NextGenEU PCI2022-135018-2, MICIN & FEDER PID2021-125273NB, RYC2019-028510-I, RYC2020-030254-I, RYC2021-031273-I, RYC2022-038164-I); Sweden: Carl Trygger Foundation (Carl Trygger Foundation CTS 22:2312), Swedish Research Council (Swedish Research Council 2023-04654, VR 2018-00482, VR 2022-03845, VR 2022-04683, VR 2023-03403, VR grant 2021-03651), Knut and Alice Wallenberg Foundation (KAW 2018.0458, KAW 2019.0447, KAW 2022.0358); Switzerland: Swiss National Science Foundation (SNSF - PCEFP2_194658); United Kingdom: Leverhulme Trust (Leverhulme Trust RPG-2020-004), Royal Society (NIF-R1-231091); United States of America: U.S. Department of Energy (ECA DE-AC02-76SF00515), Neubauer Family Foundation.

References

- [1] L. Evans and P. Bryant, *LHC Machine*, [JINST 3 \(2008\) S08001](#).

- [2] ATLAS Collaboration, *The ATLAS Experiment at the CERN Large Hadron Collider*, [JINST 3 \(2008\) S08003](#).
- [3] CMS Collaboration, *The CMS Experiment at the CERN LHC*, [JINST 3 \(2008\) S08004](#).
- [4] O. Aberle et al., *High-Luminosity Large Hadron Collider (HL-LHC): Technical design report*, CERN-2020-010, 2020, URL: <https://cds.cern.ch/record/2749422>.
- [5] ATLAS Collaboration, *ATLAS Inner Detector: Technical Design Report, Volume 1*, ATLAS-TDR-4; CERN-LHCC-97-016, 1997, URL: <https://cds.cern.ch/record/331063>.
- [6] ATLAS Collaboration, *ATLAS Inner Detector: Technical Design Report, Volume 2*, ATLAS-TDR-5, CERN-LHCC-97-017, 1997, URL: <https://cds.cern.ch/record/331064>.
- [7] ATLAS Collaboration, *Modelling radiation damage to pixel sensors in the ATLAS detector*, [JINST 14 \(2019\) P06012](#), arXiv: [1905.03739 \[physics.ins-det\]](#).
- [8] ATLAS Collaboration, *Measurements of sensor radiation damage in the ATLAS inner detector using leakage currents*, [JINST 16 \(2021\) P08025](#), arXiv: [2106.09287 \[hep-ex\]](#).
- [9] ATLAS Collaboration, *ATLAS Inner Tracker Strip Detector: Technical Design Report*, ATLAS-TDR-025; CERN-LHCC-2017-005, 2017, URL: <https://cds.cern.ch/record/2257755>.
- [10] ATLAS Collaboration, *ATLAS Inner Tracker Pixel Detector: Technical Design Report*, ATLAS-TDR-030; CERN-LHCC-2017-021, 2017, URL: <https://cds.cern.ch/record/2285585>.
- [11] ATLAS Collaboration, *Letter of Intent for the Phase-II Upgrade of the ATLAS Experiment*, CERN-LHCC-2012-022, LHCC-I-023, 2012, URL: <https://cds.cern.ch/record/1502664>.
- [12] ATLAS Collaboration, *ATLAS Phase-II Upgrade Scoping Document*, CERN-LHCC-2015-020, LHCC-G-166, 2015, URL: <https://cds.cern.ch/record/2055248>.
- [13] ATLAS Collaboration, *Jet reconstruction and performance using particle flow with the ATLAS Detector*, [Eur. Phys. J. C 77 \(2017\) 466](#), arXiv: [1703.10485 \[hep-ex\]](#).
- [14] ATLAS Collaboration, *ATLAS flavour-tagging algorithms for the LHC Run 2 pp collision dataset*, [Eur. Phys. J. C 83 \(2023\) 681](#), arXiv: [2211.16345 \[physics.data-an\]](#).
- [15] ATLAS Collaboration, *Graph Neural Network Jet Flavour Tagging with the ATLAS Detector*, ATL-PHYS-PUB-2022-027, 2022, URL: <https://cds.cern.ch/record/2811135>.
- [16] ATLAS Collaboration, *Electron and photon efficiencies in LHC Run 2 with the ATLAS experiment*, [JHEP 05 \(2024\) 162](#), arXiv: [2308.13362 \[hep-ex\]](#).
- [17] ATLAS Collaboration, *Reconstruction, Identification, and Calibration of hadronically decaying tau leptons with the ATLAS detector for the LHC Run 3 and reprocessed Run 2 data*, ATL-PHYS-PUB-2022-044, 2022, URL: <https://cds.cern.ch/record/2827111>.
- [18] ATLAS Collaboration, *Muon reconstruction and identification efficiency in ATLAS using the full Run 2 pp collision data set at $\sqrt{s} = 13$ TeV*, [Eur. Phys. J. C 81 \(2021\) 578](#), arXiv: [2012.00578 \[hep-ex\]](#).

- [19] ATLAS Collaboration, *Measurement of angular and momentum distributions of charged particles within and around jets in Pb+Pb and pp collisions at $\sqrt{s_{NN}} = 5.02$ TeV with the ATLAS detector*, *Phys. Rev. C* **100** (2019) 064901, arXiv: 1908.05264 [nucl-ex], Erratum: *Phys. Rev. C* **101** (2019) 059903.
- [20] ATLAS Collaboration, *Search for long-lived charginos based on a disappearing-track signature using 136fb^{-1} of pp collisions at $\sqrt{s} = 13$ TeV with the ATLAS detector*, *Eur. Phys. J. C* **82** (2022) 606, arXiv: 2201.02472 [hep-ex].
- [21] ATLAS Collaboration, *Measurement of the production of a W boson in association with a charmed hadron in pp collisions at $\sqrt{s} = 13$ TeV with the ATLAS detector*, *Phys. Rev. D* **108** (2023) 032012, arXiv: 2302.00336 [hep-ex].
- [22] T. Cornelissen et al., *The new ATLAS track reconstruction (NEWT)*, *J. Phys. Conf. Ser.* **119** (2008) 032014.
- [23] ATLAS Collaboration, *Software Performance of the ATLAS Track Reconstruction for LHC Run 3*, *Comput. Softw. Big Sci.* **8** (2024) 9, arXiv: 2308.09471 [hep-ex].
- [24] R. Frühwirth, *Application of Kalman filtering to track and vertex fitting*, *Nucl. Instrum. Meth. A* **262** (1987) 444.
- [25] ATLAS Collaboration, *Expected b-tagging Performance with the upgraded ATLAS Inner Tracker Detector at the High-Luminosity LHC*, ATL-PHYS-PUB-2020-005, 2020, URL: <https://cds.cern.ch/record/2713377>.
- [26] ATLAS Collaboration, *Neural Network Jet Flavour Tagging with the Upgraded ATLAS Inner Tracker Detector at the High-Luminosity LHC*, ATL-PHYS-PUB-2022-047, 2022, URL: <https://cds.cern.ch/record/2839913>.
- [27] ATLAS Collaboration, *Expected performance of the ATLAS detector at the High-Luminosity LHC*, ATL-PHYS-PUB-2019-005, 2019, URL: <https://cds.cern.ch/record/2655304>.
- [28] ATLAS Collaboration, *Expected performance of the ATLAS detector under different High-Luminosity LHC conditions*, ATL-PHYS-PUB-2021-023, 2021, URL: <https://cds.cern.ch/record/2776650>.
- [29] CMS Collaboration, *Technical Proposal for the Phase-II Upgrade of the CMS Detector*, CERN-LHCC-2015-010, LHCC-P-008, CMS-TDR-15-02, 2015, URL: <https://cds.cern.ch/record/2020886>.
- [30] CMS Collaboration, *The Phase-2 Upgrade of the CMS Tracker*, CERN-LHCC-2017-009, CMS-TDR-014, 2017, URL: <https://cds.cern.ch/record/2272264>.
- [31] ATLAS and CMS Collaborations, *Report on the Physics at the HL-LHC and Perspectives for the HE-LHC*, 2019, arXiv: 1902.10229 [hep-ex].
- [32] ATLAS and CMS Collaborations, *Snowmass White Paper Contribution: Physics with the Phase-2 ATLAS and CMS Detectors*, ATL-PHYS-PUB-2022-018, CMS PAS FTR-22-001, 2022, URL: <https://cds.cern.ch/record/2805993>.
- [33] ATLAS Collaboration, *A High-Granularity Timing Detector for the ATLAS Phase-II Upgrade: Technical Design Report*, ATLAS-TDR-031; CERN-LHCC-2020-007, 2020, URL: <https://cds.cern.ch/record/2719855>.

- [34] ATLAS Collaboration, *Software and computing for Run 3 of the ATLAS experiment at the LHC*, (2024), arXiv: [2404.06335 \[hep-ex\]](#).
- [35] M. Bandieramonte, R. M. Bianchi, J. Boudreau, A. Dell'Acqua and V. Tsulaia, *The GeoModel tool suite for detector description*, [EPJ Web Conf. **251** \(2021\) 03007](#).
- [36] ATLAS Collaboration, *ATLAS HL-LHC Computing Conceptual Design Report*, CERN-LHCC-2020-015, LHCC-G-178, 2020, URL: <https://cds.cern.ch/record/2729668>.
- [37] S. Frixione, G. Ridolfi and P. Nason, *A positive-weight next-to-leading-order Monte Carlo for heavy flavour hadroproduction*, [JHEP **09** \(2007\) 126](#), arXiv: [0707.3088 \[hep-ph\]](#).
- [38] P. Nason, *A new method for combining NLO QCD with shower Monte Carlo algorithms*, [JHEP **11** \(2004\) 040](#), arXiv: [hep-ph/0409146](#).
- [39] S. Frixione, P. Nason and C. Oleari, *Matching NLO QCD computations with parton shower simulations: the POWHEG method*, [JHEP **11** \(2007\) 070](#), arXiv: [0709.2092 \[hep-ph\]](#).
- [40] S. Alioli, P. Nason, C. Oleari and E. Re, *A general framework for implementing NLO calculations in shower Monte Carlo programs: the POWHEG BOX*, [JHEP **06** \(2010\) 043](#), arXiv: [1002.2581 \[hep-ph\]](#).
- [41] NNPDF Collaboration, R. D. Ball et al., *Parton distributions for the LHC run II*, [JHEP **04** \(2015\) 040](#), arXiv: [1410.8849 \[hep-ph\]](#).
- [42] ATLAS Collaboration, *Studies on top-quark Monte Carlo modelling for Top2016*, ATL-PHYS-PUB-2016-020, 2016, URL: <https://cds.cern.ch/record/2216168>.
- [43] T. Sjöstrand et al., *An introduction to PYTHIA 8.2*, [Comput. Phys. Commun. **191** \(2015\) 159](#), arXiv: [1410.3012 \[hep-ph\]](#).
- [44] ATLAS Collaboration, *ATLAS Pythia 8 tunes to 7 TeV data*, ATL-PHYS-PUB-2014-021, 2014, URL: <https://cds.cern.ch/record/1966419>.
- [45] NNPDF Collaboration, R. D. Ball et al., *Parton distributions with LHC data*, [Nucl. Phys. B **867** \(2013\) 244](#), arXiv: [1207.1303 \[hep-ph\]](#).
- [46] D. J. Lange, *The EvtGen particle decay simulation package*, [Nucl. Instrum. Meth. A **462** \(2001\) 152](#).
- [47] C. Bierlich et al., *A comprehensive guide to the physics and usage of PYTHIA 8.3*, [SciPost Phys. Codeb. \(2022\) 8](#), arXiv: [2203.11601 \[hep-ph\]](#).
- [48] ATLAS Collaboration, *The ATLAS Simulation Infrastructure*, [Eur. Phys. J. C **70** \(2010\) 823](#), arXiv: [1005.4568 \[physics.ins-det\]](#).
- [49] S. Agostinelli et al., *GEANT4 – a simulation toolkit*, [Nucl. Instrum. Meth. A **506** \(2003\) 250](#).
- [50] H. Bichsel, *Straggling in thin silicon detectors*, [Rev. Mod. Phys. **60** \(1988\) 663](#).
- [51] RD53 Collaboration, *RD53 pixel chips for the ATLAS and CMS Phase-2 upgrades at HL-LHC*, [Nucl. Instrum. Meth. A **1067** \(2024\) 169682](#).
- [52] I. Gorelov et al., *A Measurement of Lorentz Angle and Spatial Resolution of Radiation Hard Silicon Pixel Sensors*, [Nucl. Instrum. Meth. A **481** \(2002\) 204](#).

- [53] ATLAS Collaboration, *ATLAS Run 3 charged particle track seed finding performance*, ATL-PHYS-PUB-2023-034, 2023, URL: <https://cds.cern.ch/record/2882156>.
- [54] E. Lund, L. Bugge, I. Gavrilenko and A. Strandlie, *Track parameter propagation through the application of a new adaptive Runge-Kutta-Nyström method in the ATLAS experiment*, *JINST* **4** (2009) P04001.
- [55] T. Cornelissen et al., *The global χ^2 track fitter in ATLAS*, *J. Phys. Conf. Ser.* **119** (2008) 032013.
- [56] T. Cornelissen et al., *Concepts, Design and Implementation of the ATLAS New Tracking (NEWT)*, ATL-SOFT-PUB-2007-007, 2007, URL: <https://cds.cern.ch/record/1020106>.
- [57] ATLAS Collaboration, *A neural network clustering algorithm for the ATLAS silicon pixel detector*, *JINST* **9** (2014) P09009, arXiv: [1406.7690](https://arxiv.org/abs/1406.7690) [hep-ex].
- [58] ATLAS Collaboration, *Performance of the ATLAS track reconstruction algorithms in dense environments in LHC Run 2*, *Eur. Phys. J. C* **77** (2017) 673, arXiv: [1704.07983](https://arxiv.org/abs/1704.07983) [hep-ex].
- [59] ATLAS Collaboration, *Development of ATLAS Primary Vertex Reconstruction for LHC Run 3*, ATL-PHYS-PUB-2019-015, 2019, URL: <https://cds.cern.ch/record/2670380>.
- [60] M. Cacciari, G. P. Salam and G. Soyez, *The anti- k_t jet clustering algorithm*, *JHEP* **04** (2008) 063, arXiv: [0802.1189](https://arxiv.org/abs/0802.1189) [hep-ph].
- [61] M. Cacciari, G. P. Salam and G. Soyez, *FastJet user manual*, *Eur. Phys. J. C* **72** (2012) 1896, arXiv: [1111.6097](https://arxiv.org/abs/1111.6097) [hep-ph].
- [62] ATLAS Collaboration, *ATLAS Insertable B-Layer Technical Design Report*, ATLAS-TDR-19; CERN-LHCC-2010-013, 2010, URL: <https://cds.cern.ch/record/1291633>, Addendum: ATLAS-TDR-19-ADD-1; CERN-LHCC-2012-009, 2012, URL: <https://cds.cern.ch/record/1451888>.
- [63] B. Abbott et al., *Production and integration of the ATLAS Insertable B-Layer*, *JINST* **13** (2018) T05008, arXiv: [1803.00844](https://arxiv.org/abs/1803.00844) [physics.ins-det].
- [64] ATLAS Collaboration, *ATLAS Computing Acknowledgements*, ATL-SOFT-PUB-2023-001, 2023, URL: <https://cds.cern.ch/record/2869272>.

The ATLAS Collaboration

G. Aad ¹⁰⁵, E. Aakvaag ¹⁷, B. Abbott ¹²⁴, S. Abdelhameed ^{120a}, K. Abeling ⁵⁶, N.J. Abicht ⁵⁰, S.H. Abidi ³⁰, M. Aboeela ⁴⁶, A. Aboulhorma ^{36e}, H. Abramowicz ¹⁵⁸, Y. Abulaiti ¹²¹, B.S. Acharya ^{70a,70b,o}, A. Ackermann ^{64a}, C. Adam Bourdarios ⁴, L. Adamczyk ^{87a}, S.V. Addepalli ¹⁵⁰, M.J. Addison ¹⁰⁴, J. Adelman ¹¹⁹, A. Adiguzel ^{22c}, T. Adye ¹³⁸, A.A. Affolder ¹⁴⁰, Y. Afik ⁴¹, M.N. Agaras ¹³, A. Aggarwal ¹⁰³, C. Agheorghiesei ^{28c}, F. Ahmadov ^{40,ad}, S. Ahuja ⁹⁸, X. Ai ^{144b}, G. Aielli ^{77a,77b}, A. Aikot ¹⁷⁰, M. Ait Tamlihat ^{36e}, B. Aitbenkikh ^{36a}, M. Akbiyik ¹⁰³, T.P.A. Åkesson ¹⁰¹, A.V. Akimov ¹⁵², D. Akiyama ¹⁷⁵, N.N. Akolkar ²⁵, S. Aktas ^{22a}, G.L. Alberghi ^{24b}, J. Albert ¹⁷², P. Albicocco ⁵⁴, G.L. Albouy ⁶¹, S. Alderweireldt ⁵³, Z.L. Alegria ¹²⁵, M. Aleksa ³⁷, I.N. Aleksandrov ⁴⁰, C. Alexa ^{28b}, T. Alexopoulos ¹⁰, F. Alfonsi ^{24b}, M. Algren ⁵⁷, M. Alhroob ¹⁷⁴, B. Ali ¹³⁶, H.M.J. Ali ^{94,x}, S. Ali ³², S.W. Alibocus ⁹⁵, M. Aliev ^{34c}, G. Alimonti ^{72a}, W. Alkahi ⁵⁶, C. Allaire ⁶⁷, B.M.M. Allbrooke ¹⁵³, J.S. Allen ¹⁰⁴, J.F. Allen ⁵³, P.P. Allport ²¹, A. Aloisio ^{73a,73b}, F. Alonso ⁹³, C. Alpigiani ¹⁴³, Z.M.K. Alsolami ⁹⁴, A. Alvarez Fernandez ¹⁰³, M. Alves Cardoso ⁵⁷, M.G. Alviggi ^{73a,73b}, M. Aly ¹⁰⁴, Y. Amaral Coutinho ^{84b}, A. Ambler ¹⁰⁷, C. Amelung ³⁷, M. Amerl ¹⁰⁴, C.G. Ames ¹¹², D. Amidei ¹⁰⁹, B. Amini ⁵⁵, K.J. Amirie ¹⁶², A. Amirkhanov ⁴⁰, S.P. Amor Dos Santos ^{134a}, K.R. Amos ¹⁷⁰, D. Amperiadou ¹⁵⁹, S. An ⁸⁵, V. Ananiev ¹²⁹, C. Anastopoulos ¹⁴⁶, T. Andeen ¹¹, J.K. Anders ⁹⁵, A.C. Anderson ⁶⁰, A. Andreazza ^{72a,72b}, S. Angelidakis ⁹, A. Angerami ⁴³, A.V. Anisenkov ⁴⁰, A. Annovi ^{75a}, C. Antel ⁵⁷, E. Antipov ¹⁵², M. Antonelli ⁵⁴, F. Anulli ^{76a}, M. Aoki ⁸⁵, T. Aoki ¹⁶⁰, M.A. Aparo ¹⁵³, L. Aperio Bella ⁴⁹, C. Appelt ¹⁵⁸, A. Apyan ²⁷, S.J. Arbiol Val ⁸⁸, C. Arcangeletti ⁵⁴, A.T.H. Arce ⁵², J-F. Arguin ¹¹¹, S. Argyropoulos ¹⁵⁹, J.-H. Arling ⁴⁹, O. Arnaez ⁴, H. Arnold ¹⁵², G. Artoni ^{76a,76b}, H. Asada ¹¹⁴, K. Asai ¹²², S. Asai ¹⁶⁰, N.A. Asbah ³⁷, R.A. Ashby Pickering ¹⁷⁴, A.M. Aslam ⁹⁸, K. Assamagan ³⁰, R. Astalos ^{29a}, K.S.V. Astrand ¹⁰¹, S. Atashi ¹⁶⁶, R.J. Atkin ^{34a}, H. Atmani ^{36f}, P.A. Atlasiddha ¹³², K. Augsten ¹³⁶, A.D. Auriol ⁴², V.A. Austrup ¹⁰⁴, G. Avolio ³⁷, K. Axiotis ⁵⁷, G. Azuelos ^{111,ah}, A. Azzam ¹³, D. Babal ^{29b}, H. Bachacou ¹³⁹, K. Bachas ^{159,s}, A. Bachiu ³⁵, E. Bachmann ⁵¹, M.J. Backes ^{64a}, A. Badea ⁴¹, T.M. Baer ¹⁰⁹, P. Bagnaia ^{76a,76b}, M. Bahmani ¹⁹, D. Bahner ⁵⁵, K. Bai ¹²⁷, J.T. Baines ¹³⁸, L. Baines ⁹⁷, O.K. Baker ¹⁷⁹, E. Bakos ¹⁶, D. Bakshi Gupta ⁸, L.E. Balabram Filho ^{84b}, V. Balakrishnan ¹²⁴, R. Balasubramanian ⁴, E.M. Baldin ³⁸, P. Balek ^{87a}, E. Ballabene ^{24b,24a}, F. Balli ¹³⁹, L.M. Baltes ^{64a}, W.K. Balunas ³³, J. Balz ¹⁰³, I. Bamwidhi ^{120b}, E. Banas ⁸⁸, M. Bandieramonte ¹³³, A. Bandyopadhyay ²⁵, S. Bansal ²⁵, L. Barak ¹⁵⁸, M. Barakat ⁴⁹, E.L. Barberio ¹⁰⁸, D. Barberis ^{18b}, M. Barbero ¹⁰⁵, M.Z. Barel ¹¹⁸, T. Barillari ¹¹³, M-S. Barisits ³⁷, T. Barklow ¹⁵⁰, P. Baron ¹²⁶, D.A. Baron Moreno ¹⁰⁴, A. Baroncelli ⁶³, A.J. Barr ¹³⁰, J.D. Barr ⁹⁹, F. Barreiro ¹⁰², J. Barreiro Guimarães da Costa ¹⁴, M.G. Barros Teixeira ^{134a}, S. Barsov ³⁸, F. Bartels ^{64a}, R. Bartoldus ¹⁵⁰, A.E. Barton ⁹⁴, P. Bartos ^{29a}, A. Basan ¹⁰³, M. Baselga ⁵⁰, S. Bashiri ⁸⁸, A. Bassalat ^{67,b}, M.J. Basso ^{163a}, S. Bataju ⁴⁶, R. Bate ¹⁷¹, R.L. Bates ⁶⁰, S. Batlamous ¹⁰², M. Battaglia ¹⁴⁰, D. Battulga ¹⁹, M. Bauge ^{76a,76b}, M. Bauer ⁸⁰, P. Bauer ²⁵, L.T. Bayer ⁴⁹, L.T. Bazzano Hurrell ³¹, J.B. Beacham ¹¹³, T. Beau ¹³¹, J.Y. Beauchamp ⁹³, P.H. Beauchemin ¹⁶⁵, P. Bechtel ²⁵, H.P. Beck ^{20,r}, K. Becker ¹⁷⁴, A.J. Beddall ⁸³, V.A. Bednyakov ⁴⁰, C.P. Bee ¹⁵², L.J. Beemster ¹⁶, M. Begalli ^{84d}, M. Begel ³⁰, J.K. Behr ⁴⁹, J.F. Beirer ³⁷, F. Beisiegel ²⁵, M. Belfkir ^{120b}, G. Bella ¹⁵⁸, L. Bellagamba ^{24b}, A. Bellerive ³⁵, P. Bellos ²¹, K. Beloborodov ³⁸, D. Bencheikroun ^{36a}, F. Bendebba ^{36a}, Y. Benhammou ¹⁵⁸, K.C. Benkendorfer ⁶², L. Beresford ⁴⁹, M. Beretta ⁵⁴, E. Bergeas Kuutmann ¹⁶⁸, N. Berger ⁴,

B. Bergmann [ID136](#), J. Beringer [ID18a](#), G. Bernardi [ID5](#), C. Bernius [ID150](#), F.U. Bernlochner [ID25](#),
 F. Bernon [ID37](#), A. Berrocal Guardia [ID13](#), T. Berry [ID98](#), P. Berta [ID137](#), A. Berthold [ID51](#), S. Bethke [ID113](#),
 A. Betti [ID76a,76b](#), A.J. Bevan [ID97](#), L. Bezio [ID57](#), N.K. Bhalla [ID55](#), S. Bharthuar [ID113](#), S. Bhatta [ID152](#),
 D.S. Bhattacharya [ID173](#), P. Bhattarai [ID150](#), Z.M. Bhatti [ID121](#), K.D. Bhide [ID55](#), V.S. Bhopatkar [ID125](#),
 R.M. Bianchi [ID133](#), G. Bianco [ID24b,24a](#), O. Biebel [ID112](#), M. Biglietti [ID78a](#), C.S. Billingsley [ID46](#),
 Y. Bimgdi [ID36f](#), M. Bindi [ID56](#), A. Bingham [ID178](#), A. Bingul [ID22b](#), C. Bini [ID76a,76b](#), G.A. Bird [ID33](#),
 M. Birman [ID176](#), M. Biros [ID137](#), S. Biryukov [ID153](#), T. Bisanz [ID50](#), E. Bisceglie [ID24b,24a](#), J.P. Biswal [ID138](#),
 D. Biswas [ID148](#), I. Bloch [ID49](#), A. Blue [ID60](#), U. Blumenschein [ID97](#), J. Blumenthal [ID103](#),
 V.S. Bobrovnikov [ID40](#), M. Boehler [ID55](#), B. Boehm [ID173](#), D. Bogavac [ID37](#), A.G. Bogdanchikov [ID38](#),
 L.S. Boggia [ID131](#), V. Boisvert [ID98](#), P. Bokan [ID37](#), T. Bold [ID87a](#), M. Bomben [ID5](#), M. Bona [ID97](#),
 M. Boonekamp [ID139](#), A.G. Borbély [ID60](#), I.S. Bordulev [ID38](#), G. Borissov [ID94](#), D. Bortoletto [ID130](#),
 D. Boscherini [ID24b](#), M. Bosman [ID13](#), K. Bouaouda [ID36a](#), N. Bouchhar [ID170](#), L. Boudet [ID4](#),
 J. Boudreau [ID133](#), E.V. Bouhova-Thacker [ID94](#), D. Boumediene [ID42](#), R. Bouquet [ID58b,58a](#), A. Boveia [ID123](#),
 J. Boyd [ID37](#), D. Boye [ID30](#), I.R. Boyko [ID40](#), L. Bozianu [ID57](#), J. Bracinek [ID21](#), N. Brahimi [ID4](#),
 G. Brandt [ID178](#), O. Brandt [ID33](#), B. Brau [ID106](#), J.E. Brau [ID127](#), R. Brener [ID176](#), L. Brenner [ID118](#),
 R. Brenner [ID168](#), S. Bressler [ID176](#), G. Brianti [ID79a,79b](#), D. Britton [ID60](#), D. Britzger [ID113](#), I. Brock [ID25](#),
 R. Brock [ID110](#), G. Brooijmans [ID43](#), A.J. Brooks [ID69](#), E.M. Brooks [ID163b](#), E. Brost [ID30](#), L.M. Brown [ID172](#),
 L.E. Bruce [ID62](#), T.L. Bruckler [ID130](#), P.A. Bruckman de Renstrom [ID88](#), B. Brüers [ID49](#), A. Bruni [ID24b](#),
 G. Bruni [ID24b](#), D. Brunner [ID48a,48b](#), M. Bruschi [ID24b](#), N. Bruscinò [ID76a,76b](#), T. Buanes [ID17](#), Q. Buat [ID143](#),
 D. Buchin [ID113](#), A.G. Buckley [ID60](#), O. Bulekov [ID38](#), B.A. Bullard [ID150](#), S. Burdin [ID95](#), C.D. Burgard [ID50](#),
 A.M. Burger [ID37](#), B. Burghgrave [ID8](#), O. Burlayenko [ID55](#), J. Burleson [ID169](#), J.T.P. Burr [ID33](#),
 J.C. Burzynski [ID149](#), E.L. Busch [ID43](#), V. Büscher [ID103](#), P.J. Bussey [ID60](#), J.M. Butler [ID26](#), C.M. Buttar [ID60](#),
 J.M. Butterworth [ID99](#), W. Buttinger [ID138](#), C.J. Buxo Vazquez [ID110](#), A.R. Buzykaev [ID40](#),
 S. Cabrera Urbán [ID170](#), L. Cadamuro [ID67](#), D. Caforio [ID59](#), H. Cai [ID133](#), Y. Cai [ID24b,115c,24a](#), Y. Cai [ID115a](#),
 V.M.M. Cairo [ID37](#), O. Cakir [ID3a](#), N. Calace [ID37](#), P. Calafiura [ID18a](#), G. Calderini [ID131](#), P. Calfayan [ID35](#),
 G. Callea [ID60](#), L.P. Caloba [ID84b](#), D. Calvet [ID42](#), S. Calvet [ID42](#), R. Camacho Toro [ID131](#), S. Camarda [ID37](#),
 D. Camarero Munoz [ID27](#), P. Camarri [ID77a,77b](#), M.T. Camerlingo [ID73a,73b](#), C. Camincher [ID172](#),
 M. Campanelli [ID99](#), A. Camplani [ID44](#), V. Canale [ID73a,73b](#), A.C. Canbay [ID3a](#), E. Canonero [ID98](#),
 J. Cantero [ID170](#), Y. Cao [ID169](#), F. Capocasa [ID27](#), M. Capua [ID45b,45a](#), A. Carbone [ID72a,72b](#),
 R. Cardarelli [ID77a](#), J.C.J. Cardenas [ID8](#), M.P. Cardiff [ID27](#), G. Carducci [ID45b,45a](#), T. Carli [ID37](#),
 G. Carlino [ID73a](#), J.I. Carlotto [ID13](#), B.T. Carlson [ID133,t](#), E.M. Carlson [ID172](#), J. Carmignani [ID95](#),
 L. Carminati [ID72a,72b](#), A. Carnelli [ID4](#), M. Carnesale [ID37](#), S. Caron [ID117](#), E. Carquin [ID141f](#), I.B. Carr [ID108](#),
 S. Carrá [ID72a](#), G. Carratta [ID24b,24a](#), A.M. Carroll [ID127](#), M.P. Casado [ID13,i](#), M. Caspar [ID49](#),
 F.L. Castillo [ID4](#), L. Castillo Garcia [ID13](#), V. Castillo Gimenez [ID170](#), N.F. Castro [ID134a,134e](#),
 A. Catinaccio [ID37](#), J.R. Catmore [ID129](#), T. Cavaliere [ID4](#), V. Cavaliere [ID30](#), L.J. Caviedes Betancourt [ID23b](#),
 Y.C. Cekmecelioglu [ID49](#), E. Celebi [ID83](#), S. Cella [ID37](#), V. Cepaitis [ID57](#), K. Cerny [ID126](#),
 A.S. Cerqueira [ID84a](#), A. Cerri [ID75a,75b](#), L. Cerrito [ID77a,77b](#), F. Cerutti [ID18a](#), B. Cervato [ID72a,72b](#),
 A. Cervelli [ID24b](#), G. Cesarini [ID54](#), S.A. Cetin [ID83](#), P.M. Chabrilat [ID131](#), J. Chan [ID18a](#), W.Y. Chan [ID160](#),
 J.D. Chapman [ID33](#), E. Chapon [ID139](#), B. Chargeishvili [ID156b](#), D.G. Charlton [ID21](#), C. Chauhan [ID137](#),
 Y. Che [ID115a](#), S. Chekanov [ID6](#), S.V. Chekulaev [ID163a](#), G.A. Chelkov [ID40,a](#), B. Chen [ID158](#), B. Chen [ID172](#),
 H. Chen [ID115a](#), H. Chen [ID30](#), J. Chen [ID145a](#), J. Chen [ID149](#), M. Chen [ID130](#), S. Chen [ID90](#), S.J. Chen [ID115a](#),
 X. Chen [ID145a](#), X. Chen [ID15,ag](#), Z. Chen [ID63](#), C.L. Cheng [ID177](#), H.C. Cheng [ID65a](#), S. Cheong [ID150](#),
 A. Cheplakov [ID40](#), E. Cheremushkina [ID49](#), E. Cherepanova [ID118](#), R. Cherkaoui El Moursli [ID36e](#),
 E. Cheu [ID7](#), K. Cheung [ID66](#), L. Chevalier [ID139](#), V. Chiarella [ID54](#), G. Chiarelli [ID75a](#), N. Chiedde [ID105](#),
 G. Chiodini [ID71a](#), A.S. Chisholm [ID21](#), A. Chitan [ID28b](#), M. Chitishvili [ID170](#), M.V. Chizhov [ID40,u](#),
 K. Choi [ID11](#), Y. Chou [ID143](#), E.Y.S. Chow [ID117](#), K.L. Chu [ID176](#), M.C. Chu [ID65a](#), X. Chu [ID14,115c](#),
 Z. Chubinidze [ID54](#), J. Chudoba [ID135](#), J.J. Chwastowski [ID88](#), D. Cieri [ID113](#), K.M. Ciesla [ID87a](#),

V. Cindro ⁹⁶, A. Ciocio ^{18a}, F. Cirotto ^{73a,73b}, Z.H. Citron ¹⁷⁶, M. Citterio ^{72a}, D.A. Ciubotaru ^{28b}, A. Clark ⁵⁷, P.J. Clark ⁵³, N. Clarke Hall ⁹⁹, C. Clarry ¹⁶², S.E. Clawson ⁴⁹, C. Clement ^{48a,48b}, Y. Coadou ¹⁰⁵, M. Cobal ^{70a,70c}, A. Coccaro ^{58b}, R.F. Coelho Barrue ^{134a}, R. Coelho Lopes De Sa ¹⁰⁶, S. Coelli ^{72a}, L.S. Colangeli ¹⁶², B. Cole ⁴³, P. Collado Soto ¹⁰², J. Collot ⁶¹, P. Conde Muiño ^{134a,134g}, M.P. Connell ^{34c}, S.H. Connell ^{34c}, E.I. Conroy ¹³⁰, F. Conventi ^{73a,ai}, H.G. Cooke ²¹, A.M. Cooper-Sarkar ¹³⁰, F.A. Corchia ^{24b,24a}, A. Cordeiro Oudot Choi ¹³¹, L.D. Corpe ⁴², M. Corradi ^{76a,76b}, F. Corriveau ^{107,ac}, A. Cortes-Gonzalez ¹⁹, M.J. Costa ¹⁷⁰, F. Costanza ⁴, D. Costanzo ¹⁴⁶, B.M. Cote ¹²³, J. Couthures ⁴, G. Cowan ⁹⁸, K. Cranmer ¹⁷⁷, L. Cremer ⁵⁰, D. Cremonini ^{24b,24a}, S. Crépe-Renaudin ⁶¹, F. Crescioli ¹³¹, T. Cresta ^{74a,74b}, M. Cristinziani ¹⁴⁸, M. Cristoforetti ^{79a,79b}, V. Croft ¹¹⁸, J.E. Crosby ¹²⁵, G. Crosetti ^{45b,45a}, A. Cueto ¹⁰², H. Cui ⁹⁹, Z. Cui ⁷, W.R. Cunningham ⁶⁰, F. Curcio ¹⁷⁰, J.R. Curran ⁵³, P. Czodrowski ³⁷, M.J. Da Cunha Sargedas De Sousa ^{58b,58a}, J.V. Da Fonseca Pinto ^{84b}, C. Da Via ¹⁰⁴, W. Dabrowski ^{87a}, T. Dado ³⁷, S. Dahbi ¹⁵⁵, T. Dai ¹⁰⁹, D. Dal Santo ²⁰, C. Dallapiccola ¹⁰⁶, M. Dam ⁴⁴, G. D'amen ³⁰, V. D'Amico ¹¹², J. Damp ¹⁰³, J.R. Dandoy ³⁵, D. Dannheim ³⁷, M. Danninger ¹⁴⁹, V. Dao ¹⁵², G. Darbo ^{58b}, S.J. Das ³⁰, F. Dattola ⁴⁹, S. D'Auria ^{72a,72b}, A. D'Avanzo ^{73a,73b}, T. Davidek ¹³⁷, I. Dawson ⁹⁷, H.A. Day-hall ¹³⁶, K. De ⁸, C. De Almeida Rossi ¹⁶², R. De Asmundis ^{73a}, N. De Biase ⁴⁹, S. De Castro ^{24b,24a}, N. De Groot ¹¹⁷, P. de Jong ¹¹⁸, H. De la Torre ¹¹⁹, A. De Maria ^{115a}, A. De Salvo ^{76a}, U. De Sanctis ^{77a,77b}, F. De Santis ^{71a,71b}, A. De Santo ¹⁵³, J.B. De Vivie De Regie ⁶¹, J. Debevc ⁹⁶, D.V. Dedovich ⁴⁰, J. Degens ⁹⁵, A.M. Deiana ⁴⁶, J. Del Peso ¹⁰², L. Delagrangé ¹³¹, F. Deliot ¹³⁹, C.M. Delitzsch ⁵⁰, M. Della Pietra ^{73a,73b}, D. Della Volpe ⁵⁷, A. Dell'Acqua ³⁷, L. Dell'Asta ^{72a,72b}, M. Delmastro ⁴, C.C. Delogu ¹⁰³, P.A. Delsart ⁶¹, S. Demers ¹⁷⁹, M. Demichev ⁴⁰, S.P. Denisov ³⁸, H. Denizli ^{22a,m}, L. D'Eramo ⁴², D. Derendarz ⁸⁸, F. Derue ¹³¹, P. Dervan ⁹⁵, K. Desch ²⁵, C. Deutsch ²⁵, F.A. Di Bello ^{58b,58a}, A. Di Ciaccio ^{77a,77b}, L. Di Ciaccio ⁴, A. Di Domenico ^{76a,76b}, C. Di Donato ^{73a,73b}, A. Di Girolamo ³⁷, G. Di Gregorio ³⁷, A. Di Luca ^{79a,79b}, B. Di Micco ^{78a,78b}, R. Di Nardo ^{78a,78b}, K.F. Di Petrillo ⁴¹, M. Diamantopoulou ³⁵, F.A. Dias ¹¹⁸, T. Dias Do Vale ¹⁴⁹, M.A. Diaz ^{141a,141b}, A.R. Didenko ⁴⁰, M. Didenko ¹⁷⁰, E.B. Diehl ¹⁰⁹, S. Díez Cornell ⁴⁹, C. Diez Pardos ¹⁴⁸, C. Dimitriadi ¹⁵¹, A. Dimitrievska ²¹, A. Dimri ¹⁵², J. Dingfelder ²⁵, T. Dingley ¹³⁰, I-M. Dinu ^{28b}, S.J. Dittmeier ^{64b}, F. Dittus ³⁷, M. Divisek ¹³⁷, B. Dixit ⁹⁵, F. Djama ¹⁰⁵, T. Djobava ^{156b}, C. Doglioni ^{104,101}, A. Dohnalova ^{29a}, Z. Dolezal ¹³⁷, K. Domijan ^{87a}, K.M. Dona ⁴¹, M. Donadelli ^{84d}, B. Dong ¹¹⁰, J. Donini ⁴², A. D'Onofrio ^{73a,73b}, M. D'Onofrio ⁹⁵, J. Dopke ¹³⁸, A. Doria ^{73a}, N. Dos Santos Fernandes ^{134a}, P. Dougan ¹⁰⁴, M.T. Dova ⁹³, A.T. Doyle ⁶⁰, M.A. Draguet ¹³⁰, M.P. Drescher ⁵⁶, E. Dreyer ¹⁷⁶, I. Drivas-koulouris ¹⁰, M. Drnevich ¹²¹, M. Drozdova ⁵⁷, D. Du ⁶³, T.A. du Pree ¹¹⁸, F. Dubinin ⁴⁰, M. Dubovsky ^{29a}, E. Duchovni ¹⁷⁶, G. Duckeck ¹¹², P.K. Duckett ⁹⁹, O.A. Ducu ^{28b}, D. Duda ⁵³, A. Dudarev ³⁷, E.R. Duden ²⁷, M. D'uffizi ¹⁰⁴, L. Duflot ⁶⁷, M. Dührssen ³⁷, I. Duminica ^{28g}, A.E. Dumitriu ^{28b}, M. Dunford ^{64a}, S. Dungs ⁵⁰, K. Dunne ^{48a,48b}, A. Duperrin ¹⁰⁵, H. Duran Yildiz ^{3a}, M. Düren ⁵⁹, A. Durglishvili ^{156b}, D. Duvnjak ³⁵, B.L. Dwyer ¹¹⁹, G.I. Dyckes ^{18a}, M. Dyndal ^{87a}, B.S. Dziedzic ³⁷, Z.O. Earnshaw ¹⁵³, G.H. Eberwein ¹³⁰, B. Eckerova ^{29a}, S. Eggebrecht ⁵⁶, E. Egidio Purcino De Souza ^{84e}, G. Eigen ¹⁷, K. Einsweiler ^{18a}, T. Ekelof ¹⁶⁸, P.A. Ekman ¹⁰¹, S. El Farkh ^{36b}, Y. El Ghazali ⁶³, H. El Jarrari ³⁷, A. El Moussaouy ^{36a}, V. Ellajosyula ¹⁶⁸, M. Ellert ¹⁶⁸, F. Ellinghaus ¹⁷⁸, N. Ellis ³⁷, J. Elmsheuser ³⁰, M. Elsayy ^{120a}, M. Elsing ³⁷, D. Emeliyanov ¹³⁸, Y. Enari ⁸⁵, I. Ene ^{18a}, S. Epari ¹¹¹, D. Ernani Martins Neto ⁸⁸, M. Errenst ¹⁷⁸, M. Escalier ⁶⁷, C. Escobar ¹⁷⁰, E. Etzion ¹⁵⁸, G. Evans ^{134a,134b}, H. Evans ⁶⁹, L.S. Evans ⁹⁸, A. Ezhilov ³⁸,

S. Ezzarqtouni [id](#)^{36a}, F. Fabbri [id](#)^{24b,24a}, L. Fabbri [id](#)^{24b,24a}, G. Facini [id](#)⁹⁹, V. Fadeyev [id](#)¹⁴⁰,
 R.M. Fakhrutdinov [id](#)³⁸, D. Fakoudis [id](#)¹⁰³, S. Falciano [id](#)^{76a}, L.F. Falda Ulhoa Coelho [id](#)^{134a},
 F. Fallavollita [id](#)¹¹³, G. Falsetti [id](#)^{45b,45a}, J. Faltova [id](#)¹³⁷, C. Fan [id](#)¹⁶⁹, K.Y. Fan [id](#)^{65b}, Y. Fan [id](#)¹⁴,
 Y. Fang [id](#)^{14,115c}, M. Fanti [id](#)^{72a,72b}, M. Faraj [id](#)^{70a,70b}, Z. Farazpay [id](#)¹⁰⁰, A. Farbin [id](#)⁸, A. Farilla [id](#)^{78a},
 T. Farooque [id](#)¹¹⁰, J.N. Farr [id](#)¹⁷⁹, S.M. Farrington [id](#)^{138,53}, F. Fassi [id](#)^{36c}, D. Fassouliotis [id](#)⁹,
 L. Fayard [id](#)⁶⁷, P. Federic [id](#)¹³⁷, P. Federicova [id](#)¹³⁵, O.L. Fedin [id](#)^{38,a}, M. Feickert [id](#)¹⁷⁷, L. Feligioni [id](#)¹⁰⁵,
 D.E. Fellers [id](#)^{18a}, C. Feng [id](#)^{144a}, Z. Feng [id](#)¹¹⁸, M.J. Fenton [id](#)¹⁶⁶, L. Ferencz [id](#)⁴⁹,
 B. Fernandez Barbadillo⁹⁴, P. Fernandez Martinez [id](#)⁶⁸, M.J.V. Fernoux [id](#)¹⁰⁵, J. Ferrando [id](#)⁹⁴,
 A. Ferrari [id](#)¹⁶⁸, P. Ferrari [id](#)^{118,117}, R. Ferrari [id](#)^{74a}, D. Ferrere [id](#)⁵⁷, C. Ferretti [id](#)¹⁰⁹, M.P. Fewell [id](#)¹,
 D. Fiacco [id](#)^{76a,76b}, F. Fiedler [id](#)¹⁰³, P. Fiedler [id](#)¹³⁶, S. Filimonov [id](#)⁴⁰, A. Filipičič [id](#)⁹⁶, E.K. Filmer [id](#)^{163a},
 F. Filthaut [id](#)¹¹⁷, M.C.N. Fiolhais [id](#)^{134a,134c,c}, L. Fiorini [id](#)¹⁷⁰, W.C. Fisher [id](#)¹¹⁰, T. Fitschen [id](#)¹⁰⁴,
 P.M. Fitzhugh¹³⁹, I. Fleck [id](#)¹⁴⁸, P. Fleischmann [id](#)¹⁰⁹, T. Flick [id](#)¹⁷⁸, M. Flores [id](#)^{34d,ae},
 L.R. Flores Castillo [id](#)^{65a}, L. Flores Sanz De Acedo [id](#)³⁷, F.M. Follega [id](#)^{79a,79b}, N. Fomin [id](#)³³,
 J.H. Foo [id](#)¹⁶², A. Formica [id](#)¹³⁹, A.C. Forti [id](#)¹⁰⁴, E. Fortin [id](#)³⁷, A.W. Fortman [id](#)^{18a}, L. Fountas [id](#)^{9,j},
 D. Fournier [id](#)⁶⁷, H. Fox [id](#)⁹⁴, P. Francavilla [id](#)^{75a,75b}, S. Francescato [id](#)⁶², S. Franchellucci [id](#)⁵⁷,
 M. Franchini [id](#)^{24b,24a}, S. Franchino [id](#)^{64a}, D. Francis³⁷, L. Franco [id](#)¹¹⁷, V. Franco Lima [id](#)³⁷,
 L. Franconi [id](#)⁴⁹, M. Franklin [id](#)⁶², G. Frattari [id](#)²⁷, Y.Y. Frid [id](#)¹⁵⁸, J. Friend [id](#)⁶⁰, N. Fritzsche [id](#)³⁷,
 A. Froch [id](#)⁵⁷, D. Froidevaux [id](#)³⁷, J.A. Frost [id](#)¹³⁰, Y. Fu [id](#)¹¹⁰, S. Fuenzalida Garrido [id](#)^{141f},
 M. Fujimoto [id](#)¹⁰⁵, K.Y. Fung [id](#)^{65a}, E. Furtado De Simas Filho [id](#)^{84e}, M. Furukawa [id](#)¹⁶⁰, J. Fuster [id](#)¹⁷⁰,
 A. Gaa [id](#)⁵⁶, A. Gabrielli [id](#)^{24b,24a}, A. Gabrielli [id](#)¹⁶², P. Gadow [id](#)³⁷, G. Gagliardi [id](#)^{58b,58a},
 L.G. Gagnon [id](#)^{18a}, S. Gaid [id](#)^{89b}, S. Galantzan [id](#)¹⁵⁸, J. Gallagher [id](#)¹, E.J. Gallas [id](#)¹³⁰, A.L. Gallen [id](#)¹⁶⁸,
 B.J. Gallop [id](#)¹³⁸, K.K. Gan [id](#)¹²³, S. Ganguly [id](#)¹⁶⁰, Y. Gao [id](#)⁵³, A. Garabaglu [id](#)¹⁴³,
 F.M. Garay Walls [id](#)^{141a,141b}, B. Garcia³⁰, C. García [id](#)¹⁷⁰, A. Garcia Alonso [id](#)¹¹⁸,
 A.G. Garcia Caffaro [id](#)¹⁷⁹, J.E. García Navarro [id](#)¹⁷⁰, M. Garcia-Sciveres [id](#)^{18a}, G.L. Gardner [id](#)¹³²,
 R.W. Gardner [id](#)⁴¹, N. Garelli [id](#)¹⁶⁵, R.B. Garg [id](#)¹⁵⁰, J.M. Gargan [id](#)⁵³, C.A. Garner¹⁶², C.M. Garvey [id](#)^{34a},
 V.K. Gassmann¹⁶⁵, G. Gaudio [id](#)^{74a}, V. Gautam¹³, P. Gauzzi [id](#)^{76a,76b}, J. Gavranovic [id](#)⁹⁶,
 I.L. Gavrilenko [id](#)^{134a}, A. Gavrilyuk [id](#)³⁸, C. Gay [id](#)¹⁷¹, G. Gaycken [id](#)¹²⁷, E.N. Gazis [id](#)¹⁰, A. Gekow¹²³,
 C. Gemme [id](#)^{58b}, M.H. Genest [id](#)⁶¹, A.D. Gentry [id](#)¹¹⁶, S. George [id](#)⁹⁸, W.F. George [id](#)²¹, T. Geralis [id](#)⁴⁷,
 A.A. Gerwin [id](#)¹²⁴, P. Gessinger-Befurt [id](#)³⁷, M.E. Geyik [id](#)¹⁷⁸, M. Ghani [id](#)¹⁷⁴, K. Ghorbanian [id](#)⁹⁷,
 A. Ghosal [id](#)¹⁴⁸, A. Ghosh [id](#)¹⁶⁶, A. Ghosh [id](#)⁷, B. Giacobbe [id](#)^{24b}, S. Giagu [id](#)^{76a,76b}, T. Giani [id](#)¹¹⁸,
 A. Giannini [id](#)⁶³, S.M. Gibson [id](#)⁹⁸, M. Gignac [id](#)¹⁴⁰, D.T. Gil [id](#)^{87b}, A.K. Gilbert [id](#)^{87a}, B.J. Gilbert [id](#)⁴³,
 D. Gillberg [id](#)³⁵, G. Gilles [id](#)¹¹⁸, L. Ginabat [id](#)¹³¹, D.M. Gingrich [id](#)^{2,ah}, M.P. Giordani [id](#)^{70a,70c},
 P.F. Giraud [id](#)¹³⁹, G. Giugliarelli [id](#)^{70a,70c}, D. Giugni [id](#)^{72a}, F. Giuli [id](#)^{77a,77b}, I. Gkialas [id](#)^{9,j},
 L.K. Gladilin [id](#)³⁸, C. Glasman [id](#)¹⁰², G. Glemža [id](#)⁴⁹, M. Glisic¹²⁷, I. Gnesi [id](#)^{45b}, Y. Go [id](#)³⁰,
 M. Goblirsch-Kolb [id](#)³⁷, B. Gocke [id](#)⁵⁰, D. Godin¹¹¹, B. Gokturk [id](#)^{22a}, S. Goldfarb [id](#)¹⁰⁸, T. Golling [id](#)⁵⁷,
 M.G.D. Gololo [id](#)^{34c}, D. Golubkov [id](#)³⁸, J.P. Gombas [id](#)¹¹⁰, A. Gomes [id](#)^{134a,134b}, G. Gomes Da Silva [id](#)¹⁴⁸,
 A.J. Gomez Delegido [id](#)¹⁷⁰, R. Gonçalves [id](#)^{134a}, L. Gonella [id](#)²¹, A. Gongadze [id](#)^{156c}, F. Gonnella [id](#)²¹,
 J.L. Gonski [id](#)¹⁵⁰, R.Y. González Andana [id](#)⁵³, S. González de la Hoz [id](#)¹⁷⁰, C. Gonzalez Renteria [id](#)^{18a},
 M.V. Gonzalez Rodrigues [id](#)⁴⁹, R. Gonzalez Suarez [id](#)¹⁶⁸, S. Gonzalez-Sevilla [id](#)⁵⁷, L. Goossens [id](#)³⁷,
 B. Gorini [id](#)³⁷, E. Gorini [id](#)^{71a,71b}, A. Gorišek [id](#)⁹⁶, T.C. Gosart [id](#)¹³², A.T. Goshaw [id](#)⁵², M.I. Gostkin [id](#)⁴⁰,
 S. Goswami [id](#)¹²⁵, C.A. Gottardo [id](#)³⁷, S.A. Gotz [id](#)¹¹², M. Gouighri [id](#)^{36b}, A.G. Goussiou [id](#)¹⁴³,
 N. Govender [id](#)^{34c}, R.P. Grabarczyk [id](#)¹³⁰, I. Grabowska-Bold [id](#)^{87a}, K. Graham [id](#)³⁵, E. Gramstad [id](#)¹²⁹,
 S. Grancagnolo [id](#)^{71a,71b}, C.M. Grant^{1,139}, P.M. Gravila [id](#)^{28f}, F.G. Gravili [id](#)^{71a,71b}, H.M. Gray [id](#)^{18a},
 M. Greco [id](#)¹¹³, M.J. Green [id](#)¹, C. Grefe [id](#)²⁵, A.S. Grefsrud [id](#)¹⁷, I.M. Gregor [id](#)⁴⁹, K.T. Greif [id](#)¹⁶⁶,
 P. Grenier [id](#)¹⁵⁰, S.G. Grewe¹¹³, A.A. Grillo [id](#)¹⁴⁰, K. Grimm [id](#)³², S. Grinstein [id](#)^{13,y}, J.-F. Grivaz [id](#)⁶⁷,
 E. Gross [id](#)¹⁷⁶, J. Grosse-Knetter [id](#)⁵⁶, L. Guan [id](#)¹⁰⁹, G. Guerrieri [id](#)³⁷, R. Guevara [id](#)¹²⁹, R. Gugel [id](#)¹⁰³,
 J.A.M. Guhit [id](#)¹⁰⁹, A. Guida [id](#)¹⁹, E. Guilloton [id](#)¹⁷⁴, S. Guindon [id](#)³⁷, F. Guo [id](#)^{14,115c}, J. Guo [id](#)^{145a},

L. Guo ⁴⁹, L. Guo ^{115b,w}, Y. Guo ¹⁰⁹, A. Gupta ⁵⁰, R. Gupta ¹³³, S. Gurbuz ²⁵,
 S.S. Gurdasani ⁴⁹, G. Gustavino ^{76a,76b}, P. Gutierrez ¹²⁴, L.F. Gutierrez Zagazeta ¹³²,
 M. Gutsche ⁵¹, C. Gutschow ⁹⁹, C. Gwenlan ¹³⁰, C.B. Gwilliam ⁹⁵, E.S. Haaland ¹²⁹,
 A. Haas ¹²¹, M. Habedank ⁶⁰, C. Haber ^{18a}, H.K. Hadavand ⁸, A. Haddad ⁴², A. Hadeef ⁵¹,
 A.I. Hagan ⁹⁴, J.J. Hahn ¹⁴⁸, E.H. Haines ⁹⁹, M. Haleem ¹⁷³, J. Haley ¹²⁵, G.D. Hallewell ¹⁰⁵,
 L. Halser ²⁰, K. Hamano ¹⁷², M. Hamer ²⁵, S.E.D. Hammoud ⁶⁷, E.J. Hampshire ⁹⁸,
 J. Han ^{144a}, L. Han ^{115a}, L. Han ⁶³, S. Han ^{18a}, K. Hanagaki ⁸⁵, M. Hance ¹⁴⁰, D.A. Hangal ⁴³,
 H. Hanif ¹⁴⁹, M.D. Hank ¹³², J.B. Hansen ⁴⁴, P.H. Hansen ⁴⁴, D. Harada ⁵⁷, T. Harenberg ¹⁷⁸,
 S. Harkusha ¹⁸⁰, M.L. Harris ¹⁰⁶, Y.T. Harris ²⁵, J. Harrison ¹³, N.M. Harrison ¹²³,
 P.F. Harrison ¹⁷⁴, N.M. Hartman ¹¹³, N.M. Hartmann ¹¹², R.Z. Hasan ^{98,138}, Y. Hasegawa ¹⁴⁷,
 F. Haslbeck ¹³⁰, S. Hassan ¹⁷, R. Hauser ¹¹⁰, M. Haviernik ¹³⁷, C.M. Hawkes ²¹,
 R.J. Hawkings ³⁷, Y. Hayashi ¹⁶⁰, D. Hayden ¹¹⁰, C. Hayes ¹⁰⁹, R.L. Hayes ¹¹⁸, C.P. Hays ¹³⁰,
 J.M. Hays ⁹⁷, H.S. Hayward ⁹⁵, F. He ⁶³, M. He ^{14,115c}, Y. He ⁴⁹, Y. He ⁹⁹, N.B. Heatley ⁹⁷,
 V. Hedberg ¹⁰¹, A.L. Heggelund ¹²⁹, C. Heidegger ⁵⁵, K.K. Heidegger ⁵⁵, J. Heilman ³⁵,
 S. Heim ⁴⁹, T. Heim ^{18a}, J.G. Heinlein ¹³², J.J. Heinrich ¹²⁷, L. Heinrich ^{113,af}, J. Hejbal ¹³⁵,
 A. Held ¹⁷⁷, S. Hellesund ¹⁷, C.M. Helling ¹⁷¹, S. Hellman ^{48a,48b}, L. Henkelmann ³³,
 A.M. Henriques Correia ³⁷, H. Herde ¹⁰¹, Y. Hernández Jiménez ¹⁵², L.M. Herrmann ²⁵,
 T. Herrmann ⁵¹, G. Herten ⁵⁵, R. Hertenberger ¹¹², L. Hervas ³⁷, M.E. Hesping ¹⁰³,
 N.P. Hessey ^{163a}, J. Hessler ¹¹³, M. Hidaoui ^{36b}, N. Hidic ¹³⁷, E. Hill ¹⁶², S.J. Hillier ²¹,
 J.R. Hinds ¹¹⁰, F. Hinterkeuser ²⁵, M. Hirose ¹²⁸, S. Hirose ¹⁶⁴, D. Hirschbuehl ¹⁷⁸,
 T.G. Hitchings ¹⁰⁴, B. Hiti ⁹⁶, J. Hobbs ¹⁵², R. Hobincu ^{28e}, N. Hod ¹⁷⁶, M.C. Hodgkinson ¹⁴⁶,
 B.H. Hodgkinson ¹³⁰, A. Hoecker ³⁷, D.D. Hofer ¹⁰⁹, J. Hofer ¹⁷⁰, M. Holzbock ³⁷,
 L.B.A.H. Hommels ³³, V. Homsak ¹³⁰, B.P. Honan ¹⁰⁴, J.J. Hong ⁶⁹, J. Hong ^{145a},
 T.M. Hong ¹³³, B.H. Hooberman ¹⁶⁹, W.H. Hopkins ⁶, M.C. Hoppesch ¹⁶⁹, Y. Horii ¹¹⁴,
 M.E. Horstmann ¹¹³, S. Hou ¹⁵⁵, M.R. Housenga ¹⁶⁹, A.S. Howard ⁹⁶, J. Howarth ⁶⁰, J. Hoya ⁶,
 M. Hrabovsky ¹²⁶, T. Hryn'ova ⁴, P.J. Hsu ⁶⁶, S.-C. Hsu ¹⁴³, T. Hsu ⁶⁷, M. Hu ^{18a}, Q. Hu ⁶³,
 S. Huang ³³, X. Huang ^{14,115c}, Y. Huang ¹³⁷, Y. Huang ^{115b}, Y. Huang ¹⁰³, Y. Huang ¹⁴,
 Z. Huang ¹⁰⁴, Z. Hubacek ¹³⁶, M. Huebner ²⁵, F. Huegging ²⁵, T.B. Huffman ¹³⁰,
 M. Hufnagel Maranha De Faria ^{84a}, C.A. Hugli ⁴⁹, M. Huhtinen ³⁷, S.K. Huiberts ¹⁷,
 R. Hulskens ¹⁰⁷, C.E. Hultquist ^{18a}, N. Huseynov ^{12,g}, J. Huston ¹¹⁰, J. Huth ⁶², R. Hyneman ⁷,
 G. Iacobucci ⁵⁷, G. Iakovidis ³⁰, L. Iconomidou-Fayard ⁶⁷, J.P. Iddon ³⁷, P. Iengo ^{73a,73b},
 R. Iguchi ¹⁶⁰, Y. Iiyama ¹⁶⁰, T. Iizawa ¹³⁰, Y. Ikegami ⁸⁵, D. Iliadis ¹⁵⁹, N. Ilic ¹⁶²,
 H. Imam ^{84c}, G. Inacio Goncalves ^{84d}, S.A. Infante Cabanas ^{141c}, T. Ingebretsen Carlson ^{48a,48b},
 J.M. Inglis ⁹⁷, G. Introzzi ^{74a,74b}, M. Iodice ^{78a}, V. Ippolito ^{76a,76b}, R.K. Irwin ⁹⁵, M. Ishino ¹⁶⁰,
 W. Islam ¹⁷⁷, C. Issever ¹⁹, S. Istin ^{22a,am}, K. Itabashi ⁸⁵, H. Ito ¹⁷⁵, R. Iuppa ^{79a,79b}, A. Ivina ¹⁷⁶,
 V. Izzo ^{73a}, P. Jacka ¹³⁵, P. Jackson ¹, P. Jain ⁴⁹, K. Jakobs ⁵⁵, T. Jakoubek ¹⁷⁶, J. Jamieson ⁶⁰,
 W. Jang ¹⁶⁰, S. Jankovych ¹³⁷, M. Javurkova ¹⁰⁶, P. Jawahar ¹⁰⁴, L. Jeanty ¹²⁷, J. Jejelava ^{156a},
 P. Jenni ^{55,f}, C.E. Jessiman ³⁵, C. Jia ^{144a}, H. Jia ¹⁷¹, J. Jia ¹⁵², X. Jia ^{14,115c}, Z. Jia ^{115a},
 C. Jiang ⁵³, Q. Jiang ^{65b}, S. Jiggins ⁴⁹, J. Jimenez Pena ¹³, S. Jin ^{115a}, A. Jinaru ^{28b},
 O. Jinnouchi ¹⁴², P. Johansson ¹⁴⁶, K.A. Johns ⁷, J.W. Johnson ¹⁴⁰, F.A. Jolly ⁴⁹,
 D.M. Jones ¹⁵³, E. Jones ⁴⁹, K.S. Jones ⁸, P. Jones ³³, R.W.L. Jones ⁹⁴, T.J. Jones ⁹⁵,
 H.L. Joos ^{56,37}, R. Joshi ¹²³, J. Jovicevic ¹⁶, X. Ju ^{18a}, J.J. Junggeburth ³⁷, T. Junkermann ^{64a},
 A. Juste Rozas ^{13,y}, M.K. Juzek ⁸⁸, S. Kabana ^{141e}, A. Kaczmarska ⁸⁸, M. Kado ¹¹³,
 H. Kagan ¹²³, M. Kagan ¹⁵⁰, A. Kahn ¹³², C. Kahra ¹⁰³, T. Kaji ¹⁶⁰, E. Kajomovitz ¹⁵⁷,
 N. Kakati ¹⁷⁶, N. Kakoty ¹³, I. Kalaitzidou ⁵⁵, S. Kandel ⁸, N.J. Kang ¹⁴⁰, D. Kar ^{34g},
 K. Karava ¹³⁰, E. Karentzos ²⁵, O. Karkout ¹¹⁸, S.N. Karpov ⁴⁰, Z.M. Karpova ⁴⁰,
 V. Kartvelishvili ⁹⁴, A.N. Karyukhin ³⁸, E. Kasimi ¹⁵⁹, J. Katzy ⁴⁹, S. Kaur ³⁵, K. Kawade ¹⁴⁷,

M.P. Kawale [ID124](#), C. Kawamoto [ID90](#), T. Kawamoto [ID63](#), E.F. Kay [ID37](#), F.I. Kaya [ID165](#), S. Kazakos [ID110](#),
V.F. Kazanin [ID38](#), Y. Ke [ID152](#), J.M. Keaveney [ID34a](#), R. Keeler [ID172](#), G.V. Kehris [ID62](#), J.S. Keller [ID35](#),
J.J. Kempster [ID153](#), O. Kepka [ID135](#), J. Kerr [ID163b](#), B.P. Kerridge [ID138](#), B.P. Kerševan [ID96](#),
L. Keszeghova [ID29a](#), R.A. Khan [ID133](#), A. Khanov [ID125](#), A.G. Kharlamov [ID38](#), T. Kharlamova [ID38](#),
E.E. Khoda [ID143](#), M. Kholodenko [ID134a](#), T.J. Khoo [ID19](#), G. Khoriali [ID173](#), J. Khubua [ID156b,*](#),
Y.A.R. Khwaira [ID131](#), B. Kibirige [ID34g](#), D. Kim [ID6](#), D.W. Kim [ID48a,48b](#), Y.K. Kim [ID41](#), N. Kimura [ID99](#),
M.K. Kingston [ID56](#), A. Kirchhoff [ID56](#), C. Kirfel [ID25](#), F. Kirfel [ID25](#), J. Kirk [ID138](#), A.E. Kiryunin [ID113](#),
S. Kita [ID164](#), C. Kitsaki [ID10](#), O. Kivernyk [ID25](#), M. Klassen [ID165](#), C. Klein [ID35](#), L. Klein [ID173](#),
M.H. Klein [ID46](#), S.B. Klein [ID57](#), U. Klein [ID95](#), A. Klimentov [ID30](#), T. Klioutchnikova [ID37](#), P. Kluit [ID118](#),
S. Kluth [ID113](#), E. Kneringer [ID80](#), T.M. Knight [ID162](#), A. Knue [ID50](#), D. Kobylanskii [ID176](#), S.F. Koch [ID130](#),
M. Kocian [ID150](#), P. Kodyš [ID137](#), D.M. Koeck [ID127](#), P.T. Koenig [ID25](#), T. Koffas [ID35](#), O. Kolay [ID51](#),
I. Koletsou [ID4](#), T. Komarek [ID88](#), K. Köneke [ID56](#), A.X.Y. Kong [ID1](#), T. Kono [ID122](#), N. Konstantinidis [ID99](#),
P. Kontaxakis [ID57](#), B. Konya [ID101](#), R. Kopeliansky [ID43](#), S. Koperny [ID87a](#), K. Korcyl [ID88](#),
K. Kordas [ID159,e](#), A. Korn [ID99](#), S. Korn [ID56](#), I. Korolkov [ID13](#), N. Korotkova [ID38](#), B. Kortman [ID118](#),
O. Kortner [ID113](#), S. Kortner [ID113](#), W.H. Kostecka [ID119](#), M. Kostov [ID29a](#), V.V. Kostyukhin [ID148](#),
A. Kotsokechagia [ID37](#), A. Kotwal [ID52](#), A. Koulouris [ID37](#), A. Kourkoumeli-Charalampidi [ID74a,74b](#),
C. Kourkoumelis [ID9](#), E. Kourlitis [ID113,af](#), O. Kovanda [ID127](#), R. Kowalewski [ID172](#), W. Kozanecki [ID127](#),
A.S. Kozhin [ID38](#), V.A. Kramarenko [ID38](#), G. Kramberger [ID96](#), P. Kramer [ID25](#), M.W. Krasny [ID131](#),
A. Krasznahorkay [ID106](#), A.C. Kraus [ID119](#), J.W. Kraus [ID178](#), J.A. Kremer [ID49](#), N.B. Kregel [ID148](#),
T. Kresse [ID51](#), L. Kretschmann [ID178](#), J. Kretzschmar [ID95](#), K. Kreul [ID19](#), P. Krieger [ID162](#), K. Krizka [ID21](#),
K. Kroeninger [ID50](#), H. Kroha [ID113](#), J. Kroll [ID135](#), J. Kroll [ID132](#), K.S. Krowpman [ID110](#), U. Kruchonak [ID40](#),
H. Krüger [ID25](#), N. Krumnack [ID82](#), M.C. Kruse [ID52](#), O. Kuchinskaia [ID40](#), S. Kuday [ID3a](#), S. Kuehn [ID37](#),
R. Kuesters [ID55](#), T. Kuhl [ID49](#), V. Kukhtin [ID40](#), Y. Kulchitsky [ID40](#), S. Kuleshov [ID141d,141b](#), M. Kumar [ID34g](#),
N. Kumari [ID49](#), P. Kumari [ID163b](#), A. Kupco [ID135](#), T. Kupfer [ID50](#), A. Kupich [ID38](#), O. Kuprash [ID55](#),
H. Kurashige [ID86](#), L.L. Kurchaninov [ID163a](#), O. Kurdysh [ID4](#), Y.A. Kurochkin [ID39](#), A. Kurova [ID38](#),
M. Kuze [ID142](#), A.K. Kvam [ID106](#), J. Kvita [ID126](#), N.G. Kyriacou [ID109](#), L.A.O. Laatu [ID105](#), C. Lacasta [ID170](#),
F. Lacava [ID76a,76b](#), H. Lacker [ID19](#), D. Lacour [ID131](#), N.N. Lad [ID99](#), E. Ladygin [ID40](#), A. Lafarge [ID42](#),
B. Laforge [ID131](#), T. Lagouri [ID179](#), F.Z. Lahbabi [ID36a](#), S. Lai [ID56](#), J.E. Lambert [ID172](#), S. Lammers [ID69](#),
W. Lampl [ID7](#), C. Lampoudis [ID159,e](#), G. Lamprinoudis [ID103](#), A.N. Lancaster [ID119](#), E. Lançon [ID30](#),
U. Landgraf [ID55](#), M.P.J. Landon [ID97](#), V.S. Lang [ID55](#), O.K.B. Langrekken [ID129](#), A.J. Lankford [ID166](#),
F. Lanni [ID37](#), K. Lantzsch [ID25](#), A. Lanza [ID74a](#), M. Lanzac Berrocal [ID170](#), J.F. Laporte [ID139](#), T. Lari [ID72a](#),
D. Larsen [ID17](#), F. Lasagni Manghi [ID24b](#), M. Lassnig [ID37](#), V. Latonova [ID135](#), S.D. Lawlor [ID146](#),
Z. Lawrence [ID104](#), R. Lazaridou [ID174](#), M. Lazzaroni [ID72a,72b](#), H.D.M. Le [ID110](#), E.M. Le Boulicaut [ID179](#),
L.T. Le Pottier [ID18a](#), B. Leban [ID24b,24a](#), M. LeBlanc [ID104](#), F. Ledroit-Guillon [ID61](#), S.C. Lee [ID155](#),
T.F. Lee [ID95](#), L.L. Leeuw [ID34c,ak](#), M. Lefebvre [ID172](#), C. Leggett [ID18a](#), G. Lehmann Miotto [ID37](#),
M. Leigh [ID57](#), W.A. Leight [ID106](#), W. Leinonen [ID117](#), A. Leisos [ID159,v](#), M.A.L. Leite [ID84c](#),
C.E. Leitgeb [ID19](#), R. Leitner [ID137](#), K.J.C. Leney [ID46](#), T. Lenz [ID25](#), S. Leone [ID75a](#), C. Leonidopoulos [ID53](#),
A. Leopold [ID151](#), J.H. Lepage Bourbonnais [ID35](#), R. Les [ID110](#), C.G. Lester [ID33](#), M. Levchenko [ID38](#),
J. Levêque [ID4](#), L.J. Levinson [ID176](#), G. Levrini [ID24b,24a](#), M.P. Lewicki [ID88](#), C. Lewis [ID143](#), D.J. Lewis [ID4](#),
L. Lewitt [ID146](#), A. Li [ID30](#), B. Li [ID144a](#), C. Li [ID109](#), C-Q. Li [ID113](#), H. Li [ID63](#), H. Li [ID144a](#), H. Li [ID104](#),
H. Li [ID15](#), H. Li [ID144a](#), J. Li [ID145a](#), K. Li [ID14](#), L. Li [ID145a](#), R. Li [ID179](#), S. Li [ID14,115c](#), S. Li [ID145b,145a,d](#),
T. Li [ID5](#), X. Li [ID107](#), Z. Li [ID160](#), Z. Li [ID14,115c](#), Z. Li [ID63](#), S. Liang [ID14,115c](#), Z. Liang [ID14](#),
M. Liberatore [ID139](#), B. Liberti [ID77a](#), K. Lie [ID65c](#), J. Lieber Marin [ID84e](#), H. Lien [ID69](#), H. Lin [ID109](#),
L. Linden [ID112](#), R.E. Lindley [ID7](#), J.H. Lindon [ID2](#), J. Ling [ID62](#), E. Lipeles [ID132](#), A. Lipniacka [ID17](#),
A. Lister [ID171](#), J.D. Little [ID69](#), B. Liu [ID14](#), B.X. Liu [ID115b](#), D. Liu [ID145b,145a](#), E.H.L. Liu [ID21](#),
J.K.K. Liu [ID33](#), K. Liu [ID145b](#), K. Liu [ID145b,145a](#), M. Liu [ID63](#), M.Y. Liu [ID63](#), P. Liu [ID14](#),
Q. Liu [ID145b,143,145a](#), X. Liu [ID63](#), X. Liu [ID144a](#), Y. Liu [ID115b,115c](#), Y.L. Liu [ID144a](#), Y.W. Liu [ID63](#),



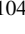















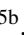





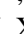




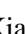









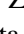
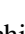
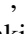
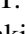




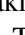
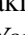




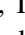



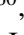
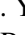
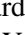



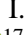
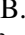
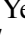
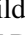



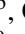
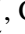
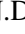


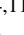
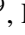
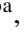

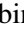




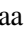

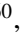

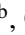
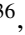








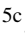
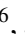

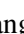




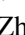
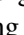


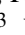
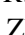
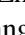




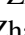

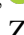





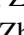

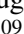


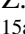
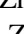



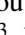

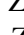




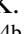
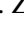




Z. Liu ^{67,1}, S.L. Lloyd ⁹⁷, E.M. Lobodzinska ⁴⁹, P. Loch ⁷, E. Lodhi ¹⁶², T. Lohse ¹⁹, K. Lohwasser ¹⁴⁶, E. Loiacono ⁴⁹, J.D. Lomas ²¹, J.D. Long ⁴³, I. Longarini ¹⁶⁶, R. Longo ¹⁶⁹, A. Lopez Solis ⁴⁹, N.A. Lopez-canelas ⁷, N. Lorenzo Martinez ⁴, A.M. Lory ¹¹², M. Losada ^{120a}, G. Löschcke Centeno ¹⁵³, O. Loseva ³⁸, X. Lou ^{48a,48b}, X. Lou ^{14,115c}, A. Lounis ⁶⁷, P.A. Love ⁹⁴, G. Lu ^{14,115c}, M. Lu ⁶⁷, S. Lu ¹³², Y.J. Lu ¹⁵⁵, H.J. Lubatti ¹⁴³, C. Luci ^{76a,76b}, F.L. Lucio Alves ^{115a}, F. Luehring ⁶⁹, B.S. Lunday ¹³², O. Lundberg ¹⁵¹, B. Lund-Jensen ^{151,*}, N.A. Luongo ⁶, M.S. Lutz ³⁷, A.B. Lux ²⁶, D. Lynn ³⁰, R. Lysak ¹³⁵, V. Lysenko ¹³⁶, E. Lytken ¹⁰¹, V. Lyubushkin ⁴⁰, T. Lyubushkina ⁴⁰, M.M. Lyukova ¹⁵², M.Firdaus M. Soberi ⁵³, H. Ma ³⁰, K. Ma ⁶³, L.L. Ma ^{144a}, W. Ma ⁶³, Y. Ma ¹²⁵, J.C. MacDonald ¹⁰³, P.C. Machado De Abreu Farias ^{84e}, R. Madar ⁴², T. Madula ⁹⁹, J. Maeda ⁸⁶, T. Maeno ³⁰, P.T. Mafa ^{34c,k}, H. Maguire ¹⁴⁶, V. Maiboroda ⁶⁷, A. Maio ^{134a,134b,134d}, K. Maj ^{87a}, O. Majersky ⁴⁹, S. Majewski ¹²⁷, R. Makhmanazarov ³⁸, N. Makovec ⁶⁷, V. Maksimovic ¹⁶, B. Malaescu ¹³¹, J. Malamant ¹²⁹, Pa. Malecki ⁸⁸, V.P. Maleev ³⁸, F. Malek ^{61,q}, M. Mali ⁹⁶, D. Malito ⁹⁸, U. Mallik ^{81,*}, S. Maltezos ¹⁰, A. Malvezzi Lopes ^{84d}, S. Malyukov ⁴⁰, J. Mamuzic ¹³, G. Mancini ⁵⁴, M.N. Mancini ²⁷, G. Manco ^{74a,74b}, J.P. Mandalia ⁹⁷, S.S. Mandarray ¹⁵³, I. Mandić ⁹⁶, L. Manhaes de Andrade Filho ^{84a}, I.M. Maniatis ¹⁷⁶, J. Manjarres Ramos ⁹², D.C. Mankad ¹⁷⁶, A. Mann ¹¹², S. Manzoni ³⁷, L. Mao ^{145a}, X. Mapekula ^{34c}, A. Marantis ^{159,v}, R.R. Marcelo Gregorio ⁹⁷, G. Marchiori ⁵, M. Marcisovsky ¹³⁵, C. Marcon ^{72a}, M. Marinescu ²¹, S. Marium ⁴⁹, M. Marjanovic ¹²⁴, A. Markhoos ⁵⁵, M. Markovitch ⁶⁷, M.K. Maroun ¹⁰⁶, E.J. Marshall ⁹⁴, Z. Marshall ^{18a}, S. Marti-Garcia ¹⁷⁰, J. Martin ⁹⁹, T.A. Martin ¹³⁸, V.J. Martin ⁵³, B. Martin dit Latour ¹⁷, L. Martinelli ^{76a,76b}, M. Martinez ^{13,y}, P. Martinez Agullo ¹⁷⁰, V.I. Martinez Outschoorn ¹⁰⁶, P. Martinez Suarez ¹³, S. Martin-Haugh ¹³⁸, G. Martinovicova ¹³⁷, V.S. Martoiu ^{28b}, A.C. Martyniuk ⁹⁹, A. Marzin ³⁷, D. Mascione ^{79a,79b}, L. Masetti ¹⁰³, J. Masik ¹⁰⁴, A.L. Maslennikov ⁴⁰, S.L. Mason ⁴³, P. Massarotti ^{73a,73b}, P. Mastrandrea ^{75a,75b}, A. Mastroberardino ^{45b,45a}, T. Masubuchi ¹²⁸, T.T. Mathew ¹²⁷, J. Matousek ¹³⁷, D.M. Mattern ⁵⁰, J. Maurer ^{28b}, T. Maurin ⁶⁰, A.J. Maury ⁶⁷, B. Maček ⁹⁶, D.A. Maximov ³⁸, A.E. May ¹⁰⁴, E. Mayer ⁴², R. Mazini ^{34g}, I. Maznas ¹¹⁹, M. Mazza ¹¹⁰, S.M. Mazza ¹⁴⁰, E. Mazzeo ^{72a,72b}, J.P. Mc Gowan ¹⁷², S.P. Mc Kee ¹⁰⁹, C.A. Mc Lean ⁶, C.C. McCracken ¹⁷¹, E.F. McDonald ¹⁰⁸, A.E. McDougall ¹¹⁸, L.F. Mcelhinney ⁹⁴, J.A. Mcfayden ¹⁵³, R.P. McGovern ¹³², R.P. Mckenzie ^{34g}, T.C. Mclachlan ⁴⁹, D.J. Mclaughlin ⁹⁹, S.J. McMahon ¹³⁸, C.M. Mcpartland ⁹⁵, R.A. McPherson ^{172,ac}, S. Mehlhase ¹¹², A. Mehta ⁹⁵, D. Melini ¹⁷⁰, B.R. Mellado Garcia ^{34g}, A.H. Melo ⁵⁶, F. Meloni ⁴⁹, A.M. Mendes Jacques Da Costa ¹⁰⁴, H.Y. Meng ¹⁶², L. Meng ⁹⁴, S. Menke ¹¹³, M. Mentink ³⁷, E. Meoni ^{45b,45a}, G. Mercado ¹¹⁹, S. Merianos ¹⁵⁹, C. Merlassino ^{70a,70c}, C. Meroni ^{72a,72b}, J. Metcalfe ⁶, A.S. Mete ⁶, E. Meuser ¹⁰³, C. Meyer ⁶⁹, J-P. Meyer ¹³⁹, R.P. Middleton ¹³⁸, L. Mijović ⁵³, G. Mikenberg ¹⁷⁶, M. Mikesstikova ¹³⁵, M. Mikuš ⁹⁶, H. Mildner ¹⁰³, A. Milic ³⁷, D.W. Miller ⁴¹, E.H. Miller ¹⁵⁰, L.S. Miller ³⁵, A. Milov ¹⁷⁶, D.A. Milstead ^{48a,48b}, T. Min ^{115a}, A.A. Minaenko ³⁸, I.A. Minashvili ^{156b}, A.I. Mincer ¹²¹, B. Mindur ^{87a}, M. Mineev ⁴⁰, Y. Mino ⁹⁰, L.M. Mir ¹³, M. Miralles Lopez ⁶⁰, M. Mironova ^{18a}, M.C. Missio ¹¹⁷, A. Mitra ¹⁷⁴, V.A. Mitsou ¹⁷⁰, Y. Mitsumori ¹¹⁴, O. Miu ¹⁶², P.S. Miyagawa ⁹⁷, T. Mkrtchyan ^{64a}, M. Mlinarevic ⁹⁹, T. Mlinarevic ⁹⁹, M. Mlynarikova ³⁷, S. Mobius ²⁰, P. Mogg ¹¹², M.H. Mohamed Farook ¹¹⁶, A.F. Mohammed ^{14,115c}, S. Mohapatra ⁴³, S. Mohiuddin ¹²⁵, G. Mokgatitwane ^{34g}, L. Moleri ¹⁷⁶, B. Mondal ¹⁴⁸, S. Mondal ¹³⁶, K. Mönig ⁴⁹, E. Monnier ¹⁰⁵, L. Monsonis Romero ¹⁷⁰, J. Montejo Berlingen ¹³, A. Montella ^{48a,48b}, M. Montella ¹²³, F. Montekali ^{78a,78b}, F. Monticelli ⁹³, S. Monzani ^{70a,70c}, A. Morancho Tarda ⁴⁴, N. Morange ⁶⁷, A.L. Moreira De Carvalho ⁴⁹, M. Moreno Llácer ¹⁷⁰, C. Moreno Martinez ⁵⁷, J.M. Moreno Perez ^{23b}, P. Morettini ^{58b}, S. Morgenstern ³⁷, M. Morii ⁶², M. Morinaga ¹⁶⁰,

M. Moritsu ⁹¹, F. Morodei ^{76a,76b}, P. Moschovakos ³⁷, B. Moser ¹³⁰, M. Mosidze ^{156b},
T. Moskalets ⁴⁶, P. Moskvitina ¹¹⁷, J. Moss ^{32,n}, P. Moszkowicz ^{87a}, A. Moussa ^{36d},
Y. Moyal ¹⁷⁶, E.J.W. Moyse ¹⁰⁶, O. Mtintsilana ^{34g}, S. Muanza ¹⁰⁵, J. Mueller ¹³³, R. Müller ³⁷,
G.A. Mullier ¹⁶⁸, A.J. Mullin ³³, J.J. Mullin ⁵², A.E. Mulski ⁶², D.P. Mungo ¹⁶², D. Munoz Perez ¹⁷⁰,
F.J. Munoz Sanchez ¹⁰⁴, M. Murin ¹⁰⁴, W.J. Murray ^{174,138}, M. Muškinja ⁹⁶, C. Mwewa ³⁰,
A.G. Myagkov ^{38,a}, A.J. Myers ⁸, G. Myers ¹⁰⁹, M. Myska ¹³⁶, B.P. Nachman ^{18a}, K. Nagai ¹³⁰,
K. Nagano ⁸⁵, R. Nagasaka ¹⁶⁰, J.L. Nagle ^{30,aj}, E. Nagy ¹⁰⁵, A.M. Nairz ³⁷, Y. Nakahama ⁸⁵,
K. Nakamura ⁸⁵, K. Nakkalil ⁵, H. Nanjo ¹²⁸, E.A. Narayanan ⁴⁶, Y. Narukawa ¹⁶⁰,
I. Naryshkin ³⁸, L. Nasella ^{72a,72b}, S. Nasri ^{120b}, C. Nass ²⁵, G. Navarro ^{23a},
J. Navarro-Gonzalez ¹⁷⁰, A. Nayaz ¹⁹, P.Y. Nechaeva ³⁸, S. Nechaeva ^{24b,24a}, F. Nechansky ¹³⁵,
L. Nedic ¹³⁰, T.J. Neep ²¹, A. Negri ^{74a,74b}, M. Negrini ^{24b}, C. Nellist ¹¹⁸, C. Nelson ¹⁰⁷,
K. Nelson ¹⁰⁹, S. Nemecek ¹³⁵, M. Nessi ^{37,h}, M.S. Neubauer ¹⁶⁹, J. Newell ⁹⁵,
P.R. Newman ²¹, Y.W.Y. Ng ¹⁶⁹, B. Ngair ^{120a}, H.D.N. Nguyen ¹¹¹, R.B. Nickerson ¹³⁰,
R. Nicolaidou ¹³⁹, J. Nielsen ¹⁴⁰, M. Niemeyer ⁵⁶, J. Niermann ³⁷, N. Nikiforou ³⁷,
V. Nikolaenko ^{38,a}, I. Nikolic-Audit ¹³¹, P. Nilsson ³⁰, I. Ninca ⁴⁹, G. Ninio ¹⁵⁸, A. Nisati ^{76a},
N. Nishu ², R. Nisius ¹¹³, N. Nitika ^{70a,70c}, J-E. Nitschke ⁵¹, E.K. Nkadimeng ^{34g}, T. Nobe ¹⁶⁰,
T. Nommensen ¹⁵⁴, M.B. Norfolk ¹⁴⁶, B.J. Norman ³⁵, M. Noury ^{36a}, J. Novak ⁹⁶, T. Novak ⁹⁶,
R. Novotny ¹¹⁶, L. Nozka ¹²⁶, K. Ntekas ¹⁶⁶, N.M.J. Nunes De Moura Junior ^{84b}, J. Ocariz ¹³¹,
A. Ochi ⁸⁶, I. Ochoa ^{134a}, S. Oerdek ^{49,z}, J.T. Offermann ⁴¹, A. Ogrodnik ¹³⁷, A. Oh ¹⁰⁴,
C.C. Ohm ¹⁵¹, H. Oide ⁸⁵, R. Oishi ¹⁶⁰, M.L. Ojeda ³⁷, Y. Okumura ¹⁶⁰, L.F. Oleiro Seabra ^{134a},
I. Oleksiyuk ⁵⁷, S.A. Olivares Pino ^{141d}, G. Oliveira Correa ¹³, D. Oliveira Damazio ³⁰,
J.L. Oliver ¹⁶⁶, Ö.O. Öncel ⁵⁵, A.P. O'Neill ²⁰, A. Onofre ^{134a,134e}, P.U.E. Onyisi ¹¹,
M.J. Oreglia ⁴¹, D. Orestano ^{78a,78b}, R. Orlandini ^{78a,78b}, R.S. Orr ¹⁶², L.M. Osojnak ¹³²,
Y. Osumi ¹¹⁴, G. Otero y Garzon ³¹, H. Otono ⁹¹, G.J. Ottino ^{18a}, M. Ouchrif ^{36d},
F. Ould-Saada ¹²⁹, T. Ovsiannikova ¹⁴³, M. Owen ⁶⁰, R.E. Owen ¹³⁸, V.E. Ozcan ^{22a},
F. Ozturk ⁸⁸, N. Ozturk ⁸, S. Ozturk ⁸³, H.A. Pacey ¹³⁰, K. Pachal ^{163a}, A. Pacheco Pages ¹³,
C. Padilla Aranda ¹³, G. Padovano ^{76a,76b}, S. Pagan Griso ^{18a}, G. Palacino ⁶⁹, A. Palazzo ^{71a,71b},
J. Pampel ²⁵, J. Pan ¹⁷⁹, T. Pan ^{65a}, D.K. Panchal ¹¹, C.E. Pandini ¹¹⁸,
J.G. Panduro Vazquez ¹³⁸, H.D. Pandya ¹, H. Pang ¹³⁹, P. Pani ⁴⁹, G. Panizzo ^{70a,70c},
L. Panwar ¹³¹, L. Paolozzi ⁵⁷, S. Parajuli ¹⁶⁹, A. Paramonov ⁶, C. Paraskevopoulos ⁵⁴,
D. Paredes Hernandez ^{65b}, A. Pareti ^{74a,74b}, K.R. Park ⁴³, T.H. Park ¹¹³, F. Parodi ^{58b,58a},
J.A. Parsons ⁴³, U. Parzefall ⁵⁵, B. Pascual Dias ⁴², L. Pascual Dominguez ¹⁰², E. Pasqualucci ^{76a},
S. Passaggio ^{58b}, F. Pastore ⁹⁸, P. Patel ⁸⁸, U.M. Patel ⁵², J.R. Pater ¹⁰⁴, T. Pauly ³⁷,
F. Pauwels ¹³⁷, C.I. Pazos ¹⁶⁵, M. Pedersen ¹²⁹, R. Pedro ^{134a}, S.V. Peleganchuk ³⁸, O. Penc ³⁷,
E.A. Pender ⁵³, S. Peng ¹⁵, G.D. Penn ¹⁷⁹, K.E. Pensi ¹¹², M. Penzin ³⁸, B.S. Peralva ^{84d},
A.P. Pereira Peixoto ¹⁴³, L. Pereira Sanchez ¹⁵⁰, D.V. Perepelitsa ^{30,aj}, G. Perera ¹⁰⁶,
E. Perez Codina ^{163a}, M. Perganti ¹⁰, H. Pernegger ³⁷, S. Perrella ^{76a,76b}, O. Perrin ⁴²,
K. Peters ⁴⁹, R.F.Y. Peters ¹⁰⁴, B.A. Petersen ³⁷, T.C. Petersen ⁴⁴, E. Petit ¹⁰⁵, V. Petousis ¹³⁶,
A.R. Petri ^{72a,72b}, C. Petridou ^{159,e}, T. Petru ¹³⁷, A. Petrukhin ¹⁴⁸, M. Pettee ^{18a}, A. Petukhov ⁸³,
K. Petukhova ³⁷, R. Pezoa ^{141f}, L. Pezzotti ^{24b,24a}, G. Pezzullo ¹⁷⁹, L. Pfaffenbichler ³⁷,
A.J. Pflieger ³⁷, T.M. Pham ¹⁷⁷, T. Pham ¹⁰⁸, P.W. Phillips ¹³⁸, G. Piacquadio ¹⁵², E. Pianori ^{18a},
F. Piazza ¹²⁷, R. Piegai ³¹, D. Pietreanu ^{28b}, A.D. Pilkington ¹⁰⁴, M. Pinamonti ^{70a,70c},
J.L. Pinfeld ², B.C. Pinheiro Pereira ^{134a}, J. Pinol Bel ¹³, A.E. Pinto Pinoargote ¹³¹,
L. Pintucci ^{70a,70c}, K.M. Piper ¹⁵³, A. Pirttikoski ⁵⁷, D.A. Pizzi ³⁵, L. Pizzimento ^{65b},
A. Plebani ³³, M.-A. Pleier ³⁰, V. Pleskot ¹³⁷, E. Plotnikova ⁴⁰, G. Poddar ⁹⁷, R. Poettgen ¹⁰¹,
L. Poggioli ¹³¹, S. Polacek ¹³⁷, G. Polesello ^{74a}, A. Poley ^{149,163a}, A. Polini ^{24b}, C.S. Pollard ¹⁷⁴,
Z.B. Pollock ¹²³, E. Pompa Pacchi ¹²⁴, N.I. Pond ⁹⁹, D. Ponomarenko ⁶⁹, L. Pontecorvo ³⁷,

S. Popa [ID28a](#), G.A. Popeneciu [ID28d](#), A. Poreba [ID37](#), D.M. Portillo Quintero [ID163a](#), S. Pospisil [ID136](#),
 M.A. Postill [ID146](#), P. Postolache [ID28c](#), K. Potamianos [ID174](#), P.A. Potepa [ID87a](#), I.N. Potrap [ID40](#),
 C.J. Potter [ID33](#), H. Potti [ID154](#), J. Poveda [ID170](#), M.E. Pozo Astigarraga [ID37](#), A. Prades Ibanez [ID77a,77b](#),
 J. Pretel [ID172](#), D. Price [ID104](#), M. Primavera [ID71a](#), L. Primomo [ID70a,70c](#), M.A. Principe Martin [ID102](#),
 R. Privara [ID126](#), T. Procter [ID60](#), M.L. Proffitt [ID143](#), N. Proklova [ID132](#), K. Prokofiev [ID65c](#), G. Proto [ID113](#),
 J. Proudfoot [ID6](#), M. Przybycien [ID87a](#), W.W. Przygoda [ID87b](#), A. Psallidas [ID47](#), J.E. Puddefoot [ID146](#),
 D. Pudzha [ID55](#), D. Pyatiiizbyantseva [ID117](#), J. Qian [ID109](#), R. Qian [ID110](#), D. Qichen [ID104](#), Y. Qin [ID13](#),
 T. Qiu [ID53](#), A. Quadt [ID56](#), M. Queitsch-Maitland [ID104](#), G. Quetant [ID57](#), R.P. Quinn [ID171](#),
 G. Rabanal Bolanos [ID62](#), D. Rafanoharana [ID55](#), F. Raffaelli [ID77a,77b](#), F. Ragusa [ID72a,72b](#), J.L. Rainbolt [ID41](#),
 J.A. Raine [ID57](#), S. Rajagopalan [ID30](#), E. Ramakoti [ID38](#), L. Rambelli [ID58b,58a](#), I.A. Ramirez-Berend [ID35](#),
 K. Ran [ID49,115c](#), D.S. Rankin [ID132](#), N.P. Rapheeha [ID34g](#), H. Rasheed [ID28b](#), V. Raskina [ID131](#),
 D.F. Rassloff [ID64a](#), A. Rastogi [ID18a](#), S. Rave [ID103](#), S. Ravera [ID58b,58a](#), B. Ravina [ID37](#), I. Ravinovich [ID176](#),
 M. Raymond [ID37](#), A.L. Read [ID129](#), N.P. Readioff [ID146](#), D.M. Rebuzzi [ID74a,74b](#), A.S. Reed [ID113](#),
 K. Reeves [ID27](#), J.A. Reidelsturz [ID178](#), D. Reikher [ID127](#), A. Rej [ID50](#), C. Rembser [ID37](#), H. Ren [ID63](#),
 M. Renda [ID28b](#), F. Renner [ID49](#), A.G. Rennie [ID166](#), A.L. Rescia [ID49](#), S. Resconi [ID72a](#),
 M. Ressegotti [ID58b,58a](#), S. Rettie [ID37](#), W.F. Rettie [ID35](#), J.G. Reyes Rivera [ID110](#), E. Reynolds [ID18a](#),
 O.L. Rezanova [ID40](#), P. Reznicek [ID137](#), H. Riani [ID36d](#), N. Ribaric [ID52](#), E. Ricci [ID79a,79b](#), R. Richter [ID113](#),
 S. Richter [ID48a,48b](#), E. Richter-Was [ID87b](#), M. Ridel [ID131](#), S. Ridouani [ID36d](#), P. Rieck [ID121](#), P. Riedler [ID37](#),
 E.M. Riefel [ID48a,48b](#), J.O. Rieger [ID118](#), M. Rijssenbeek [ID152](#), M. Rimoldi [ID37](#), L. Rinaldi [ID24b,24a](#),
 P. Rincke [ID56,168](#), G. Ripellino [ID168](#), I. Riu [ID13](#), J.C. Rivera Vergara [ID172](#), F. Rizatdinova [ID125](#),
 E. Rizvi [ID97](#), B.R. Roberts [ID18a](#), S.S. Roberts [ID140](#), D. Robinson [ID33](#), M. Robles Manzano [ID103](#),
 A. Robson [ID60](#), A. Rocchi [ID77a,77b](#), C. Roda [ID75a,75b](#), S. Rodriguez Bosca [ID37](#), Y. Rodriguez Garcia [ID23a](#),
 A.M. Rodríguez Vera [ID119](#), S. Roe [ID37](#), J.T. Roemer [ID37](#), O. Røhne [ID129](#), C.P.A. Roland [ID131](#), J. Roloff [ID30](#),
 A. Romaniouk [ID80](#), E. Romano [ID74a,74b](#), M. Romano [ID24b](#), A.C. Romero Hernandez [ID169](#),
 N. Rompotis [ID95](#), L. Roos [ID131](#), S. Rosati [ID76a](#), B.J. Rosser [ID41](#), E. Rossi [ID130](#), E. Rossi [ID73a,73b](#),
 L.P. Rossi [ID62](#), L. Rossini [ID55](#), R. Rosten [ID123](#), M. Rotaru [ID28b](#), B. Rottler [ID55](#), D. Rousseau [ID67](#),
 D. Rousso [ID49](#), S. Roy-Garand [ID162](#), A. Rozanov [ID105](#), Z.M.A. Rozario [ID60](#), Y. Rozen [ID157](#),
 A. Rubio Jimenez [ID170](#), V.H. Ruelas Rivera [ID19](#), T.A. Ruggeri [ID1](#), A. Ruggiero [ID130](#),
 A. Ruiz-Martinez [ID170](#), A. Rummler [ID37](#), Z. Rurikova [ID55](#), N.A. Rusakovich [ID40](#), H.L. Russell [ID172](#),
 G. Russo [ID76a,76b](#), J.P. Rutherford [ID7](#), S. Rutherford Colmenares [ID33](#), M. Rybar [ID137](#),
 P. Rybczynski [ID87a](#), E.B. Rye [ID129](#), A. Ryzhov [ID46](#), J.A. Sabater Iglesias [ID57](#), H.F.W. Sadrozinski [ID140](#),
 F. Safai Tehrani [ID76a](#), S. Saha [ID1](#), M. Sahinsoy [ID83](#), A. Saibel [ID170](#), B.T. Saifuddin [ID124](#),
 M. Saimpert [ID139](#), M. Saito [ID160](#), T. Saito [ID160](#), A. Sala [ID72a,72b](#), D. Salamani [ID37](#), A. Salnikov [ID150](#),
 J. Salt [ID170](#), A. Salvador Salas [ID158](#), D. Salvatore [ID45b,45a](#), F. Salvatore [ID153](#), A. Salzburger [ID37](#),
 D. Sammel [ID55](#), E. Sampson [ID94](#), D. Sampsonidis [ID159,e](#), D. Sampsonidou [ID127](#), J. Sánchez [ID170](#),
 V. Sanchez Sebastian [ID170](#), H. Sandaker [ID129](#), C.O. Sander [ID49](#), J.A. Sandesara [ID106](#), M. Sandhoff [ID178](#),
 C. Sandoval [ID23b](#), L. Sanfilippo [ID64a](#), D.P.C. Sankey [ID138](#), T. Sano [ID90](#), A. Sansoni [ID54](#), L. Santi [ID37](#),
 C. Santoni [ID42](#), H. Santos [ID134a,134b](#), A. Santra [ID176](#), E. Sanzani [ID24b,24a](#), K.A. Saoucha [ID89b](#),
 J.G. Saraiva [ID134a,134d](#), J. Sardain [ID7](#), O. Sasaki [ID85](#), K. Sato [ID164](#), C. Sauer [ID37](#), E. Sauvan [ID4](#),
 P. Savard [ID162,ah](#), R. Sawada [ID160](#), C. Sawyer [ID138](#), L. Sawyer [ID100](#), C. Sbarra [ID24b](#), A. Sbrizzi [ID24b,24a](#),
 T. Scanlon [ID99](#), J. Schaarschmidt [ID143](#), U. Schäfer [ID103](#), A.C. Schaffer [ID67,46](#), D. Schaile [ID112](#),
 R.D. Schamberger [ID152](#), C. Scharf [ID19](#), M.M. Schefer [ID20](#), V.A. Schegelsky [ID38](#), D. Scheirich [ID137](#),
 M. Schernau [ID141e](#), C. Scheulen [ID57](#), C. Schiavi [ID58b,58a](#), M. Schioppa [ID45b,45a](#), B. Schlag [ID150](#),
 S. Schlenker [ID37](#), J. Schmeing [ID178](#), M.A. Schmidt [ID178](#), K. Schmieden [ID103](#), C. Schmitt [ID103](#),
 N. Schmitt [ID103](#), S. Schmitt [ID49](#), L. Schoeffel [ID139](#), A. Schoening [ID64b](#), P.G. Scholer [ID35](#), E. Schopf [ID148](#),
 M. Schott [ID25](#), S. Schramm [ID57](#), T. Schroer [ID57](#), H-C. Schultz-Coulon [ID64a](#), M. Schumacher [ID55](#),
 B.A. Schumm [ID140](#), Ph. Schune [ID139](#), H.R. Schwartz [ID140](#), A. Schwartzman [ID150](#), T.A. Schwarz [ID109](#),

Ph. Schwemling ¹³⁹, R. Schwienhorst ¹¹⁰, F.G. Sciacca ²⁰, A. Sciandra ³⁰, G. Sciolla ²⁷,
 F. Scuri ^{75a}, C.D. Sebastiani ³⁷, K. Sedlaczek ¹¹⁹, S.C. Seidel ¹¹⁶, A. Seiden ¹⁴⁰,
 B.D. Seidlitz ⁴³, C. Seitz ⁴⁹, J.M. Seixas ^{84b}, G. Sekhniaidze ^{73a}, L. Selem ⁶¹,
 N. Semprini-Cesari ^{24b,24a}, A. Semushin ^{180,38}, D. Sengupta ⁵⁷, V. Senthilkumar ¹⁷⁰, L. Serin ⁶⁷,
 M. Sessa ^{77a,77b}, H. Severini ¹²⁴, F. Sforza ^{58b,58a}, A. Sfyrla ⁵⁷, Q. Sha ¹⁴, E. Shabalina ⁵⁶,
 H. Shaddix ¹¹⁹, A.H. Shah ³³, R. Shaheen ¹⁵¹, J.D. Shahinian ¹³², D. Shaked Renous ¹⁷⁶,
 M. Shamim ³⁷, L.Y. Shan ¹⁴, M. Shapiro ^{18a}, A. Sharma ³⁷, A.S. Sharma ¹⁷¹, P. Sharma ³⁰,
 P.B. Shatalov ³⁸, K. Shaw ¹⁵³, S.M. Shaw ¹⁰⁴, Q. Shen ^{145a}, D.J. Sheppard ¹⁴⁹, P. Sherwood ⁹⁹,
 L. Shi ⁹⁹, X. Shi ¹⁴, S. Shimizu ⁸⁵, C.O. Shimmin ¹⁷⁹, I.P.J. Shipsey ^{130,*}, S. Shirabe ⁹¹,
 M. Shiyakova ^{40,aa}, M.J. Shochet ⁴¹, D.R. Shope ¹²⁹, B. Shrestha ¹²⁴, S. Shrestha ^{123,al},
 I. Shreyber ⁴⁰, M.J. Shroff ¹⁷², P. Sicho ¹³⁵, A.M. Sickles ¹⁶⁹, E. Sideras Haddad ^{34g,167},
 A.C. Sidley ¹¹⁸, A. Sidoti ^{24b}, F. Siegert ⁵¹, Dj. Sijacki ¹⁶, F. Sili ⁹³, J.M. Silva ⁵³,
 I. Silva Ferreira ^{84b}, M.V. Silva Oliveira ³⁰, S.B. Silverstein ^{48a}, S. Simion ⁶⁷, R. Simoniello ³⁷,
 E.L. Simpson ¹⁰⁴, H. Simpson ¹⁵³, L.R. Simpson ¹⁰⁹, S. Simsek ⁸³, S. Sindhu ⁵⁶, P. Sinervo ¹⁶²,
 S.N. Singh ²⁷, S. Singh ³⁰, S. Sinha ⁴⁹, S. Sinha ¹⁰⁴, M. Sioli ^{24b,24a}, K. Sioulas ⁹, I. Siral ³⁷,
 E. Sitnikova ⁴⁹, J. Sjölin ^{48a,48b}, A. Skaf ⁵⁶, E. Skorda ²¹, P. Skubic ¹²⁴, M. Slawinska ⁸⁸,
 I. Slazyk ¹⁷, V. Smakhtin ¹⁷⁶, B.H. Smart ¹³⁸, S.Yu. Smirnov ^{141b}, Y. Smirnov ⁸³,
 L.N. Smirnova ^{38,a}, O. Smirnova ¹⁰¹, A.C. Smith ⁴³, D.R. Smith ¹⁶⁶, E.A. Smith ⁴¹, J.L. Smith ¹⁰⁴,
 M.B. Smith ³⁵, R. Smith ¹⁵⁰, H. Smitmanns ¹⁰³, M. Smizanska ⁹⁴, K. Smolek ¹³⁶,
 P. Smolyanskiy ¹³⁶, A.A. Snesarev ⁴⁰, H.L. Snoek ¹¹⁸, S. Snyder ³⁰, R. Sobie ^{172,ac}, A. Soffer ¹⁵⁸,
 C.A. Solans Sanchez ³⁷, E.Yu. Soldatov ⁴⁰, U. Soldevila ¹⁷⁰, A.A. Solodkov ^{34g}, S. Solomon ²⁷,
 A. Soloshenko ⁴⁰, K. Solovieva ⁵⁵, O.V. Solovyanov ⁴², P. Sommer ⁵¹, A. Sonay ¹³,
 W.Y. Song ^{163b}, A. Sopczak ¹³⁶, A.L. Sopio ⁵³, F. Sopkova ^{29b}, J.D. Sorenson ¹¹⁶,
 I.R. Sotarriva Alvarez ¹⁴², V. Sothilingam ^{64a}, O.J. Soto Sandoval ^{141c,141b}, S. Sottocornola ⁶⁹,
 R. Soualah ^{89a}, Z. Soumami ^{36e}, D. South ⁴⁹, N. Soybelman ¹⁷⁶, S. Spagnolo ^{71a,71b},
 M. Spalla ¹¹³, D. Sperlich ⁵⁵, B. Spisso ^{73a,73b}, D.P. Spiteri ⁶⁰, L. Splendori ¹⁰⁵, M. Spousta ¹³⁷,
 E.J. Staats ³⁵, R. Stamen ^{64a}, E. Stanecka ⁸⁸, W. Stanek-Maslouska ⁴⁹, M.V. Stange ⁵¹,
 B. Stanislaus ^{18a}, M.M. Stanitzki ⁴⁹, B. Stapf ⁴⁹, E.A. Starchenko ³⁸, G.H. Stark ¹⁴⁰, J. Stark ⁹²,
 P. Staroba ¹³⁵, P. Starovoitov ^{89b}, R. Staszewski ⁸⁸, G. Stavropoulos ⁴⁷, A. Stefl ³⁷,
 P. Steinberg ³⁰, B. Stelzer ^{149,163a}, H.J. Stelzer ¹³³, O. Stelzer-Chilton ^{163a}, H. Stenzel ⁵⁹,
 T.J. Stevenson ¹⁵³, G.A. Stewart ³⁷, J.R. Stewart ¹²⁵, M.C. Stockton ³⁷, G. Stoicea ^{28b},
 M. Stolarski ^{134a}, S. Stonjek ¹¹³, A. Straessner ⁵¹, J. Strandberg ¹⁵¹, S. Strandberg ^{48a,48b},
 M. Stratmann ¹⁷⁸, M. Strauss ¹²⁴, T. Strebler ¹⁰⁵, P. Strizenec ^{29b}, R. Ströhmer ¹⁷³,
 D.M. Strom ¹²⁷, R. Stroynowski ⁴⁶, A. Strubig ^{48a,48b}, S.A. Stucci ³⁰, B. Stugu ¹⁷, J. Stupak ¹²⁴,
 N.A. Styles ⁴⁹, D. Su ¹⁵⁰, S. Su ⁶³, W. Su ^{145b}, X. Su ⁶³, D. Suchy ^{29a}, K. Sugizaki ¹³²,
 V.V. Sulin ³⁸, M.J. Sullivan ⁹⁵, D.M.S. Sultan ¹³⁰, L. Sultanaliev ³⁸, S. Sultansoy ^{3b},
 S. Sun ¹⁷⁷, W. Sun ¹⁴, O. Sunneborn Gudnadottir ¹⁶⁸, N. Sur ¹⁰⁵, M.R. Sutton ¹⁵³,
 H. Suzuki ¹⁶⁴, M. Svatos ¹³⁵, P.N. Swallow ³³, M. Swiatlowski ^{163a}, T. Swirski ¹⁷³,
 I. Sykora ^{29a}, M. Sykora ¹³⁷, T. Sykora ¹³⁷, D. Ta ¹⁰³, K. Tackmann ^{49,z}, A. Taffard ¹⁶⁶,
 R. Tafirout ^{163a}, Y. Takubo ⁸⁵, M. Talby ¹⁰⁵, A.A. Talyshv ³⁸, K.C. Tam ^{65b}, N.M. Tamir ¹⁵⁸,
 A. Tanaka ¹⁶⁰, J. Tanaka ¹⁶⁰, R. Tanaka ⁶⁷, M. Tanasini ¹⁵², Z. Tao ¹⁷¹, S. Tapia Araya ^{141f},
 S. Tapprogge ¹⁰³, A. Tarek Abouelfadl Mohamed ¹¹⁰, S. Tarem ¹⁵⁷, K. Tariq ¹⁴, G. Tarna ^{28b},
 G.F. Tartarelli ^{72a}, M.J. Tartarin ⁹², P. Tas ¹³⁷, M. Tasevsky ¹³⁵, E. Tassi ^{45b,45a}, A.C. Tate ¹⁶⁹,
 G. Tateno ¹⁶⁰, Y. Tayalati ^{36e,ab}, G.N. Taylor ¹⁰⁸, W. Taylor ^{163b}, A.S. Tegetmeier ⁹²,
 P. Teixeira-Dias ⁹⁸, J.J. Teoh ¹⁶², K. Terashi ¹⁶⁰, J. Terron ¹⁰², S. Terzo ¹³, M. Testa ⁵⁴,
 R.J. Teuscher ^{162,ac}, A. Thaler ⁸⁰, O. Theiner ⁵⁷, T. Theveneaux-Pelzer ¹⁰⁵, O. Thielmann ¹⁷⁸,
 D.W. Thomas ⁹⁸, J.P. Thomas ²¹, E.A. Thompson ^{18a}, P.D. Thompson ²¹, E. Thomson ¹³²,

R.E. Thornberry ⁴⁶, C. Tian ⁶³, Y. Tian ⁵⁷, V. Tikhomirov ⁸³, Yu.A. Tikhonov ³⁸, S. Timoshenko ³⁸, D. Timoshyn ¹³⁷, E.X.L. Ting ¹, P. Tipton ¹⁷⁹, A. Tishelman-Charny ³⁰, S.H. Tlou ^{34g}, K. Todome ¹⁴², S. Todorova-Nova ¹³⁷, S. Todt ⁵¹, L. Toffolin ^{70a,70c}, M. Togawa ⁸⁵, J. Tojo ⁹¹, S. Tokár ^{29a}, O. Toldaiev ⁶⁹, G. Tolkachev ¹⁰⁵, M. Tomoto ^{85,114}, L. Tompkins ^{150,p}, E. Torrence ¹²⁷, H. Torres ⁹², E. Torró Pastor ¹⁷⁰, M. Toscani ³¹, C. Tosciri ⁴¹, M. Tost ¹¹, D.R. Tovey ¹⁴⁶, T. Trefzger ¹⁷³, P.M. Tricarico ¹³, A. Tricoli ³⁰, I.M. Trigger ^{163a}, S. Trincaz-Duvoid ¹³¹, D.A. Trischuk ²⁷, A. Tropina ⁴⁰, L. Truong ^{34c}, M. Trzebinski ⁸⁸, A. Trzupiek ⁸⁸, F. Tsai ¹⁵², M. Tsai ¹⁰⁹, A. Tsiamis ¹⁵⁹, P.V. Tsiareshka ⁴⁰, S. Tsigaridas ^{163a}, A. Tsirigotis ^{159,v}, V. Tsiskaridze ¹⁶², E.G. Tskhadadze ^{156a}, M. Tsopoulou ¹⁵⁹, Y. Tsujikawa ⁹⁰, I.I. Tsukerman ³⁸, V. Tsulaia ^{18a}, S. Tsuno ⁸⁵, K. Tsuru ¹²², D. Tsybychev ¹⁵², Y. Tu ^{65b}, A. Tudorache ^{28b}, V. Tudorache ^{28b}, S. Turchikhin ^{58b,58a}, I. Turk Cakir ^{3a}, R. Turra ^{72a}, T. Turtuvshin ⁴⁰, P.M. Tuts ⁴³, S. Tzamarias ^{159,e}, E. Tzovara ¹⁰³, Y. Uematsu ⁸⁵, F. Ukegawa ¹⁶⁴, P.A. Ulloa Poblete ^{141c,141b}, E.N. Umaka ³⁰, G. Unal ³⁷, A. Undrus ³⁰, G. Unel ¹⁶⁶, J. Urban ^{29b}, P. Urrejola ^{141a}, G. Usai ⁸, R. Ushioda ¹⁶¹, M. Usman ¹¹¹, F. Ustuner ⁵³, Z. Uysal ⁸³, V. Vacek ¹³⁶, B. Vachon ¹⁰⁷, T. Vafeiadis ³⁷, A. Vaitkus ⁹⁹, C. Valderanis ¹¹², E. Valdes Santurio ^{48a,48b}, M. Valente ^{163a}, S. Valentinetti ^{24b,24a}, A. Valero ¹⁷⁰, E. Valiente Moreno ¹⁷⁰, A. Vallier ⁹², J.A. Valls Ferrer ¹⁷⁰, D.R. Van Arneman ¹¹⁸, T.R. Van Daalen ¹⁴³, A. Van Der Graaf ⁵⁰, H.Z. Van Der Schyf ^{34g}, P. Van Gemmeren ⁶, M. Van Rijnbach ³⁷, S. Van Stroud ⁹⁹, I. Van Vulpen ¹¹⁸, P. Vana ¹³⁷, M. Vanadia ^{77a,77b}, U.M. Vande Voorde ¹⁵¹, W. Vandelli ³⁷, E.R. Vandewall ¹²⁵, D. Vannicola ¹⁵⁸, L. Vannoli ⁵⁴, R. Vari ^{76a}, E.W. Varnes ⁷, C. Varni ^{18b}, D. Varouchas ⁶⁷, L. Varriale ¹⁷⁰, K.E. Varvell ¹⁵⁴, M.E. Vasile ^{28b}, L. Vaslin ⁸⁵, A. Vasyukov ⁴⁰, L.M. Vaughan ¹²⁵, R. Vavricka ¹³⁷, T. Vazquez Schroeder ¹³, J. Veatch ³², V. Vecchio ¹⁰⁴, M.J. Veen ¹⁰⁶, I. Veliscek ³⁰, L.M. Veloce ¹⁶², F. Veloso ^{134a,134c}, S. Veneziano ^{76a}, A. Ventura ^{71a,71b}, S. Ventura Gonzalez ¹³⁹, A. Verbytskyi ¹¹³, M. Verducci ^{75a,75b}, C. Vergis ⁹⁷, M. Verissimo De Araujo ^{84b}, W. Verkerke ¹¹⁸, J.C. Vermeulen ¹¹⁸, C. Vernieri ¹⁵⁰, M. Vessella ¹⁶⁶, M.C. Vetterli ^{149,ah}, A. Vgenopoulos ¹⁰³, N. Viaux Maira ^{141f}, T. Vickey ¹⁴⁶, O.E. Vickey Boeriu ¹⁴⁶, G.H.A. Viehhauser ¹³⁰, L. Vigani ^{64b}, M. Vigl ¹¹³, M. Villa ^{24b,24a}, M. Villaplana Perez ¹⁷⁰, E.M. Villhauer ⁵³, E. Vilucchi ⁵⁴, M.G. Vinciter ³⁵, A. Visibile ¹¹⁸, C. Vittori ³⁷, I. Vivarelli ^{24b,24a}, E. Voevodina ¹¹³, F. Vogel ¹¹², J.C. Voigt ⁵¹, P. Vokac ¹³⁶, Yu. Volkotrub ^{87b}, E. Von Toerne ²⁵, B. Vormwald ³⁷, K. Vorobev ³⁸, M. Vos ¹⁷⁰, K. Voss ¹⁴⁸, M. Vozak ³⁷, L. Vozdecky ¹²⁴, N. Vranjes ¹⁶, M. Vranjes Milosavljevic ¹⁶, M. Vreeswijk ¹¹⁸, N.K. Vu ^{145b,145a}, R. Vuillermet ³⁷, O. Vujanovic ¹⁰³, I. Vukotic ⁴¹, I.K. Vyas ³⁵, J.F. Wack ³³, S. Wada ¹⁶⁴, C. Wagner ¹⁵⁰, J.M. Wagner ^{18a}, W. Wagner ¹⁷⁸, S. Wahdan ¹⁷⁸, H. Wahlberg ⁹³, C.H. Waits ¹²⁴, J. Walder ¹³⁸, R. Walker ¹¹², W. Walkowiak ¹⁴⁸, A. Wall ¹³², E.J. Wallin ¹⁰¹, T. Wamorkar ^{18a}, A.Z. Wang ¹⁴⁰, C. Wang ¹⁰³, C. Wang ¹¹, H. Wang ^{18a}, J. Wang ^{65c}, P. Wang ¹⁰⁴, P. Wang ⁹⁹, R. Wang ⁶², R. Wang ⁶, S.M. Wang ¹⁵⁵, S. Wang ¹⁴, T. Wang ⁶³, T. Wang ⁶³, W.T. Wang ⁸¹, W. Wang ¹⁴, X. Wang ¹⁶⁹, X. Wang ^{145a}, X. Wang ⁴⁹, Y. Wang ^{115a}, Y. Wang ⁶³, Z. Wang ¹⁰⁹, Z. Wang ^{145b,52,145a}, Z. Wang ¹⁰⁹, C. Wanotayaroj ⁸⁵, A. Warburton ¹⁰⁷, R.J. Ward ²¹, A.L. Warnerbring ¹⁴⁸, N. Warrack ⁶⁰, S. Waterhouse ⁹⁸, A.T. Watson ²¹, H. Watson ⁵³, M.F. Watson ²¹, E. Watton ⁶⁰, G. Watts ¹⁴³, B.M. Waugh ⁹⁹, J.M. Webb ⁵⁵, C. Weber ³⁰, H.A. Weber ¹⁹, M.S. Weber ²⁰, S.M. Weber ^{64a}, C. Wei ⁶³, Y. Wei ⁵⁵, A.R. Weidberg ¹³⁰, E.J. Weik ¹²¹, J. Weingarten ⁵⁰, C. Weiser ⁵⁵, C.J. Wells ⁴⁹, T. Wenaus ³⁰, B. Wendland ⁵⁰, T. Wengler ³⁷, N.S. Wenke ¹¹³, N. Wermes ²⁵, M. Wessels ^{64a}, A.M. Wharton ⁹⁴, A.S. White ⁶², A. White ⁸, M.J. White ¹, D. Whiteson ¹⁶⁶, L. Wickremasinghe ¹²⁸, W. Wiedenmann ¹⁷⁷, M. Wielers ¹³⁸, C. Wiglesworth ⁴⁴, D.J. Wilbern ¹²⁴, H.G. Wilkens ³⁷, J.J.H. Wilkinson ³³, D.M. Williams ⁴³, H.H. Williams ¹³², S. Williams ³³,

S. Willocq ¹⁰⁶, B.J. Wilson ¹⁰⁴, D.J. Wilson ¹⁰⁴, P.J. Windischhofer ⁴¹, F.I. Winkel ³¹, F. Winklmeier ¹²⁷, B.T. Winter ⁵⁵, M. Wittgen¹⁵⁰, M. Wobisch ¹⁰⁰, T. Wojtkowski⁶¹, Z. Wolffs ¹¹⁸, J. Wollrath³⁷, M.W. Wolter ⁸⁸, H. Wolters ^{134a,134c}, M.C. Wong¹⁴⁰, E.L. Woodward ⁴³, S.D. Worm ⁴⁹, B.K. Wosiek ⁸⁸, K.W. Woźniak ⁸⁸, S. Wozniowski ⁵⁶, K. Wraight ⁶⁰, C. Wu ²¹, M. Wu ^{115b}, M. Wu ¹¹⁷, S.L. Wu ¹⁷⁷, X. Wu ⁵⁷, X. Wu ⁶³, Y. Wu ⁶³, Z. Wu ⁴, J. Wuerzinger ^{113,af}, T.R. Wyatt ¹⁰⁴, B.M. Wynne ⁵³, S. Xella ⁴⁴, L. Xia ^{115a}, M. Xia ¹⁵, M. Xie ⁶³, A. Xiong ¹²⁷, J. Xiong ^{18a}, D. Xu ¹⁴, H. Xu ⁶³, L. Xu ⁶³, R. Xu ¹³², T. Xu ¹⁰⁹, Y. Xu ¹⁴³, Z. Xu ⁵³, Z. Xu^{115a}, B. Yabsley ¹⁵⁴, S. Yacoob ^{34a}, Y. Yamaguchi ⁸⁵, E. Yamashita ¹⁶⁰, H. Yamauchi ¹⁶⁴, T. Yamazaki ^{18a}, Y. Yamazaki ⁸⁶, S. Yan ⁶⁰, Z. Yan ¹⁰⁶, H.J. Yang ^{145a,145b}, H.T. Yang ⁶³, S. Yang ⁶³, T. Yang ^{65c}, X. Yang ³⁷, X. Yang ¹⁴, Y. Yang ¹⁶⁰, Y. Yang⁶³, W.-M. Yao ^{18a}, C.L. Yardley ¹⁵³, H. Ye ⁵⁶, J. Ye ¹⁴, S. Ye ³⁰, X. Ye ⁶³, Y. Yeh ⁹⁹, I. Yeletsikh ⁴⁰, B. Yeo ^{18b}, M.R. Yexley ⁹⁹, T.P. Yildirim ¹³⁰, P. Yin ⁴³, K. Yorita ¹⁷⁵, S. Younas ^{28b}, C.J.S. Young ³⁷, C. Young ¹⁵⁰, N.D. Young¹²⁷, Y. Yu ⁶³, J. Yuan ^{14,115c}, M. Yuan ¹⁰⁹, R. Yuan ^{145b,145a}, L. Yue ⁹⁹, M. Zaazoua ⁶³, B. Zabinski ⁸⁸, I. Zahir ^{36a}, A. Zaio^{58b,58a}, Z.K. Zak ⁸⁸, T. Zakareishvili ¹⁷⁰, S. Zambito ⁵⁷, J.A. Zamora Saa ^{141d}, J. Zang ¹⁶⁰, D. Zanzi ⁵⁵, R. Zanzottera ^{72a,72b}, O. Zaplatilek ¹³⁶, C. Zeitnitz ¹⁷⁸, H. Zeng ¹⁴, J.C. Zeng ¹⁶⁹, D.T. Zenger Jr ²⁷, O. Zenin ³⁸, T. Ženiš ^{29a}, S. Zenz ⁹⁷, S. Zerradi ^{36a}, D. Zerwas ⁶⁷, M. Zhai ^{14,115c}, D.F. Zhang ¹⁴⁶, J. Zhang ^{144a}, J. Zhang ⁶, K. Zhang ^{14,115c}, L. Zhang ⁶³, L. Zhang ^{115a}, P. Zhang ^{14,115c}, R. Zhang ¹⁷⁷, S. Zhang ⁹², T. Zhang ¹⁶⁰, X. Zhang ^{145a}, Y. Zhang ¹⁴³, Y. Zhang ⁹⁹, Y. Zhang ⁶³, Y. Zhang ^{115a}, Z. Zhang ^{18a}, Z. Zhang ^{144a}, Z. Zhang ⁶⁷, H. Zhao ¹⁴³, T. Zhao ^{144a}, Y. Zhao ³⁵, Z. Zhao ⁶³, Z. Zhao ⁶³, A. Zhemchugov ⁴⁰, J. Zheng ^{115a}, K. Zheng ¹⁶⁹, X. Zheng ⁶³, Z. Zheng ¹⁵⁰, D. Zhong ¹⁶⁹, B. Zhou ¹⁰⁹, H. Zhou ⁷, N. Zhou ^{145a}, Y. Zhou ¹⁵, Y. Zhou ^{115a}, Y. Zhou⁷, C.G. Zhu ^{144a}, J. Zhu ¹⁰⁹, X. Zhu^{145b}, Y. Zhu ^{145a}, Y. Zhu ⁶³, X. Zhuang ¹⁴, K. Zhukov ⁶⁹, N.I. Zimine ⁴⁰, J. Zinsser ^{64b}, M. Ziolkowski ¹⁴⁸, L. Živković ¹⁶, A. Zoccoli ^{24b,24a}, K. Zoch ⁶², T.G. Zorbas ¹⁴⁶, O. Zormpa ⁴⁷, W. Zou ⁴³, L. Zwalinski ³⁷.

¹Department of Physics, University of Adelaide, Adelaide; Australia.

²Department of Physics, University of Alberta, Edmonton AB; Canada.

^{3(a)}Department of Physics, Ankara University, Ankara; ^(b)Division of Physics, TOBB University of Economics and Technology, Ankara; Türkiye.

⁴LAPP, Université Savoie Mont Blanc, CNRS/IN2P3, Annecy; France.

⁵APC, Université Paris Cité, CNRS/IN2P3, Paris; France.

⁶High Energy Physics Division, Argonne National Laboratory, Argonne IL; United States of America.

⁷Department of Physics, University of Arizona, Tucson AZ; United States of America.

⁸Department of Physics, University of Texas at Arlington, Arlington TX; United States of America.

⁹Physics Department, National and Kapodistrian University of Athens, Athens; Greece.

¹⁰Physics Department, National Technical University of Athens, Zografou; Greece.

¹¹Department of Physics, University of Texas at Austin, Austin TX; United States of America.

¹²Institute of Physics, Azerbaijan Academy of Sciences, Baku; Azerbaijan.

¹³Institut de Física d'Altes Energies (IFAE), Barcelona Institute of Science and Technology, Barcelona; Spain.

¹⁴Institute of High Energy Physics, Chinese Academy of Sciences, Beijing; China.

¹⁵Physics Department, Tsinghua University, Beijing; China.

¹⁶Institute of Physics, University of Belgrade, Belgrade; Serbia.

¹⁷Department for Physics and Technology, University of Bergen, Bergen; Norway.

^{18(a)}Physics Division, Lawrence Berkeley National Laboratory, Berkeley CA; ^(b)University of California,

Berkeley CA; United States of America.

¹⁹Institut für Physik, Humboldt Universität zu Berlin, Berlin; Germany.

²⁰Albert Einstein Center for Fundamental Physics and Laboratory for High Energy Physics, University of Bern, Bern; Switzerland.

²¹School of Physics and Astronomy, University of Birmingham, Birmingham; United Kingdom.

²²(^a)Department of Physics, Bogazici University, Istanbul; (^b)Department of Physics Engineering, Gaziantep University, Gaziantep; (^c)Department of Physics, Istanbul University, Istanbul; Türkiye.

²³(^a)Facultad de Ciencias y Centro de Investigaciones, Universidad Antonio Nariño,

Bogotá; (^b)Departamento de Física, Universidad Nacional de Colombia, Bogotá; Colombia.

²⁴(^a)Dipartimento di Fisica e Astronomia A. Righi, Università di Bologna, Bologna; (^b)INFN Sezione di Bologna; Italy.

²⁵Physikalisches Institut, Universität Bonn, Bonn; Germany.

²⁶Department of Physics, Boston University, Boston MA; United States of America.

²⁷Department of Physics, Brandeis University, Waltham MA; United States of America.

²⁸(^a)Transilvania University of Brasov, Brasov; (^b)Horia Hulubei National Institute of Physics and Nuclear Engineering, Bucharest; (^c)Department of Physics, Alexandru Ioan Cuza University of Iasi, Iasi; (^d)National Institute for Research and Development of Isotopic and Molecular Technologies, Physics Department, Cluj-Napoca; (^e)National University of Science and Technology Politehnica, Bucharest; (^f)West University in Timisoara, Timisoara; (^g)Faculty of Physics, University of Bucharest, Bucharest; Romania.

²⁹(^a)Faculty of Mathematics, Physics and Informatics, Comenius University, Bratislava; (^b)Department of Subnuclear Physics, Institute of Experimental Physics of the Slovak Academy of Sciences, Kosice; Slovak Republic.

³⁰Physics Department, Brookhaven National Laboratory, Upton NY; United States of America.

³¹Universidad de Buenos Aires, Facultad de Ciencias Exactas y Naturales, Departamento de Física, y CONICET, Instituto de Física de Buenos Aires (IFIBA), Buenos Aires; Argentina.

³²California State University, CA; United States of America.

³³Cavendish Laboratory, University of Cambridge, Cambridge; United Kingdom.

³⁴(^a)Department of Physics, University of Cape Town, Cape Town; (^b)iThemba Labs, Western

Cape; (^c)Department of Mechanical Engineering Science, University of Johannesburg,

Johannesburg; (^d)National Institute of Physics, University of the Philippines Diliman

(Philippines); (^e)University of South Africa, Department of Physics, Pretoria; (^f)University of Zululand,

KwaDlangezwa; (^g)School of Physics, University of the Witwatersrand, Johannesburg; South Africa.

³⁵Department of Physics, Carleton University, Ottawa ON; Canada.

³⁶(^a)Faculté des Sciences Ain Chock, Université Hassan II de Casablanca; (^b)Faculté des Sciences, Université Ibn-Tofail, Kénitra; (^c)Faculté des Sciences Semlalia, Université Cadi Ayyad,

LPHEA-Marrakech; (^d)LPMR, Faculté des Sciences, Université Mohamed Premier, Oujda; (^e)Faculté des

sciences, Université Mohammed V, Rabat; (^f)Institute of Applied Physics, Mohammed VI Polytechnic

University, Ben Guerir; Morocco.

³⁷CERN, Geneva; Switzerland.

³⁸Affiliated with an institute covered by a cooperation agreement with CERN.

³⁹Affiliated with an institute formerly covered by a cooperation agreement with CERN.

⁴⁰Affiliated with an international laboratory covered by a cooperation agreement with CERN.

⁴¹Enrico Fermi Institute, University of Chicago, Chicago IL; United States of America.

⁴²LPC, Université Clermont Auvergne, CNRS/IN2P3, Clermont-Ferrand; France.

⁴³Nevis Laboratory, Columbia University, Irvington NY; United States of America.

⁴⁴Niels Bohr Institute, University of Copenhagen, Copenhagen; Denmark.

⁴⁵(^a)Dipartimento di Fisica, Università della Calabria, Rende; (^b)INFN Gruppo Collegato di Cosenza,

Laboratori Nazionali di Frascati; Italy.

⁴⁶Physics Department, Southern Methodist University, Dallas TX; United States of America.

⁴⁷National Centre for Scientific Research "Demokritos", Agia Paraskevi; Greece.

⁴⁸(^a) Department of Physics, Stockholm University; (^b) Oskar Klein Centre, Stockholm; Sweden.

⁴⁹Deutsches Elektronen-Synchrotron DESY, Hamburg and Zeuthen; Germany.

⁵⁰Fakultät Physik, Technische Universität Dortmund, Dortmund; Germany.

⁵¹Institut für Kern- und Teilchenphysik, Technische Universität Dresden, Dresden; Germany.

⁵²Department of Physics, Duke University, Durham NC; United States of America.

⁵³SUPA - School of Physics and Astronomy, University of Edinburgh, Edinburgh; United Kingdom.

⁵⁴INFN e Laboratori Nazionali di Frascati, Frascati; Italy.

⁵⁵Physikalisches Institut, Albert-Ludwigs-Universität Freiburg, Freiburg; Germany.

⁵⁶II. Physikalisches Institut, Georg-August-Universität Göttingen, Göttingen; Germany.

⁵⁷Département de Physique Nucléaire et Corpusculaire, Université de Genève, Genève; Switzerland.

⁵⁸(^a) Dipartimento di Fisica, Università di Genova, Genova; (^b) INFN Sezione di Genova; Italy.

⁵⁹II. Physikalisches Institut, Justus-Liebig-Universität Giessen, Giessen; Germany.

⁶⁰SUPA - School of Physics and Astronomy, University of Glasgow, Glasgow; United Kingdom.

⁶¹LPSC, Université Grenoble Alpes, CNRS/IN2P3, Grenoble INP, Grenoble; France.

⁶²Laboratory for Particle Physics and Cosmology, Harvard University, Cambridge MA; United States of America.

⁶³Department of Modern Physics and State Key Laboratory of Particle Detection and Electronics, University of Science and Technology of China, Hefei; China.

⁶⁴(^a) Kirchoff-Institut für Physik, Ruprecht-Karls-Universität Heidelberg, Heidelberg; (^b) Physikalisches Institut, Ruprecht-Karls-Universität Heidelberg, Heidelberg; Germany.

⁶⁵(^a) Department of Physics, Chinese University of Hong Kong, Shatin, N.T., Hong Kong; (^b) Department of Physics, University of Hong Kong, Hong Kong; (^c) Department of Physics and Institute for Advanced Study, Hong Kong University of Science and Technology, Clear Water Bay, Kowloon, Hong Kong; China.

⁶⁶Department of Physics, National Tsing Hua University, Hsinchu; Taiwan.

⁶⁷IJCLab, Université Paris-Saclay, CNRS/IN2P3, 91405, Orsay; France.

⁶⁸Centro Nacional de Microelectrónica (IMB-CNM-CSIC), Barcelona; Spain.

⁶⁹Department of Physics, Indiana University, Bloomington IN; United States of America.

⁷⁰(^a) INFN Gruppo Collegato di Udine, Sezione di Trieste, Udine; (^b) ICTP, Trieste; (^c) Dipartimento Politecnico di Ingegneria e Architettura, Università di Udine, Udine; Italy.

⁷¹(^a) INFN Sezione di Lecce; (^b) Dipartimento di Matematica e Fisica, Università del Salento, Lecce; Italy.

⁷²(^a) INFN Sezione di Milano; (^b) Dipartimento di Fisica, Università di Milano, Milano; Italy.

⁷³(^a) INFN Sezione di Napoli; (^b) Dipartimento di Fisica, Università di Napoli, Napoli; Italy.

⁷⁴(^a) INFN Sezione di Pavia; (^b) Dipartimento di Fisica, Università di Pavia, Pavia; Italy.

⁷⁵(^a) INFN Sezione di Pisa; (^b) Dipartimento di Fisica E. Fermi, Università di Pisa, Pisa; Italy.

⁷⁶(^a) INFN Sezione di Roma; (^b) Dipartimento di Fisica, Sapienza Università di Roma, Roma; Italy.

⁷⁷(^a) INFN Sezione di Roma Tor Vergata; (^b) Dipartimento di Fisica, Università di Roma Tor Vergata, Roma; Italy.

⁷⁸(^a) INFN Sezione di Roma Tre; (^b) Dipartimento di Matematica e Fisica, Università Roma Tre, Roma; Italy.

⁷⁹(^a) INFN-TIFPA; (^b) Università degli Studi di Trento, Trento; Italy.

⁸⁰Universität Innsbruck, Department of Astro and Particle Physics, Innsbruck; Austria.

⁸¹University of Iowa, Iowa City IA; United States of America.

⁸²Department of Physics and Astronomy, Iowa State University, Ames IA; United States of America.

⁸³Istinye University, Sariyer, Istanbul; Türkiye.

- ⁸⁴(^a) Departamento de Engenharia Elétrica, Universidade Federal de Juiz de Fora (UFJF), Juiz de Fora; (^b) Universidade Federal do Rio De Janeiro COPPE/EE/IF, Rio de Janeiro; (^c) Instituto de Física, Universidade de São Paulo, São Paulo; (^d) Rio de Janeiro State University, Rio de Janeiro; (^e) Federal University of Bahia, Bahia; Brazil.
- ⁸⁵KEK, High Energy Accelerator Research Organization, Tsukuba; Japan.
- ⁸⁶Graduate School of Science, Kobe University, Kobe; Japan.
- ⁸⁷(^a) AGH University of Krakow, Faculty of Physics and Applied Computer Science, Krakow; (^b) Marian Smoluchowski Institute of Physics, Jagiellonian University, Krakow; Poland.
- ⁸⁸Institute of Nuclear Physics Polish Academy of Sciences, Krakow; Poland.
- ⁸⁹(^a) Khalifa University of Science and Technology, Abu Dhabi; (^b) University of Sharjah, Sharjah; United Arab Emirates.
- ⁹⁰Faculty of Science, Kyoto University, Kyoto; Japan.
- ⁹¹Research Center for Advanced Particle Physics and Department of Physics, Kyushu University, Fukuoka ; Japan.
- ⁹²L2IT, Université de Toulouse, CNRS/IN2P3, UPS, Toulouse; France.
- ⁹³Instituto de Física La Plata, Universidad Nacional de La Plata and CONICET, La Plata; Argentina.
- ⁹⁴Physics Department, Lancaster University, Lancaster; United Kingdom.
- ⁹⁵Oliver Lodge Laboratory, University of Liverpool, Liverpool; United Kingdom.
- ⁹⁶Department of Experimental Particle Physics, Jožef Stefan Institute and Department of Physics, University of Ljubljana, Ljubljana; Slovenia.
- ⁹⁷School of Physics and Astronomy, Queen Mary University of London, London; United Kingdom.
- ⁹⁸Department of Physics, Royal Holloway University of London, Egham; United Kingdom.
- ⁹⁹Department of Physics and Astronomy, University College London, London; United Kingdom.
- ¹⁰⁰Louisiana Tech University, Ruston LA; United States of America.
- ¹⁰¹Fysiska institutionen, Lunds universitet, Lund; Sweden.
- ¹⁰²Departamento de Física Teórica C-15 and CIAFF, Universidad Autónoma de Madrid, Madrid; Spain.
- ¹⁰³Institut für Physik, Universität Mainz, Mainz; Germany.
- ¹⁰⁴School of Physics and Astronomy, University of Manchester, Manchester; United Kingdom.
- ¹⁰⁵CPPM, Aix-Marseille Université, CNRS/IN2P3, Marseille; France.
- ¹⁰⁶Department of Physics, University of Massachusetts, Amherst MA; United States of America.
- ¹⁰⁷Department of Physics, McGill University, Montreal QC; Canada.
- ¹⁰⁸School of Physics, University of Melbourne, Victoria; Australia.
- ¹⁰⁹Department of Physics, University of Michigan, Ann Arbor MI; United States of America.
- ¹¹⁰Department of Physics and Astronomy, Michigan State University, East Lansing MI; United States of America.
- ¹¹¹Group of Particle Physics, University of Montreal, Montreal QC; Canada.
- ¹¹²Fakultät für Physik, Ludwig-Maximilians-Universität München, München; Germany.
- ¹¹³Max-Planck-Institut für Physik (Werner-Heisenberg-Institut), München; Germany.
- ¹¹⁴Graduate School of Science and Kobayashi-Maskawa Institute, Nagoya University, Nagoya; Japan.
- ¹¹⁵(^a) Department of Physics, Nanjing University, Nanjing; (^b) School of Science, Shenzhen Campus of Sun Yat-sen University; (^c) University of Chinese Academy of Science (UCAS), Beijing; China.
- ¹¹⁶Department of Physics and Astronomy, University of New Mexico, Albuquerque NM; United States of America.
- ¹¹⁷Institute for Mathematics, Astrophysics and Particle Physics, Radboud University/Nikhef, Nijmegen; Netherlands.
- ¹¹⁸Nikhef National Institute for Subatomic Physics and University of Amsterdam, Amsterdam; Netherlands.

- ¹¹⁹Department of Physics, Northern Illinois University, DeKalb IL; United States of America.
- ¹²⁰^(a)New York University Abu Dhabi, Abu Dhabi;^(b)United Arab Emirates University, Al Ain; United Arab Emirates.
- ¹²¹Department of Physics, New York University, New York NY; United States of America.
- ¹²²Ochanomizu University, Otsuka, Bunkyo-ku, Tokyo; Japan.
- ¹²³Ohio State University, Columbus OH; United States of America.
- ¹²⁴Homer L. Dodge Department of Physics and Astronomy, University of Oklahoma, Norman OK; United States of America.
- ¹²⁵Department of Physics, Oklahoma State University, Stillwater OK; United States of America.
- ¹²⁶Palacký University, Joint Laboratory of Optics, Olomouc; Czech Republic.
- ¹²⁷Institute for Fundamental Science, University of Oregon, Eugene, OR; United States of America.
- ¹²⁸Graduate School of Science, Osaka University, Osaka; Japan.
- ¹²⁹Department of Physics, University of Oslo, Oslo; Norway.
- ¹³⁰Department of Physics, Oxford University, Oxford; United Kingdom.
- ¹³¹LPNHE, Sorbonne Université, Université Paris Cité, CNRS/IN2P3, Paris; France.
- ¹³²Department of Physics, University of Pennsylvania, Philadelphia PA; United States of America.
- ¹³³Department of Physics and Astronomy, University of Pittsburgh, Pittsburgh PA; United States of America.
- ¹³⁴^(a)Laboratório de Instrumentação e Física Experimental de Partículas - LIP, Lisboa;^(b)Departamento de Física, Faculdade de Ciências, Universidade de Lisboa, Lisboa;^(c)Departamento de Física, Universidade de Coimbra, Coimbra;^(d)Centro de Física Nuclear da Universidade de Lisboa, Lisboa;^(e)Departamento de Física, Universidade do Minho, Braga;^(f)Departamento de Física Teórica y del Cosmos, Universidad de Granada, Granada (Spain);^(g)Departamento de Física, Instituto Superior Técnico, Universidade de Lisboa, Lisboa; Portugal.
- ¹³⁵Institute of Physics of the Czech Academy of Sciences, Prague; Czech Republic.
- ¹³⁶Czech Technical University in Prague, Prague; Czech Republic.
- ¹³⁷Charles University, Faculty of Mathematics and Physics, Prague; Czech Republic.
- ¹³⁸Particle Physics Department, Rutherford Appleton Laboratory, Didcot; United Kingdom.
- ¹³⁹IRFU, CEA, Université Paris-Saclay, Gif-sur-Yvette; France.
- ¹⁴⁰Santa Cruz Institute for Particle Physics, University of California Santa Cruz, Santa Cruz CA; United States of America.
- ¹⁴¹^(a)Departamento de Física, Pontificia Universidad Católica de Chile, Santiago;^(b)Millennium Institute for Subatomic physics at high energy frontier (SAPHIR), Santiago;^(c)Instituto de Investigación Multidisciplinario en Ciencia y Tecnología, y Departamento de Física, Universidad de La Serena;^(d)Universidad Andres Bello, Department of Physics, Santiago;^(e)Instituto de Alta Investigación, Universidad de Tarapacá, Arica;^(f)Departamento de Física, Universidad Técnica Federico Santa María, Valparaíso; Chile.
- ¹⁴²Department of Physics, Institute of Science, Tokyo; Japan.
- ¹⁴³Department of Physics, University of Washington, Seattle WA; United States of America.
- ¹⁴⁴^(a)Institute of Frontier and Interdisciplinary Science and Key Laboratory of Particle Physics and Particle Irradiation (MOE), Shandong University, Qingdao;^(b)School of Physics, Zhengzhou University; China.
- ¹⁴⁵^(a)School of Physics and Astronomy, Shanghai Jiao Tong University, Key Laboratory for Particle Astrophysics and Cosmology (MOE), SKLPPC, Shanghai;^(b)Tsung-Dao Lee Institute, Shanghai; China.
- ¹⁴⁶Department of Physics and Astronomy, University of Sheffield, Sheffield; United Kingdom.
- ¹⁴⁷Department of Physics, Shinshu University, Nagano; Japan.
- ¹⁴⁸Department Physik, Universität Siegen, Siegen; Germany.
- ¹⁴⁹Department of Physics, Simon Fraser University, Burnaby BC; Canada.

- ¹⁵⁰SLAC National Accelerator Laboratory, Stanford CA; United States of America.
- ¹⁵¹Department of Physics, Royal Institute of Technology, Stockholm; Sweden.
- ¹⁵²Departments of Physics and Astronomy, Stony Brook University, Stony Brook NY; United States of America.
- ¹⁵³Department of Physics and Astronomy, University of Sussex, Brighton; United Kingdom.
- ¹⁵⁴School of Physics, University of Sydney, Sydney; Australia.
- ¹⁵⁵Institute of Physics, Academia Sinica, Taipei; Taiwan.
- ¹⁵⁶(^a) E. Andronikashvili Institute of Physics, Iv. Javakhishvili Tbilisi State University, Tbilisi; (^b) High Energy Physics Institute, Tbilisi State University, Tbilisi; (^c) University of Georgia, Tbilisi; Georgia.
- ¹⁵⁷Department of Physics, Technion, Israel Institute of Technology, Haifa; Israel.
- ¹⁵⁸Raymond and Beverly Sackler School of Physics and Astronomy, Tel Aviv University, Tel Aviv; Israel.
- ¹⁵⁹Department of Physics, Aristotle University of Thessaloniki, Thessaloniki; Greece.
- ¹⁶⁰International Center for Elementary Particle Physics and Department of Physics, University of Tokyo, Tokyo; Japan.
- ¹⁶¹Graduate School of Science and Technology, Tokyo Metropolitan University, Tokyo; Japan.
- ¹⁶²Department of Physics, University of Toronto, Toronto ON; Canada.
- ¹⁶³(^a) TRIUMF, Vancouver BC; (^b) Department of Physics and Astronomy, York University, Toronto ON; Canada.
- ¹⁶⁴Division of Physics and Tomonaga Center for the History of the Universe, Faculty of Pure and Applied Sciences, University of Tsukuba, Tsukuba; Japan.
- ¹⁶⁵Department of Physics and Astronomy, Tufts University, Medford MA; United States of America.
- ¹⁶⁶Department of Physics and Astronomy, University of California Irvine, Irvine CA; United States of America.
- ¹⁶⁷University of West Attica, Athens; Greece.
- ¹⁶⁸Department of Physics and Astronomy, University of Uppsala, Uppsala; Sweden.
- ¹⁶⁹Department of Physics, University of Illinois, Urbana IL; United States of America.
- ¹⁷⁰Instituto de Física Corpuscular (IFIC), Centro Mixto Universidad de Valencia - CSIC, Valencia; Spain.
- ¹⁷¹Department of Physics, University of British Columbia, Vancouver BC; Canada.
- ¹⁷²Department of Physics and Astronomy, University of Victoria, Victoria BC; Canada.
- ¹⁷³Fakultät für Physik und Astronomie, Julius-Maximilians-Universität Würzburg, Würzburg; Germany.
- ¹⁷⁴Department of Physics, University of Warwick, Coventry; United Kingdom.
- ¹⁷⁵Waseda University, Tokyo; Japan.
- ¹⁷⁶Department of Particle Physics and Astrophysics, Weizmann Institute of Science, Rehovot; Israel.
- ¹⁷⁷Department of Physics, University of Wisconsin, Madison WI; United States of America.
- ¹⁷⁸Fakultät für Mathematik und Naturwissenschaften, Fachgruppe Physik, Bergische Universität Wuppertal, Wuppertal; Germany.
- ¹⁷⁹Department of Physics, Yale University, New Haven CT; United States of America.
- ¹⁸⁰Yerevan Physics Institute, Yerevan; Armenia.
- ^a Also Affiliated with an institute covered by a cooperation agreement with CERN.
- ^b Also at An-Najah National University, Nablus; Palestine.
- ^c Also at Borough of Manhattan Community College, City University of New York, New York NY; United States of America.
- ^d Also at Center for High Energy Physics, Peking University; China.
- ^e Also at Center for Interdisciplinary Research and Innovation (CIRI-AUTH), Thessaloniki; Greece.
- ^f Also at CERN, Geneva; Switzerland.
- ^g Also at CMD-AC UNEC Research Center, Azerbaijan State University of Economics (UNEC); Azerbaijan.

- ^h Also at Département de Physique Nucléaire et Corpusculaire, Université de Genève, Genève; Switzerland.
- ⁱ Also at Departament de Física de la Universitat Autònoma de Barcelona, Barcelona; Spain.
- ^j Also at Department of Financial and Management Engineering, University of the Aegean, Chios; Greece.
- ^k Also at Department of Mathematical Sciences, University of South Africa, Johannesburg; South Africa.
- ^l Also at Department of Modern Physics and State Key Laboratory of Particle Detection and Electronics, University of Science and Technology of China, Hefei; China.
- ^m Also at Department of Physics, Bolu Abant İzzet Baysal University, Bolu; Türkiye.
- ⁿ Also at Department of Physics, California State University, Sacramento; United States of America.
- ^o Also at Department of Physics, King's College London, London; United Kingdom.
- ^p Also at Department of Physics, Stanford University, Stanford CA; United States of America.
- ^q Also at Department of Physics, Stellenbosch University; South Africa.
- ^r Also at Department of Physics, University of Fribourg, Fribourg; Switzerland.
- ^s Also at Department of Physics, University of Thessaly; Greece.
- ^t Also at Department of Physics, Westmont College, Santa Barbara; United States of America.
- ^u Also at Faculty of Physics, Sofia University, 'St. Kliment Ohridski', Sofia; Bulgaria.
- ^v Also at Hellenic Open University, Patras; Greece.
- ^w Also at Henan University; China.
- ^x Also at Imam Mohammad Ibn Saud Islamic University; Saudi Arabia.
- ^y Also at Institutio Catalana de Recerca i Estudis Avancats, ICREA, Barcelona; Spain.
- ^z Also at Institut für Experimentalphysik, Universität Hamburg, Hamburg; Germany.
- ^{aa} Also at Institute for Nuclear Research and Nuclear Energy (INRNE) of the Bulgarian Academy of Sciences, Sofia; Bulgaria.
- ^{ab} Also at Institute of Applied Physics, Mohammed VI Polytechnic University, Ben Guerir; Morocco.
- ^{ac} Also at Institute of Particle Physics (IPP); Canada.
- ^{ad} Also at Institute of Physics, Azerbaijan Academy of Sciences, Baku; Azerbaijan.
- ^{ae} Also at National Institute of Physics, University of the Philippines Diliman (Philippines); Philippines.
- ^{af} Also at Technical University of Munich, Munich; Germany.
- ^{ag} Also at The Collaborative Innovation Center of Quantum Matter (CICQM), Beijing; China.
- ^{ah} Also at TRIUMF, Vancouver BC; Canada.
- ^{ai} Also at Università di Napoli Parthenope, Napoli; Italy.
- ^{aj} Also at University of Colorado Boulder, Department of Physics, Colorado; United States of America.
- ^{ak} Also at University of the Western Cape; South Africa.
- ^{al} Also at Washington College, Chestertown, MD; United States of America.
- ^{am} Also at Yeditepe University, Physics Department, Istanbul; Türkiye.
- * Deceased